The application of ESCA and SIMS to the study of saccharides, protein and the C. albicans cell wall by Yong He

A thesis submitted in partial fulfillment of the requirements for the degree of Master of Science in Chemical Engineering
Montana State University

Abstract:
Polymers for permanent or temporal implantation in the human body are widely used in modern medicine. Infections associated with these polymers are frequently encountered. Candida albicans is one of the organisms associated with these infections. The attachment of C. albicans to polymer surfaces is an important step in the initiation of both superficial and deep-seated candidasis. Different methods have been used to examine the adhesion, but employing modern surface analytical instrument (ESCA, SIMS) for adhesion study has not been done previously and is employed in this study for the first time.

In order to use ESCA and static SIMS as surface analytical techniques to study the adhesion, a protocol for the interpretation of the resulting spectra must be developed. The objective of this study is to collect and interpret ESCA and SIMS spectra of model saccharides, protein and C. albicans cell wall, compare those spectra, and attempt to identify saccharides and protein constituent that contribute to SIMS spectra from the C. albicans cell wall.

Glucose, mannose, galactose, glucuronic acid, methyl α-D-mannopyranoside, cellobiose, maltose, mannan, glucan, glutamic acid and albumin were used as model saccharides and protein. ESCA analysis was performed on a Surface Science Instruments X-Probe ESCA instrument. SIMS analysis was performed on a PHI model 3700 static SIMS subsystem with a Balzers 511 quadrupole mass analyzer.

Stereoisomers looked identical in ESCA analysis, while a difference was seen in SIMS analysis. The positive ion SIMS spectra of C. albicans cell wall looked like the positive ion SIMS spectrum of mannose, while their negative ion SIMS spectra clearly indicated the. involvement of amino acids. The ESCA and SIMS spectra shown in this experiment were the first report of saccharides and C. albicans. The protocol for spectral interpretation described . in this study should be generally useful in ESCA and static SIMS saccharides, polysaccharides, saccharide acids and protein interpretation. This experiment contributed the fundamental work for further adhesion study.

THE APPLICATION OF ESCA AND SIMS TO THE STUDY OF SACCHARIDES, PROTEIN AND THE *C. albicans* CELL WALL

by

Yong He

A thesis submitted in partial fulfillment
of the requirements for the degree

of

Master of Science

in

Chemical Engineering

MONTANA STATE UNIVERSITY
Bozeman, Montana

April 1995

APPROVAL

of a thesis submitted by

Yong He

This thesis has been read by each member of the thesis committee and has been found to be satisfactory regarding content, English usage, format, citations, bibliographic style, and consistency, and is ready for submission to the College of Graduate Studies.

4/19/95
Date

Chairperson, Graduate committee

Approved for the Major Department

4/21/95
Date

Head, Major Department

Approved for the College of Graduate Studies

5/2/95
Date

Graduate Dean

STATEMENT OF PERMISSION TO USE

In presenting this thesis in partial fulfillment of the requirements for a master's degree at Montana State University, I agree that the Library shall make it available to borrowers under rules of the Library.

If I have indicated my intention to copyright this thesis by including a copyright notice page, copying is allowable only for scholarly purposes, consistent with "fair use" as prescribed in the U.S. Copyright Law. Requests for permission for extended quotation from or reproduction of this thesis in whole or in parts may be granted only by the copyright holder.

Signature 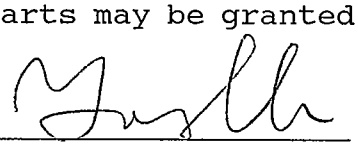

Date 4/20/1995

ACKNOWLEDGMENTS

The author wishes to thank the faculty and staff of the Chemical Engineering Department at Montana State University and Chemical Engineering Department at University of Washington for their guidance and assistance.

Thanks are extended to my advisor Dr. Bonnie Tyler, Dr. John Sears and Dr. Diane Brawner for their advice, encouragement, and support throughout the course of this research and thesis preparation.

Thanks are also extended to Pat Schamberger, Kevin Siedlecki, Ace Baty, Wayne Marchwick and Erika Johnston for their assistance and support.

TABLE OF CONTENTS

TABLE OF CONTENTS--Continued

TABLE OF CONTENTS--Continued

LIST OF TABLES

LIST OF TABLES--Continued

LIST OF TABLES--Continued

LIST OF FIGURES

LIST OF FIGURES--Continued

LIST OF FIGURES--Continued

LIST OF FIGURES--Continued

ABSTRACT

Polymers for permanent or temporal implantation in the human body are widely used in modern medicine. Infections associated with these polymers are frequently encountered. *Candida albicans* is one of the organisms associated with these infections. The attachment of *C. albicans* to polymer surfaces is an important step in the initiation of both superficial and deep-seated candidasis. Different methods have been used to examine the adhesion, but employing modern surface analytical instrument (ESCA, SIMS) for adhesion study has not been done previously and is employed in this study for the first time.

In order to use ESCA and static SIMS as surface analytical techniques to study the adhesion, a protocol for the interpretation of the resulting spectra must be developed. The objective of this study is to collect and interpret ESCA and SIMS spectra of model saccharides, protein and *C. albicans* cell wall, compare those spectra, and attempt to identify saccharides and protein constituent that contribute to SIMS spectra from the *C. albicans* cell wall.

Glucose, mannose, galactose, glucuronic acid, methyl α-D-mannopyranoside, cellobiose, maltose, mannan, glucan, glutamic acid and albumin were used as model saccharides and protein. ESCA analysis was performed on a Surface Science Instruments X-Probe ESCA instrument. SIMS analysis was performed on a PHI model 3700 static SIMS subsystem with a Balzers 511 quadrupole mass analyzer.

Stereoisomers looked identical in ESCA analysis, while a difference was seen in SIMS analysis. The positive ion SIMS spectra of *C. albicans* cell wall looked like the positive ion SIMS spectrum of mannose, while their negative ion SIMS spectra clearly indicated the involvement of amino acids. The ESCA and SIMS spectra shown in this experiment were the first report of saccharides and *C. albicans*. The protocol for spectral interpretation described in this study should be generally useful in ESCA and static SIMS saccharides, polysaccharides, saccharide acids and protein interpretation. This experiment contributed the fundamental work for further adhesion study.

INTRODUCTION

Polymers for permanent or temporal implantation in the human body have become more widely used in modern medicine. Infections associated with these polymers are frequently encountered, particularly in skin-penetrating devices [1]. These infections have proved very difficult to eradicate without the removal of the device. *Candida albicans* is one of the organisms associated with these infections [2,3]. The attachment of *Candida albicans* to various polymer surfaces is an important step in the initiation of both superficial and deep-seated candidiasis.

Problems In This Area

Although polymers are being used for tissue substitution and intravascular devices with increasing frequency, few studies on the adhesion of *C. albicans* to polymer surfaces have been reported [4]. The few studies previously reported primarily used macroscopic techniques such as microscopy to study cell adhesion. In one study, the adhesion of *C. albicans* was examined microscopically after colonized catheters were removed from patients to obtain information on the morphology of the attached fungi [5]. In another study, attached Candida species were examined quantitatively and were

shown to adhere to polyvinyl chloride and Teflon catheters in large numbers *in vitro* [6]. However, there have been few studies employing modern surface analytical methods to study cell adhesion.

Because adhesion is governed by the molecular structure of the outermost region of a solid surface, it is not enough to obtain elemental information [7]. A surface analysis technique with high sensitivity and lateral resolution that can provide detailed molecular information about surface structures is required. Concerning adhesion, there are several analytical questions that need to be answered: What is the nature, concentration, and location of all atomic and molecular species present in the surface region? Knowing the answers to these questions is an indispensable prerequisite for the controlled modification of the "molecular architecture" of the surface.

To answer these questions, researchers must consider the unambiguous identification of unknown surface species (atoms as well as molecules or molecular clusters); the quantification of these surface species (i.e., information on the relative or absolute coverage by these species), and the location of these surface species (i.e., information on their lateral and depth distributions). The identification should be universal; it should be possible to identify all types of elements and molecular species. Quantification should be possible, even for very low surface concentrations, and

locating species should be possible with high lateral and depth resolution. In addition, all types of materials and all sample shapes should be accessible.

Because most materials involved in fungal adhesion are organic in origin, the following techniques are important in this regard: X-ray photoelectron spectroscopy (XPS), also known as electron spectroscopy for chemical analysis (ESCA), surface mass spectrometry (MS), and scanning tunneling microscopy (STM) and its related counterpart, atomic force microscopy (AFM) [8].

In ESCA, information on the elemental composition of the uppermost atomic layers is obtained with sensitivities down to 0.1% of a monolayer [7]. Important information on the chemical environment of the identified elements is supplied by the chemical shift (i.e., the influence of the chemical environment on the exact energy of the emitted photoelectrons). However, identification of unknown complex molecules by this chemical shift is not possible, and the achievable lateral resolution is limited to a few micrometers. STM and AFM allow lateral resolution in the sub-nanometer range so that single atoms can be probed. However, these techniques cannot be used to identify unknown surface species [7].

Motivation of This Work

The most important feature of surface Mass Spectrometry

(MS), in addition to high sensitivity, is its ability to provide detailed molecular information and information at shallow depths. It allows the identification and quantification of all elements, isotopes, and molecular species [9]. Therefore, surface MS is an excellent technique for surface analysis. As in any MS technique, the quality and reproducibility of the data require that several criteria be met: controlled desorption of atoms and molecular species, efficient ionization of these desorbed particles, and unambiguous identification of the generated ions by their charge/mass ratios. A considerable fraction of molecular surface species should survive these processes without fragmentation. It has been shown that, static secondary ion mass spectrometry (static SIMS) meets these criteria and is well suited for elemental and molecular applications [10].

Static SIMS has been widely applied to structural characterization of polymers by using fingerprint spectra or fragments characteristic of the backbone and pendant groups. This includes the characterization of the surface chemistry of polymers of biomedical importance [11,12]. Using this powerful technique for the study of the interaction of polymers with biological molecules and systems has also been studied by Mantus and co-workers. They demonstrated that static SIMS could be used to analyze proteins adsorbed to biomaterial surfaces, and established a spectral interpretation protocol by examining homopolymers of 16 amino

acids [13].

In order to use static SIMS and ESCA as a surface analysis technique to study the adhesion of *C. albicans* to protein coated polymer surfaces, a system consisting of large biomolecules, such as proteins and polysaccharides, a protocol for the interpretation of the resulting spectra must be developed.

Objectives

The main purpose of this experiment is to demonstrate that static SIMS and ESCA can be used to identify saccharides and proteins in fungal films. The objectives are:

(1) Collect and interpret ESCA and static SIMS spectra of model saccharides and proteins. In this experiment, glucose, mannose, galactose, glucuronic acid and methyl α-D-mannopyranoside were used as model monosaccharides. Cellobiose, maltose, mannan and glucan were used as model disaccharides and polysaccharides. Bovine serum albumin was used as the model protein.

(2) Collect and interpret ESCA and static SIMS spectra of *C. albicans* cell wall purified antigens and crude antigen.

(3) Compare the ESCA and static SIMS spectra of model compounds and *Candida* cell wall antigens, and attempt to identify saccharides and protein constituents that contribute to SIMS spectra from the *C. albicans* cell wall antigens.

LITERATURE SURVEY

Static SIMS

SIMS is the mass spectrometry of ionized particles which are emitted as secondary ions when a surface is bombarded by energetic primary ions with energies on the order of several KeV. These primary ions result in the emission of secondary particles characteristic of the chemical composition and structure in the uppermost layer. Most secondary particles are emitted as neutrals, whereas only a fraction 10^{-6} - 10^{-1} of the total are positively or negatively charged secondary ions. The secondary ions consist of molecular ions, atomic ions and cluster ions. It is the secondary ions which are detected and analyzed by a mass spectrometer, either a quadrupole or time of flight analyzer.

In static SIMS the primary ions are kept at a sufficiently low energy (5-25 KeV) to allow secondary ion emission from only the top few atomic layers of a surface. It is the mass spectrum of these secondary ions that provide a detailed chemical analysis of the surface.

Principles of Sputtering And Ion Formation

Figure 1 [7] schematically outlines the mechanism of SIMS according to the current understanding of this method. In the

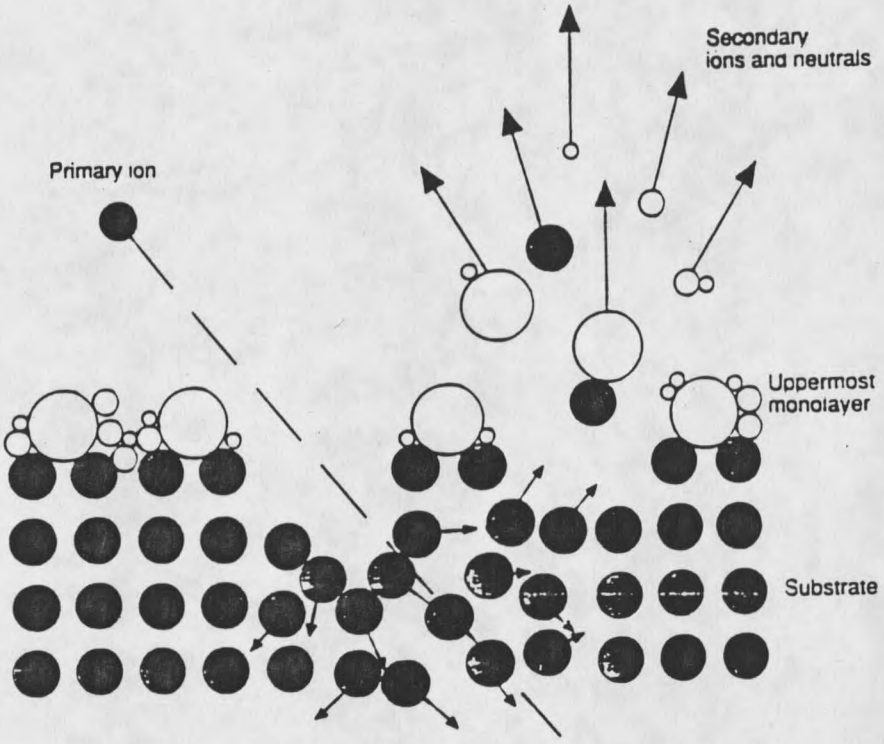

Figure 1. Particle emission from a surface after excitation with primary ions of KeV energy

case of ion bombardment, the energy of the primary beam, usually Xe^+ or Ar^+ ion beams, is transferred to the target by a collision, a billiard-ball-type process, also called "collision cascade", consisting of a cloud of target particles set in motion by the primary ions or by target particles. These primary ions and target particles are already moving. The dimension of the collision cascade depends on the energy and mass of the primary ion beam as well as the density and structure of the target material. For the bombardment of organic materials with 10-KeV Xe^+, typical values are 3 nm for the diameter of the collision cascade, and 15 nm for the depth

of the collision cascade, according to model calculations [10].

Most recoil particles have low energies, and only cascade particles from near-surface regions - with momenta directed toward the surface - can overcome the surface binding energy and thus leave the target (sputtered particles). SIMS, therefore, is a very surface-sensitive analytical technique (information depth is < 3 monolayers). The charge state of the sputtered particles depends largely on the chemical environment in the uppermost monolayer (matrix effect), which in general, prevents the direct quantification of SIMS results.

Ions originating from an elemental matrix can be positively or negatively charged, depending on their electron configurations in the outermost shell. The highest secondary ion yields (i.e., number of secondary ions X^q emitted from a surface species M per number of primary ions) of molecular ions are achieved from monolayers on noble metal substrates. Typical secondary ions are Me^+ or Me^-, $(M + H)^+$, $(M - H)^-$, $(M + Sa)^+$, and $(M + Me)^+$, where Me is a metal, M is a molecule, H is hydrogen, and Sa is either sodium or potassium. From bulk materials and thick layers, typically $(M + H)^+$ and $(M - H)^-$ and larger fragments can be obtained. To elucidate the fragmentation process, fragmentation rules that are known from electron impact mass spectrometry can be applied such as α-,β-cleavages; rearrangement processes.

Application of Static SIMS

The importance of static SIMS for surface analysis lies in the possibility of studying not only the elemental composition but also the chemical structure of surfaces. This is because the surface mass spectrum includes cluster ions as well as elemental ions. These ions directly reflect the surface chemistry of the sample [14,15].

There are two general areas of application of the static SIMS technique. The first application as a spectrometric method and the second as a surface analysis method. As a mass spectrometric method, static SIMS can be used to desorb and ionize biomolecules from specially prepared surfaces. The surface sensitivity of the static SIMS technique is not fully exploited in the purely mass spectrometric applications. As a surface analytical method, static SIMS is unrivaled in its molecular selectivity because of the groundwork provided by mass spectrometry. Static SIMS has been used to analyze a wide variety of "real" surfaces, ranging from semiconductor materials to complex copolymers. The spectra produced reflect the surface chemistry of the material but, in general, do not contain large ($m/z > 500$) molecular ions or fragments. However, useful information is readily extracted from the fragment ions in lower mass range. The ability of static SIMS to produce a surface-sensitive mass spectrum gives it great potential as a probe of proteins on surfaces.

SIMS Instrumentation

Vacuum Systems SIMS experiments are performed in high vacuum for two reasons: first, to avoid scattering of the primary and secondary beams; and second, to prevent interfering adsorption of gases on the surface under investigation.

Ion Gun For static SIMS, a broad beam source is used, with a diameter of 1 mm - 1 cm. Beam currents of 10^{-10} - 10^{-8}A are used, giving monolayer lifetimes > 100s. The beam energy lies between 500 eV and 5 KeV. The lower ion beam energies cause less disruption in the surface and sub-surface of the sample. Less disruption gives more confidence that the analysis is representative of the original surface, but also means a low sputter rate. High beam accelerating voltages give higher sputter rates, and also give higher beam currents from a given ion source. Higher values of beam energy therefore contribute to a more rapid analysis. The beam species must also be sufficiently heavy (m > 30), to produce efficient sputtering, and the inert gases argon and xenon are often chosen to preclude chemical modification of the surface.

Mass Spectrometers There are several common types of mass spectrometer: quadrupole mass spectrometers, magnetic sector mass spectrometers, and time-of-flight mass spectrometers. The one used for this thesis is the quadrupole

mass spectrometer.

A quadrupole mass spectrometer employs a combination of direct current (DC) and radio frequency (RF) potentials as a mass "filter". Mechanically, the quadrupole consists of four parallel rods arranged symmetrically. Ideally, these four rods should have the shape of a hyperbola in cross section so that idealized hyperbolic fields can be produced according to quadrupole theory. However, in practice, cylindrical rods are often used to approximate the hyperbolic-field requirements. Opposite rods (i.e., those diagonally opposite) are connected together electrically and to RF and DC voltage generators.

Ions are formed in ion source and expelled by a small electric (repeller) field. The ion current is continuous. The ions are accelerated but only to a rather low kinetic energy, about 5-15 KeV. They are then ejected along the center line between the four stainless steel rods. The ions would pass straight through to the detector at the far end if it had not been for the fact that the two pairs of opposite rods are connected, in parallel, to both a DC and an RF source. The DC voltage is kept at a constant fraction, about 16%, of the peak RF voltage. A given RF peak voltage then allows ions of only one integral mass to pass through the quadrupole - hence the name mass filter. A typical RF voltage range is a few hundred to a few thousand volts. The RF power supply has to be extremely stable while being able to deliver about 1 KW of power [9].

ESCA

Of all the contemporary surface characterization methods, electron spectroscopy for chemical analysis (ESCA) is the most widely used. ESCA is also called X-ray photoelectron spectroscopy (XPS), and these two names can be used interchangeably. The popularity of ESCA as a surface analysis technique is attributed to its high information content, its flexibility in addressing a wide variety of samples, and its sound theoretical basis [16].

Surface analysis by ESCA involves irradiation of the solid *in vacuo* with monoenergetic soft x-rays and sorting the emitted electrons by energy. Figure 2 [16] illustrates the ESCA experiment. A sample is irradiated with X-rays of known energy hν. This causes the sample to emit photoelectrons. These electrons are collected, passed through a hemispherical energy analyzer and counted. Some of these electrons will escape from the surface with no loss of kinetic energy and contribute to sharp peaks in the electron spectra. The spectrum obtained is a plot of the number of emitted electrons versus their binding energy. Each element has a unique elemental spectrum, and the spectral peaks from a mixture are approximately the sum of the elemental peaks from the individual constituents. The energies of these emitted electrons are characteristic of the compounds contained in the sample. The elements and the binding environment of elements in a sample are identified by the kinetic energy of these

photoelectrons. The intensity of the peaks can be used as a quantitative measure of the concentration of elements present in the sample.

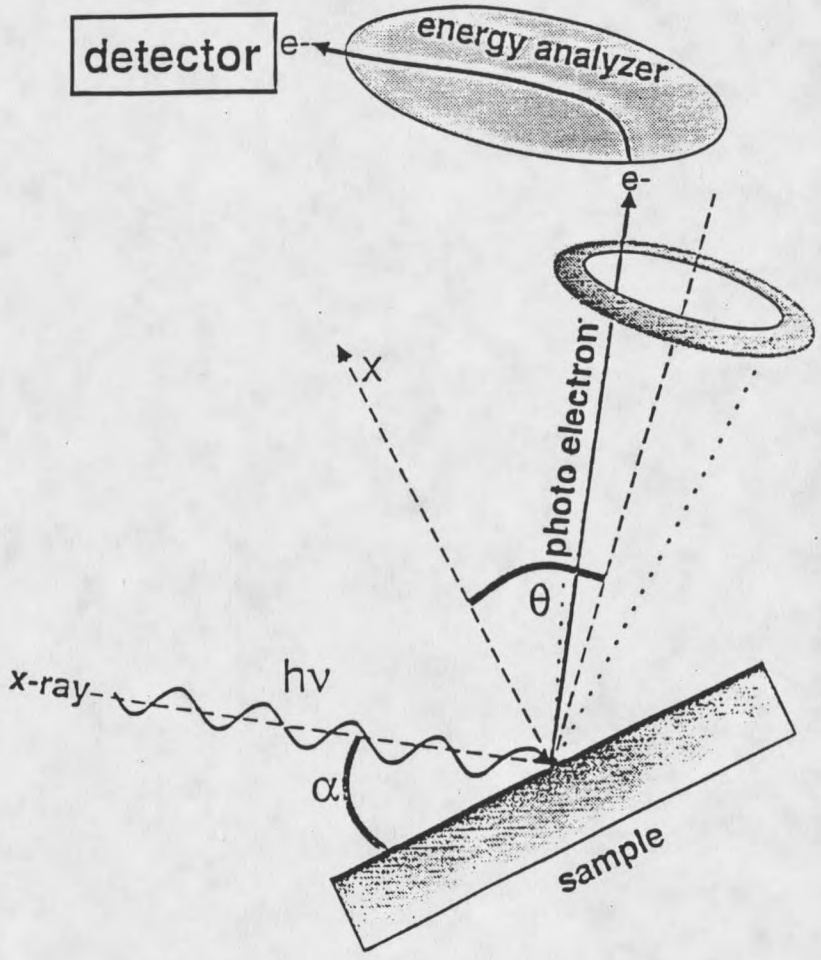

Figure 2. Cartoon illustration the principle of x-ray photoelectron spectroscopy. The sample is irradiated with x-rays and electrons are emitted from the sample. The energy of the electrons is then analyzed and electrons are counted by the detector.

Because the photoelectrons can only travel a short distance through the sample without undergoing an inelastic collision, ESCA is highly surface sensitive. Under typical

conditions, only the upper 50 Å to 100 Å of the sample is analyzed [16].

Principles of The Technique

The Photoelectric Effect Photoemission When a photon impinges upon an atom, one of three events may occur: (1) the photon can pass through with no interaction, (2) the photon can be scattered by an atomic orbital electron leading to partial energy loss, and (3) the photon may interact with an atomic orbital electron with total transfer of the photon energy to the electron, leading to electron emission from the atom. The third process accurately describes the photoemission that is the basis of ESCA. Total transfer of the photon energy to the electron is the essential element of photoemission.

No electrons will be ejected from an atom regardless of the illumination intensity unless the frequency of excitation is greater than or equal to a threshold level characteristic of each element. Thus, if the frequency (energy) of the excitation photon is too low, no photoemission will be observed. As the energy of this photon is gradually increased, at some value, the photoemission of electrons from the atom will be observed. Once the threshold frequency is exceeded, the number of electrons emitted will be proportional to the intensity of the illumination (i.e., once photon of sufficient energy were used to stimulate electron emission,

the more the photons bombarding the sample, the more photoelectrons will be produced). The kinetic energy of the emitted electrons is linearly proportional to the frequency of the exciting photons. If the photons have energy higher than the threshold value, the excess energy will be transmitted to the emitted electrons. The photoemission process from excitation to emission is extremely rapid (10^{-16} sec). The basic physics of this process can be described by the Einstein equation:

$$E_B = h\nu - KE \qquad (1)$$

where E_B is the binding energy of the electron in the atom (a function of the type of atom and its environment), $h\nu$ is the energy of the X-ray source (a known value) and KE is the kinetic energy of the emitted electron that is measured in the ESCA spectrometer. Thus, E_B, the quantity that provides valuable information about the photoemitting atom is easily obtained from $h\nu$ (known) and KE (measured).

Binding Energy Binding energies are commonly expressed in electron volts (eV; 1 eV = 1.6 x 10^{-19} joules). A negatively charged electron is bound to the atom by the positively charged nucleus. The closer the electron is to the nucleus, the more tightly bound. Binding energy will vary with the type of atom (i.e., a change in nuclear charge) and the addition of other atoms bound to that atom (bound atoms will

alter the electron distribution on the atom of interest). Different isotopes of a given element have different numbers of neutrons in the nucleus, but the same nuclear charge. Changing the isotope will not appreciably affect the binding energy. Weak interactions between atoms such as those associated with crystallization or hydrogen bonding do not alter the electron distribution sufficiently to change the binding energy. Therefore, the variations in the binding energy which provide the chemical information content of ESCA are associated with covalent or ionic bonds between atoms. These changes in binding energy are called "binding energy shifts" or "chemical shifts".

For gases, the binding energy of an electron in a given orbital is identical to the first ionization potential of that electron. In solids, the influence of the surface is present and additional energy must be accounted for removing an electron from the surface. This extra energy is called the work function ϕ_s and the Einstein equation now becomes:

$$E_B = h\nu - KE - \phi_s \qquad (2)$$

In this equation ϕ_s is the difference between the work function of the sample and the work function of the spectrometer. For a conducting sample, the sample can be grounded to the spectrometer and the ϕ_s will be sample independent and equal to the work function of the spectrometer. For an insulating sample, however, ϕ_s will be

sample dependent and an exact calculation of binding energy from the ESCA data is not possible. The contribution to the work function from the sample is typically only a few eV which is small enough that peaks can still be readily assigned. Absolute differences in binding energies for elements can be obtained, even for insulating samples, because ϕ_s is constant across the spectrum.

Binding energies for ESCA spectra of some polymers are commonly determined by shifting the spectra by a constant value based on a predefined binding energy for a reference peak. Some typical peak assignments are listed in Table 1 [16].

Table 1. Common ESCA Peak Assignments

C1s		O1s	
Binding Energy (eV)	Functional group	Binding Energy (eV)	Functional group
285.0	hydrocarbon **C**-H, **C**-C	532.2	carbonyl C=**O**, O-C=**O**
286.0	amine **C**-N	532.8	alcohol, ether C-**O**-H, C-**O**-C
286.5	alcohol, ether **C**-O-H, **C**-O-C	533.7	ester C-**O**-C=O
288.0	carbonyl **C**=O		
288.2	amide N-**C**=O		
289.0	acid, ester O-**C**=O		

Auger Electrons In addition to the photoelectrons emitted in the photoelectric process, Auger electrons are

emitted due to relaxation of the energetic ions left after photoemission. This Auger electron emission occurs roughly 10^{-14} seconds after the photoelectric event. In the Auger process, shown in Figure 3, an outer electron falls into the inner orbital vacancy, and a second electron is emitted,

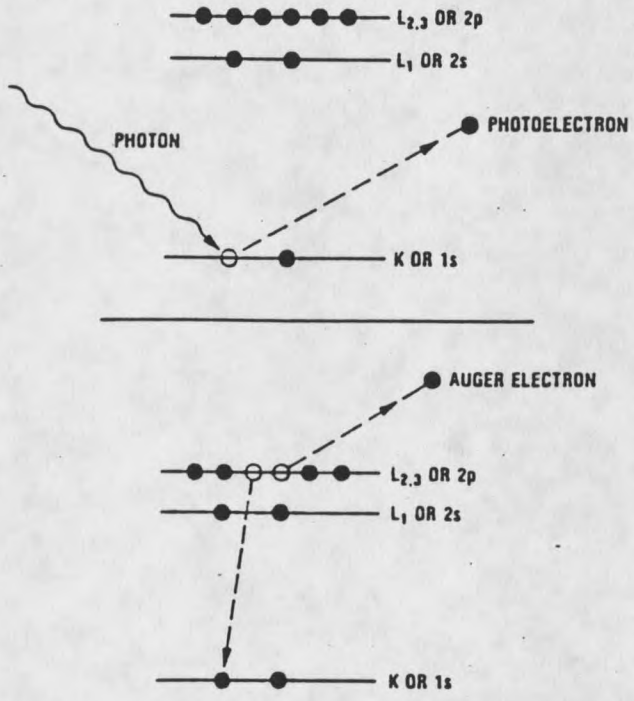

Figure 3. Diagram of the photoelectric process (top) and the Auger process (bottom)

carrying off the excess energy. The Auger electron possesses kinetic energy equal to the difference between the energy of the initial ion and the doubly-charged final ion, and is independent of the mode of the initial ionization. Thus, photoionization normally leads to two emitted electrons, a

photoelectron and an Auger electron. A characteristic of Auger electrons is that their energy is independent of irradiation energy, while photoelectron energy is proportional to irradiation energy, according to Equation 2.

Probabilities of interaction of the electrons with matter far exceed those of the photons, so, while the path length of the photons is of the order of micrometers, that of the electrons is of the order of tens of Angstroms. Thus, while ionization occurs to a depth of a few micrometers, only those electrons that originate within tens of Angstroms below the solid surface can leave the surface without energy loss. It is these electrons which produce the peaks in the spectra and are most useful.

The electrons leaving the sample are detected by an electron spectrometer according to their kinetic energy. The analyzer normally is operated as an energy "window", accepting only those electrons having an energy within the range of this fixed window, referred to as the pass energy. Scanning for different energies is accomplished by applying a variable electrostatic field, before the analyzer is reached. This retardation voltage may be varied from zero up to the photon energy. Electrons are detected as discrete events, and the number of electrons for a given detection time and energy is stored digitally or recorded using analog circuitry.

Candida albicans

Cell Wall

Candidiasis is a common life-threatening fungal disease of immunodepressed patients. The cell wall serves two unique functions in the cell: it maintains cell shape, and it is the point of contact between the cell and its environment. The contribution of the *Candida albicans* cell wall to the pathogenesis of this species has recently received substantial attention [17,18].

Cell wall constituents of *Candida albicans* include mannan, glucan, mannoproteins, chitin, proteins and lipids [17,18]. Although the synthesis of the cell wall components is dynamically influenced by growth conditions and metabolic states, the literature contains fairly consistent data

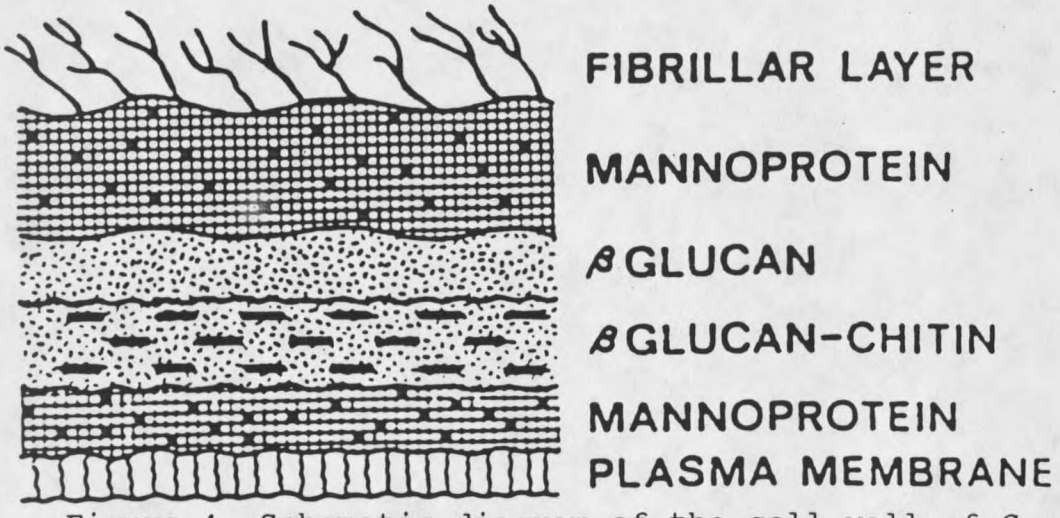

Figure 4. Schematic diagram of the cell wall of *C. albicans* [18].

regarding the chemical composition of the cell wall. Mannans represent about 15.2 to 22.9% of the yeast cell wall (dry

weight), or about 40% of the total cell wall polysaccharide. B-1,3-D-glucans and B-1,6-D-glucans account for 47 to 60% by weight of the cell wall. Proteins have been reported to account for 6 to 25%, lipids for 1 to 7%, and chitin for 0.6% by weight of the cell wall [18]. The spatial relationships of these polymers to each other are presented in Figure 4 [18].

Glucan and mannan have often been found combined with protein in cell wall extracts as glucoproteins, mannoproteins and glucomannoproteins. Of the polysaccharides in the cell wall, the mannan has received the most attention from carbohydrate chemists because of its significance as antigenic determinants in *Candida* species. The mannan polysaccharides are located throughout the cell wall and are predominant in areas of high electron density. Mannans of *C. albicans* have backbones of α-1,6-linked mannose residues with side chains based mainly on α-1,2-linked residues but with a small proportion of α-1,3 bonds [17]. The inner cell wall layers are composed mostly of glucan and chitin. There are three types of B-glucan: a highly branched B-1,6-glucan, a highly branched B-1,3-glucan, and a mixed B-1,3-B-1,6-glucan complexed with chitin. The proportions of certain kinds of glucans are quite different for yeast forms and germ tubes [19].

In this experiment, two purified *C. albicans* cell wall antigens (AgH9 and AgC6) and crude *C. albicans* cell wall antigens were used. Crude antigens were extracted from *C.*

albicans 9938 in heated 1 M NaCl [21]. AgH9 and AgC6 were further isolated by precipitation with specific monoclonal antibodies H9 and C6, and by protease digestion and dialysis [20]. They were also characterized by methods including high-pressure liquid chromatography, gas-liquid chromatography (GLC), and mass spectroscopy [20]. Lipid analysis by thin-layer chromatography of hexane-extracted fatty acids did not detect lipids in either crude or purified antigens. The protein content of crude antigen extract was approximately 30% (dry weight), but no protein was detected in isolated AgH9 or AgC6 after protease treatment. Two significant peaks representing mannose and glucose, with the mannose/glucose ratio 11 : 1, were visible when AgC6 was tested by GLC. Mannose and glucose peaks were also detected from AgH9, as well as an additional unidentified sugar. The mannose/glucose/unidentified sugar ratios in AgH9 were approximately 3 : 1 : 2.5 [20].

Model Compounds

Knowing *C. albicans* cell wall constituents, a study of some model compounds that resemble cell wall constituents may help interpret the SIMS spectra of the cell wall. The following is a list of the model compounds used for this study and their properties.

(1) **Glucose, Mannose, Galactose, Glucuronic Acid, and Methyl α-D-mannopyranoside**

In the free state, D-glucose often accompanies cane sugar

(sucrose) in plants. Sweet fruits are particularly rich in D-glucose. Animal and human organisms contain small amounts of glucose in the blood and in the cerebrospinal fluid. D-glucose takes part in the building up of di- and polysaccharides; maltose, cellobiose, starch, and cellulose are made up completely from glucose.

D-mannose occasionally occurs in the free state in plants, but more often in the form of "mannosides" [22]. Complex polysaccharides containing galactose called galactanes are abundant amongst the reserve carbohydrates in the nutritive tissue of seeds, and in certain kinds of gum [22].

Glucose, mannose and galactose have the same molecular weight (FW=180) and the same chemical formular ($C_6H_{12}O_6$), but their structures are different.

Glucuronic acid, $C_6H_{10}O_7$, has a molecular weight of 194 amu. It belongs to aldehydocarboxylic acids of the sugar series, which occur fairly abundantly in nature. D-glucuronic acid occurs in the animal organism conjugated with phenols or alcohols [23].

The molecular weight of methyl α-D-mannopyranoside, $C_7H_{14}O_6$, is 194 amu.

(2) **Cellobiose, Maltose, Mannan and Glucan.**

Cellobiose and maltose both have a molecular weight of 342 amu, and the chemical formula $C_{12}H_{22}O_{11}$.

Disaccharides are composed of two monosaccharide molecules joined together by a glycosidic linkage. Maltose

and cellobiose both yield only D-glucose on hydrolysis. In maltose the glucose moieties are joined by an α-glucoside linkage; in cellobiose they are joined by a B-glucoside linkage [24].

Mannan is known as the polysaccharide of mannose, which can be hydrolyzed to mannose. Mannan is very abundant in the cell wall.

Glucan is the polysaccharide of glucose.

(3) **Glutamic acid and Bovine serum albumin**

Glutamic acid, $C_5H_9NO_4$, is one of the common amino acids.

Bovine serum albumin is a neutral substance, soluble in water. Table 2 [13] is a summary of the Poly(amino acids) used in albumin SIMS analysis. David S. Mantus and his co-workers from University of Washington have done some SIMS work on homopolymers of amino acids. Table 3, Table 4 and Table 5 show the major positive, negative, respectively, ions in the SIMS spectra of those amino acids [13]. Albumin peak assignments in the results and discussion parts were based on Mantus's work. The polymers have the general structure (-NH-CHR-CO-). Corresponding R groups, abbreviations and the m/z of the R group are listed for each amino acid.

Table 2. Summary of Some Amino Acids [13]

amino acid	abbrev	R	m/z of R
glycine	Gly	$-H$	1
alanine	Ala	$-CH_3$	15
valine	Val	$-CH(CH_3)_2$	43
leucine	Leu	$-CH_2CH(CH_3)_2$	57
serine	Ser	$-CH_2OH$	31
methionine	Met	$-CH_2CH_2SCH_3$	75
glutamic acid	Glu	$-CH_2CH_2COOH$	73
aspartic acid	Asp	$-CH_2COOH$	59
lysine	Lys	$-(CH_2)_4-NH_2$	72
ornithine	Orn	$-(CH_2)_3-NH_2$	58
arginine	Arg	$-(CH_2)_3-NHC(NH_2)NH$	100
proline	Pro		42
phenylalanine	Phe		91
tyrosine	Tyr		107
tryptophan	Trp		130
histidine	His		81

Table 3. Summary of Major Positive Ions in the SIMS Spectra of Homopolymers of 16 Amino Acids [13]

AA	I	$I-H_2$	other
Gly	30(100)	28(8)	
Ala	44(100)	42(12)	
Val	72(100)	70(6)	
Leu	86(100)	84(10)	44(32) 30(33)
Pro	70(100)	68(24)	
Phe	120(43)	118(6)	91(100) 77(36) 58(47) 56(26) 44(35) 42(50) 30(28)
Tyr	136(40)	134(8)	107(100) 91(83) 77(72) 44(36) 30(30)
Trp			130(56) 77(100) 44(62) 30(46)
His	110(91)	108(9)	82(62) 81(100) 44(8) 30(15)
Ser	60(78)	58(24)	44(100) 30(46)
Met	104(18)	102(11)	91(23) 61(100) 56(53) 44(16) 42(17) 30(15)
Lys			84(18) 68(3) 56(24) 44(9) 30(100)
Arg	129(3)	127(4)	128(4) 97(25) 73(32) 70(100) 60(25) 44(48) 30(53)
Orn			70(100) 44(17) 30(95)
Asp	88(80)	86(12)	72(100) 62(69) 44(19) 30(18)
Glu	102(15)		84(64) 56(100) 44(86) 30(69)

* Relative intensities are given in parentheses. Peaks indicative of hydrocarbons, residual solvent, and sodium have been excluded from this summary. I = immonium ion.

Table 4. Summary of Major Negative Ion Peaks in the SIMS Spectra of Homopolymers of the Alkyl Amino Acids [13]

AA	R_1-CRHC(NH)O$^-$			OCN^-	CN^-	other
	R_1=NHCOH	R_1=NH_2	R_1=H			
Gly	101(4)	73(17)	58(8)	42(100)	26(56)	99(26)
Ala	115(6)	87(22)	72(5)	42(100)	26(64)	98(13)
Val	143(4)	115(22)	100(6)	42(100)	26(77)	
Leu	157(16)	129(31)	114(6)	42(100)	26(65)	

* Relative intensities are given in parentheses. Peaks from residual solvent have been excluded from this summary.

Table 5. Summary of Major Negative Ion Peaks in the SIMS Spectra of Homopolymers of Some Amino Acids [13]

AA	OCN^-	CN^-	other
Pro	42(100)	26(98)	165(10) 139(11) 137(7) 68(6) 66(18) 62(13)
Phe	42(61)	26(90)	91(10) 77(100) 76(58) 60(91) 25(24)
Tyr	42(97)	26(83)	134(26) 119(37) 99(18) 60(16) 25(92) 16(100)
Trp	42(95)	26(78)	189(19) 162(20) 144(43) 134(27) 108(100) 80(11)
His	42(30)	26(100)	
Ser	42(100)	26(60)	99(32) 84(16) 59(48) 58(10)
Met	42(100)	26(46)	47(87) 33(22) 32(27)

* Relative intensities are given in parentheses. Peaks from residual solvent and inorganic anions such as Cl^- and HSO_4^- have been excluded from this summary.

EXPERIMENTAL

Sample Preparation

Solution Preparation

Standard Saccharide Nine standard saccharides are listed in Table 2. Glucose was obtained from Difco Laboratories (Detroit, Mich) and the rest from Sigma Chemical Co. (St. Louis, MO.).

Table 6. Summary of Saccharides Used in This Work

	molecular weight	solvent	concentration (g/ml)
D(+)-glucose	180	deionized water	20%
D(+)-mannose	180	deionized water	20%
D(+)-galactose	180	deionized water	20%
D(+)-maltose	342	deionized water	20%
D(+)-cellobiose	342	deionized water	20%
D-glucuronic acid	194	HCl	10%
mannan		deionized water	4%
B-glucan		deionized water	4%
methyl α-D-mannopyranoside	194	deionized water	20%

C. albicans Cell Wall Purified And Crude Antigens *C. albicans* cell wall purified antigens (AgH_9 and AgC_6) [20] and crude antigen [21] were obtained from Dr. Diane Brawner from Microbiology Department at Montana State University. In this experiment, the antigens were dissloved in deionized water, at a concentration of 1% g/ml. A 30 μL volume was deposited on a 9 mm glass coverslip, air dried in a clean hood overnight before SIMS analysis. Four glass coverslips were made, two of which were used for SIMS analysis and two for ESCA analysis.

Glutamic Acid Glutamic acid (from MC&B) was dissolved in deionized water, at a concentration of 20% g/ml.

Bovine Serum Albumin In this experiment, bovine serum albumin (nitrogen content 16.0%, fatty acid content 0.006%, Sigma Chemical Co., St. Louis, MO.) was dissolved at a concentration of 2% (g/ml) in deionized water for bulk film on glass and 1 mg/ml in phosphate-buffered saline (PBS) (ph 7.2) for adsorption on Poly(ethylene terephthalate) (PET).

Spin Casting

A cleaning mixture was made by combining sulfuric acid and nochromix. Nochromix (Godax Laboratories Inc.) mixed with Sulfuric acid is a metal-free substitute for dichromates used for cleaning glass. Glass coverslips, diameter 12mm, (Ted Della Inc.) were put into the mixture for 4 - 5 days. The glass coverslips were cleaned by rinsing with deionized water,

then rinsed in an ultrasonic bath twice for 5 min each time. The glass coverslips were then cleaned with methanol, rinsed in an ultrasonic bath twice for 5 min each time. Finally the glass coverslips were placed on a holder in a clean hood and dried over night.

Films of the solutions in Table 6, glutamic acid solution, and bovine serum albumin deionized water solution were made by centrifugal casting onto 12 mm glass disks. A 20 - 40 μL volume was deposited on a 12 mm glass coverslip and spun at 4000 rpm for 30 s using a Metron Systems, Inc. (Allamuchy, NJ) LS-8000 laboratory spinner. All of these films were visible to the naked eyes and had an estimated thickness of several microns. Four glass coverslips were made for each sample, two of which were used for SIMS analysis and two for ESCA analysis.

Protein Adsorption

A 1 mg/mL bovine serum albumin solution was prepared in phosphate-buffered saline (PBS), PH 7.2. Poly(ethylene terephthalate) (PET) cover slip (22 X 60 mm) (Nunc. Inc) substrates were cut into 10 X 10 mm pieces. They were ultrasonically cleaned in methylene chloride twice, 5 minutes each, followed by acetone twice, for 5 minutes each and methanol twice for 5 minutes. Finally the pieces were ultrasonically cleaned in deionized water twice, each time for 5 minutes. The PET substrates were then placed in 2-mL vials. One mililiter of PBS was added to the vials to completely

cover the PET, and the substrates were allowed to equilibrate at room temperature for 1 hour. One milliliter of albumin solution was added to the vials and mixed once by repipetting. Adsorption was allowed to proceed for 2 hours at room temperature.

Rinsing proceeded via two steps. First, each vial was rinsed with 40 mL of clean PBS, allowing the vial to overflow during rinsing. This process of displacement and dilution ensures that the sample is never exposed to the layer of denatured protein at the air-water interface.

Subsequently, each vial was rinsed with 20 mL of deionized water, using the same dilution-displacement method. The water remaining in each vial was then removed using a clean Pasteur pipet connected to a vacuum aspirator. The samples were dried in an evacuated desiccator overnight before SIMS analysis.

Instrumentation

Static SIMS

SIMS analyses were performed on a PHI model 3700 static SIMS subsystem with a Balzers 511 quadrupole mass analyzer. A 3.5 KeV Xe^+ primary beam of ~ 0.5 nAmp/cm^2 current density was produced from a differentially pumped Leybold-Heraeus ion gun. The ion beam was rastered over an area of 4 x 4 mm during data acquisition. The total accumulated ion dose per sample was kept below 10^{13} ions/cm^2 to insure static SIMS

conditions were met. A PHI neutralization system was used to minimize sample charging.

ESCA

ESCA analyses were performed on a Surface Science Instruments (SSI) X-Probe ESCA instrument. This instrument permits analysis of the outermost 20 - 100 Å of a sample in an elliptical area whose short axis can be adjusted from 150 μm to 1000 μm. An aluminum $K_{\alpha}1,2$ monochromatized X-ray source was used to stimulate photoemission. The energy of the emitted electrons was measured with a hemispherical energy analyzer at pass energies ranging from 25 eV (resolution 1) to 150 eV (resolution 4). Lower pass energies provide higher spectral resolution. Higher pass energies permit more rapid data acquisition. SSI data analysis software was used to calculate the elemental compositions from the peak areas and to peak fit the high resolution spectra. An electron flood gun set at 5 eV was used to minimize surface charging of the samples.

The binding energy (BE) scale was referenced by setting the C-O-H peak in the C_{1s} spectrum to 286.5 eV. Typical pressure in the analysis chamber during spectral acquisition was 10^{-9} torr.

RESULTS AND DISCUSSIONS

Monosaccharides, Saccharide Acid And Pyranoside

In this experiment, glucose, mannose and galactose were used as model compounds of monosaccharides. Glucuronic acid was used as a model compound of saccharide acid. Methyl α-D-mannopyranoside was used as a model compound of pyranoside.

Glucose, Mannose And Galactose

Glucose, mannose and galactose have the same molecular weight (180 amu) and the same chemical formula ($C_6H_{12}O_6$), but the structures differ as shown below:

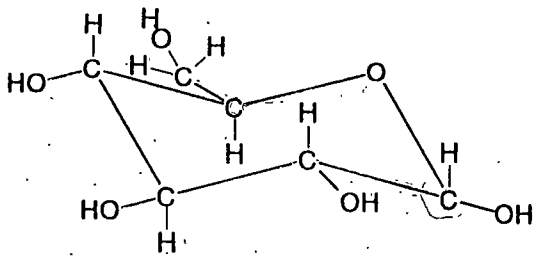

α-D-Glucose

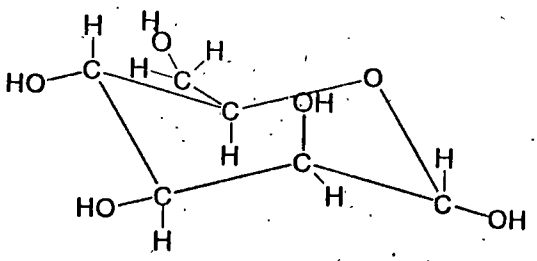

α-D-Mannose

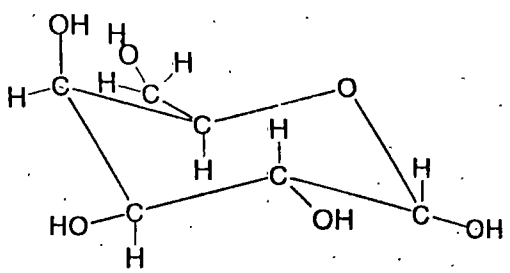

α-D-Galactose

Figure 5. Structures of glucose, mannose and galactose

ESCA Analysis From ESCA analysis (Figure 6), glucose, mannose and galactose look identical.

In glucose, the ESCA data shows a carbon to oxygen ratio of 51.13 : 48.87, for mannose this ratio is 51.78 : 48.22, and for galactose, this ratio is 51.31 : 48.69, see Table 7. That means the ratios of carbon to oxygen in these three compounds are 1 : 1. This is expected from theoretical C/O ratio, since glucose, mannose and galactose have the same chemical formula and they all have six carbons and six oxygens.

Table 7. Atom % in Glucose, Mannose and Galactose

	carbon atom %	oxygen atom %
glucose	51.13	48.87
mannose	51.78	48.22
galactose	51.31	48.69

According to Table 1 [16], **C**-O-H should have a peak at 286.50 eV, but in Figure 7(a) C-H peak appears at 278.71 eV. The reason is due to the fact that the samples used in this experiment are insulating and a charge neutralization beam has to be used to correct for any charging effects (i.e. peak broadening and peak movement). It usually brings the peak to within 7 - 10 eV of the expected values. The binding energy scale was referenced by setting the C-H peak maximum in the C 1s spectrum to 285.0 eV as a correction, and applying that same change (the difference between the raw data C-H and 285.0) to all peaks in the high resolution envelopes for that

particular spot.

However, there was no C-H peak in glucose, mannose and galactose, the binding energy scale was therefore referenced by setting the **C**-O-H peak maximum to 286.5 eV, and applying that same change to all peaks in the high resolution envelopes.

For glucose, if the **C**-O-H peak is set to 286.50 eV instead of 278.71 eV, the difference is 7.79 eV, there is another carbon peak at 288.11 eV instead of 280.32 eV, which should be a O-**C**-O peak according to Table 1 [16]. In glucose, there are two kinds of carbon bonds, **C**-O-H and O-**C**-O, see Figure 7(a). There is one oxygen peak at 532.87 eV, see Figure 8(a), instead of 525.08 eV, which should be C-**O**-H binding energy.

The same procedure of correction is applied to mannose, galactose and other samples used in this experiment. For mannose, the difference is 7.93 eV between raw data (Figure 7(b)) and 286.50 eV, yielding a second carbon peak at 288.29 eV, assigned to O-**C**-O. And the oxygen peak is at 532.87 eV, see Figure 8(b), assigned to C-**O**-H. For galactose, the difference is 8.15 eV between raw data (Figure 7(c)) and 286.50 eV, so another carbon peak is at 288.07 eV, assigned to O-**C**-O. The oxygen peak is at 532.88 eV, see Figure 8(c), assigned to C-**O**-H [16].

Table 8 summarizes carbon and oxygen peaks assignments of glucose, mannose and galactose.

Table 8. Carbon and Oxygen Peak Assignments of Glucose, Mannose and Galactose

	raw data (eV)	charge corrected data (eV)	functional group assignment
glucose	278.71	286.50	**C**-O-H
	280.32	288.11	O-**C**-O
	525.08	532.87	C-**O**-H
mannose	278.57	286.50	**C**-O-H
	280.36	288.29	O-**C**-O
	524.94	532.87	C-**O**-H
galactose	278.35	286.50	**C**-O-H
	279.92	288.07	O-**C**-O
	524.73	532.88	C-**O**-H

SIMS Analysis The ESCA spectra of glucose, mannose and galactose are identical. However, differences are seen in the SIMS spectra.

In the positive ion spectra, the most prominent ions from glucose were at m/z = 57, 61, 69, 71, 73, 85, 87, 97, 127, 145 and 163 (Figure 9). For peak assignments see Table 9. The most prominent mannose ions were at m/z = 55, 57, 69, 71, 73, 85, 91 and 97 with a diminishment of ions at m/z = 61, 71, 73, 85, 97, 127, 145 and an absence at m/z = 163, see Figure 10. The mannose spectrum showed an enhancement of ion intensity at m/z = 55. In the positive ion spectrum of galactose (Figure 11), the most prominent ions were at m/z = 55, 57, 61, 69, 73, 85, 91 and 97. Compared to glucose, the ion at m/z = 163 was

absent and the ion at m/z = 55 was enhanced, while ions at m/z = 85, 127 and 145 were diminished. In this study, all the peaks at m/z = 15, 19 and 23 in the positive ion spectra are CH_3^+, H_3O^+ and Na^+, respectively.

Table 9. Summary of Major Positive Ion Peaks in the SIMS Spectra of Glucose, Mannose and Galactose

m/z	Glucose	mannose	galactose	
27				$C_2H_3^+$
29				COH^+
31				$HOCH_2^+$
39				$C_3H_3^+$
41				C_2OH^+
43				$C_2OH_3^+$
45				$C_2OH_5^+$
53				C_3OH^+
55				$C_3OH_3^+$
57				$C_2O_2H^+$
61				$C_2O_2H_5^+$
65	-			C_4OH^+
67				$C_4OH_3^+$
69				$C_3O_2H^+$
71				$C_3O_2H_3^+$
73				$C_3O_2H_5^+$
77	-			C_5OH^+
79	-			$C_5OH_3^+$
81				$C_4O_2H^+$
83				$C_4O_2H_3^+$
85				$C_4O_2H_5^+$

Table 9 (cont'd). Summary of Major Positive Ion Peaks in the SIMS Spectra of Glucose, Mannose and Galactose

m/z	Glucose	mannose	galactose	
87				$C_3O_3H_3^+$
89		-		$C_3O_3H_5^+$
91				$C_3O_3H_7^+$
97				$C_5O_2H_5^+$
99		-		$C_4O_3H_3^+$
101				$C_4O_3H_5^+$
103				$C_4O_3H_7^+$
105	-			$C_4O_3H_9^+$
109				$C_6O_2H_5^+$
111				$C_5O_3H_3^+$
113				$C_5O_3H_5^+$
115				$C_5O_3H_7^+$
125		-	-	$C_6O_3H_5^+$
127				$C_6O_3H_7^+$
133				$C_5O_4H_9^+$
145				$C_6O_4H_9^+$
163				$C_6O_5H_{11}^+$

"-" means absence or low intensity

In the negative ion spectrum, the most prominent peaks of glucose were at m/z = 59, 71, 87, 89, 101, 117, 119, 161 and 179 (Figure 12). Peak assignments are shown in Table 10. In the negative spectrum of mannose (Figure 13), ions at m/z = 119, 179 were much diminished in intensity, and an ion at m/z = 117 was absent. The ions at m/z = 99, 113 were enhanced. Comparing this to the negative ion spectrum of glucose, many

peaks above m/z = 131 in the negative ion spectrum of galactose were unable to be detected (Figure 14). Ions at m/z = 117, 119, 179 were much diminished in intensity and the ion at m/z = 161 was absent. The ions at m/z = 73, 97, 99, 113 were enhanced. [1] In this study, all peaks at m/z = 13, 16 and 17 in the negative ion spectra are CH^-, O^- and OH^-, respectively.

Table 10. Summary of Major Negative Ion Peaks in the SIMS Spectra of Glucose, Mannose and Galactose

m/z	glucose	mannose	galactose	
25				C_2H^-
29		-		CHO^-
31		-	-	$HOCH_2^-$
41				C_2OH^-
43				$C_2OH_3^-$
45				$C_2OH_5^-$
53				C_3OH^-
55				$C_3OH_3^-$
57				$C_2O_2H^-$
58				$C_2O_2H_2^-$
59				$C_2O_2H_3^-$
67			-	$C_4OH_3^-$
69				$C_3O_2H^-$
71				$C_3O_2H_3^-$
73				$C_3O_2H_5^-$
83				$C_4O_2H_3^-$
85				$C_4O_2H_5^-$

Table 10 (cont'd). Summary of Major Negative Ion Peaks in the SIMS Spectra of Glucose, Mannose and Galactose

m/z	glucose	mannose	galactose	
87				$C_3O_3H_3^-$
89				$C_3O_3H_5^-$
95			–	$C_5O_2H_3^-$
97				$C_5O_2H_5^-$
99				$C_4O_3H_3^-$
101				$C_4O_3H_5^-$
103		–		$C_4O_3H_7^-$
107		–	–	$C_6O_2H_3^-$
111				$C_5O_3H_3^-$
113				$C_5O_3H_5^-$
115				$C_5O_3H_7^-$
117		–		$C_4O_4H_5^-$
119				$C_4O_4H_7^-$
125				$C_6O_3H_5^-$
127				$C_5O_4H_3^-$
129				$C_5O_4H_5^-$
131		–		$C_5O_4H_7^-$
141				$C_6O_4H_5^-$
143				$C_6O_4H_7^-$
149		–	–	$C_5O_5H_9^-$
159				$C_6O_5H_7^-$
161				$C_6O_5H_9^-$
177		–		$C_6O_6H_9^-$
179				$C_6O_6H_{11}^-$

Glucuronic Acid

Glucuronic acid, $C_6H_{10}O_7$, has a molecular weight of 194 amu. The structure of glucuronic acid is shown below:

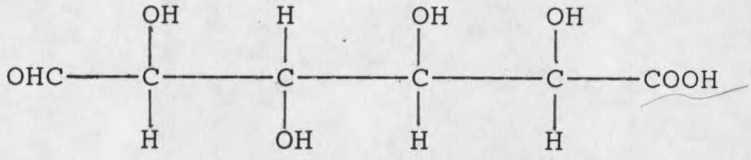

ESCA Analysis The ratio of carbon to oxygen found by ESCA analysis is 44.90 : 45.73, approximately 1 : 1, and the ratio of carbon to oxygen in its chemical formula is 6 : 7. Sodium was found during analysis (atom % 9.37) (Figure 15), and may be present because of sample contamination or from the glass substrate.

There were three peaks on carbon high resolution peak spectrum (Figure 16), but two on oxygen high resolution peak spectrum of glucuronic acid (Figure 17). The peak assignments are shown in Table 11.

Table 11. Carbon and Oxygen Peak Assignments of Glucuronic Acid

	raw data (eV)	charge corrected data (eV)	functional group assignment
carbon peak	277.30	285.00	**C**-H, C-C
	278.74	286.44	**C**-O-H
	280.44	288.14	**C**=O
oxygen peak	523.44	531.14	C=**O**
	525.00	532.70	C-**O**-H

SIMS Analysis In the positive ion spectrum of glucuronic acid (Figure 18), some prominent peaks were at m/z = 53, 55, 57, 63, 67, 69, 71, 73, 91, 105, 119, 127 and 133. Peak assignments are given in Table 12.

Table 12. Summary of Major Positive Ion Peaks in the SIMS Spectrum of Glucuronic Acid

m/z		m/z	
45	$COOH^+$	83	$C_4O_2H_3^+$
53	C_3OH^+	85	$C_4O_2H_5^+$
55	$C_3OH_3^+$	87	$C_3O_3H_3^+$
57	$C_2O_2H^+$	91	$C_3O_3H_7^+$
59	$C_2O_2H_3^+$	95	$C_5O_2H_3^+$
63	$C_2O_2H_7^+$	103	$C_4O_3H_7^+$
65	C_4OH^+	105	$C_6O_2H^+$
67	$C_4OH_3^+$	119	$C_4O_4H_7^+$
69	$C_3O_2H^+$	127	$C_6O_3H_7^+$ or $C_5O_4H_3^+$
71	$C_3O_2H_3^+$	133	$C_5O_4H_9^+$ or $C_4O_5H_5^+$
73	$C_2O_3H^+$	155	$C_6O_5H_3^+$
77	$C_2O_3H_5^+$	165	$C_5O_6H_9^+$
79	$C_5OH_3^+$		

There is less information from negative ion spectrum (Figure 19) than from positive ion spectrum. Few peaks were detected above m/z = 100. Some prominent peaks were at m/z = 59, 71, 75, 103 and 133. Peak assignments are listed in Table 13.

Table 13. Summary of Major Negative Ion Peaks in the SIMS Spectrum of Glucuronic Acid

m/z		m/z	
59	$C_2O_2H_3^-$	89	$C_3O_3H_5^-$
69	$C_3O_2H^-$	103	$C_4O_3H_7^-$
71	$C_3O_2H_3^-$	113	$C_4O_4H^-$ or $C_5O_3H_5^-$
73	$C_2O_3H^-$	127	$C_5O_4H_3^-$
75	$C_2O_3H_3^-$	133	$C_5O_4H_9^-$ or $C_4O_5H_5^-$
87	$C_3O_3H_3^-$		

Methyl α-D-Mannopyranoside

The molecular weight of methyl α-D-mannopyranoside, $C_7H_{14}O_6$, is 194 amu. The structure is shown below:

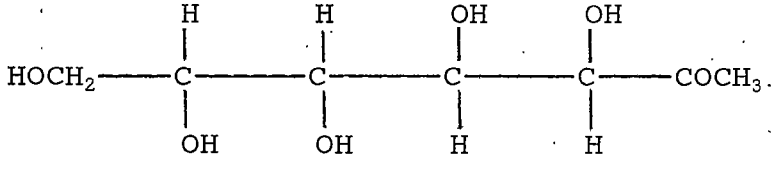

ESCA Analysis A good methyl α-D-mannopyranoside ESCA spectrum was not obtained since the methyl α-D-mannopyranoside solution did not fully cover the glass substrate when it was spin cast.

SIMS Analysis In the positive ion spectrum of methyl α-D-mannopyranoside (Figure 20), the strong peaks above m/z = 50 were m/z = 53, 57, 59, 61, 69, 71, 73, 85 and 87. Above m/z = 100, the intensity of the peaks was too weak. Peak assignments are given in Table 14.

Table 14. Summary of Major Positive Ion Peaks in the SIMS Spectrum of Methyl α-D-Mannopyranoside

m/z		m/z	
45	$C_2OH_5^+$ or $COOH^+$	69	$C_4OH_5^+$ or $C_3O_2H^+$
53	C_3OH^+	71	$C_3O_2H_3^+$
55	$C_3OH_3^+$	73	$C_3O_2H_5^+$
57	$C_2O_2H^+$	75	$C_3O_2H_7^+$
59	$C_2O_2H_3^+$	79	$C_5OH_3^+$
61	$C_2O_2H_5^+$	81	$C_4O_2H^+$
63	$C_2O_2H_7^+$	85	$C_4O_2H_5^+$
67	$C_4OH_3^+$	87	$C_3O_3H_3^+$
		99	$C_4O_3H_3^+$

In the negative ion spectrum, see Figure 21, the most prominent ions above m/z = 50 were m/z = 55, 59, 60, 61, 69, 71, 73, 76, 77, 87, 97 and 99. Above m/z = 100, high peaks were observed at m/z = 101, 111, 113, 119, 137 and 193. Peak assignments are listed in Table 15.

Table 15. Summary of Major Negative Ion Peaks in the SIMS Spectrum of Methyl α-D-Mannopyranoside

m/z		m/z	
55	$C_3OH_3^-$	87	$C_3O_3H_3^-$
57	$C_2O_2H^-$	89	$C_3O_3H_5^-$
59	$C_2O_2H_3^-$	97	$C_5O_2H_5^-$
61	$C_2O_2H_5^-$	99	$C_4O_3H_3^-$
69	C_3OH^-	101	$C_4O_3H_5^-$
71	$C_3O_2H_3^-$	137	$C_7O_3H_7^-$
73	$C_3O_2H_5^-$	193	$(M-H)^-$
77	C_5OH^-		

Discussions

Positive ion spectra of glucose, mannose and galactose were different though they were stereoisomers. There was a common pattern for mannose and galactose. They both had high intensity peaks in the low mass region, but had no strong and distinctive peaks at higher mass value ($m/z > 100$). For glucose, the highest intensity peaks were between $m/z = 50$ and $m/z = 100$. The positive ion spectrum of glucose exhibited single, strong peaks above $m/z = 100$, such as $m/z = 109$, 127, 145, 163 and 181. The peak at $m/z = 181$ was $(M+H)^+$, ion at $m/z = 163$ was due to the loss of a neutral H_2O from $(M+H)^+$. Peaks at $m/z = 145$, 127, and 109 were due to the loss of two H_2O, three H_2O and four H_2O, respectively, from $(M+H)^+$. In these ions, the pyranose ring of glucose did not break up. They were due to the loss of -H and -OH from the side chains. Mannose and galactose also had peaks at $m/z = 109$, 127, 145 and 163, but they were very weak.

In negative ion spectra, mannose and galactose still had similar patterns, which differed from the pattern of glucose. Glucose had some stronger peaks over $m/z = 100$ than mannose and galactose, such as peaks at $m/z = 129$, 143, 161 and 179. $(M-H)^-$ peaks were observable at $m/z = 179$ in all negative ion spectra with a higher intensity in glucose spectrum. The peaks at $m/z = 161$ were due to the loss of a neutral H_2O from $(M-H)^-$. The peaks at $m/z = 143$ were due to the loss of two H_2O from $(M-H)^-$.

Obviously, the pyranose ring of glucose is more stable than pyranose rings of mannose and galactose from SIMS analysis. From organic chemistry, if -H and -OH in a pyranose are both vertical to the same plane, they repel each other. This causes the ring to be less stable. In glucose, mannose and galactose, see Figure 5, mannose has a -H and a -OH both vertical to the same plane, so does galactose. The distribution of heavy functioned groups is also related to the stability of the pyranose ring. In glucose, the $-CH_2OH$ and all the -OH are equatorial bonded to C, while in mannose and galactose, a -OH is not equatorial bonded. This also causes the glucose pyranose ring to be more stable than mannose and galactose pyranose rings. The SIMS analysis showed this.

From the spectra, ions diagnostic of glucuronic acid were identified. Ions at m/z = 75 and 105 were assigned to structures uniquely diagnostic of glucuronic acid, -CH(OH)COOH and -CH(OH)CH(OH)COOH. Molecular ions were not found in either the positive ion or the negative ion spectrum. In the positive ion spectrum and the negative ion spectrum, ions diagnostic of methyl α-D-mannopyranoside were noted at m/z = 43 and 73. They were assigned to structures unique to methyl α-D-mannopyranoside, $-COCH_3$ and $-CH(OH)COCH_3$. $(M-H)^-$ peak is observed as a weak peak at m/z = 193 in the negative ion spectrum.

Disaccharides And Polysaccharides

In this experiment, cellobiose and maltose were used as model compounds of disaccharides. Mannan and glucan were used as model compounds of polysaccharides.

Cellobiose And Maltose

Cellobiose and maltose have the same molecular weight, 342 amu, and the same chemical formula, $C_{12}H_{22}O_{11}$. Their structures are different, as shown below.

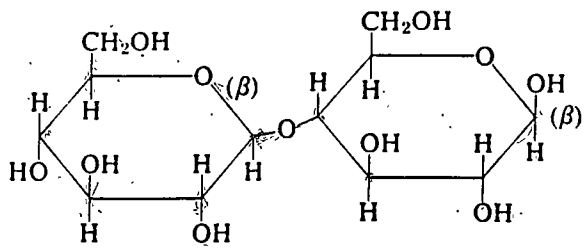

Cellobiose (β-isomer)

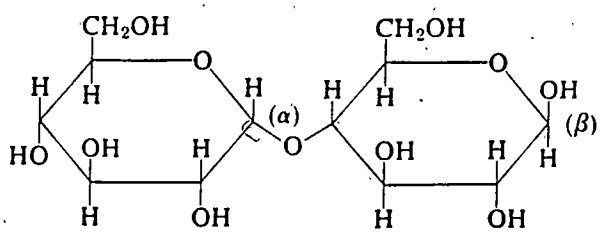

Maltose (β-isomer)

ESCA Analysis ESCA spectra (Figure 22) of maltose and cellobiose look similar. The ratio of carbon atoms to oxygen atoms in maltose is 53.90 : 46.10 and in cellobiose is 53.71 : 46.29. It is quite close to the ratio of carbon to oxygen in their chemical formulas, 12 : 11.

Two carbon peaks appeared on both cellobiose and maltose

carbon high resolution peak spectrum (Figure 23), while one peak showed in both oxygen high resolution peak spectrum (Figure 24). Their peak assignments are shown in Table 16.

Table 16. Carbon and Oxygen Peak Assignments of Cellobiose and Maltose

	raw data (eV)	charge corrected data (eV)	functional group assignment
maltose	278.72	286.50	**C**-O-H
	280.48	288.26	O-**C**-O
	525.10	532.88	C-**O**-H
cellobiose	278.32	286.50	**C**-O-H
	279.88	288.06	O-**C**-O
	524.71	532.89	C-**O**-H

SIMS Analysis In the positive ion spectrum, cellobiose has some strong peaks at m/z = 53, 55, 57, 61, 69, 71, 73, 81, 85, 87, 97, 109, 127, 145 and 163 (Figure 25). For maltose, the most prominent ions were at m/z = 55, 57, 71 and 73 (Figure 26). Above m/z = 100, few high intensity peaks were detected. Peak assignments are listed in Table 17.

Table 17. Summary of Major Positive Ion Peaks in the SIMS Spectra of Cellobiose and Maltose

m/z	Cellobiose	Maltose	
53			C_3OH^+
55			$C_3OH_3^+$
57			$C_3OH_5^+$ or $C_2O_2H^+$
59		-	$C_3OH_7^+$ or $C_2O_2H_3^+$

Table 17 (cont'd). Summary of Major Positive Ion Peaks in the SIMS Spectra of Cellobiose and Maltose

m/z	Cellobiose	Maltose	
61		-	$C_3OH_9^+$ or $C_2O_2H_5^+$
67			$C_4OH_3^+$
69			$C_4OH_5^+$ or $C_3O_2H^+$
71			$C_4OH_7^+$ or $C_3O_2H_3^+$
73			$C_4OH_9^+$ or $C_3O_2H_5^+$
81			$C_4O_2H^+$ or $C_5OH_5^+$
83			$C_4O_2H_3^+$ or $C_5OH_7^+$
85			$C_4O_2H_5^+$ $C_5OH_9^+$ or $C_3O_3H^+$
87			$C_4O_2H_7^+$ or $C_3O_3H_3^+$
89		-	$C_4O_2H_9^+$ $C_3O_3H_5^+$ or C_6OH^+
91		-	$C_4O_2H_{11}^+$ $C_3O_3H_7^+$ or $C_6OH_3^+$
97		-	$C_5O_2H_5^+$ or $C_4O_3H^+$
99		-	$C_5O_2H_7^+$ or $C_4O_3H_3^+$
101			$C_5O_2H_9^+$ or $C_4O_3H_5^+$
103		-	$C_5O_2H_{11}^+$ or $C_4O_3H_7^+$
109		-	$C_6O_2H_5^+$ or $C_5O_3H^+$
111		-	$C_6O_2H_7^+$ or $C_5O_3H_3^+$
113		-	$C_6O_2H_9^+$ $C_5O_3H_5^+$ or $C_4O_4H^+$
115		-	$C_6O_2H_{11}^+$ $C_5O_3H_7^+$ or $C_4O_4H_3^+$
127			$C_6O_3H_7^+$ or $C_5O_4H_3^+$
145		-	$C_6O_4H_7^+$ or $C_5O_5H_3^+$
163		-	$C_6O_5H_{11}^+$

In the negative ion spectrum, the most prominent peaks above m/z = 50 in cellobiose were m/z = 59, 71, 87, 101, 113, 119, 161 and 179 (Figure 27). Table 18 lists the ions

corresponding to each m/z ratio. The ion at m/z = 221 may be ($M-H+SiO_2-H_2O$). In the maltose negative ion spectrum, Figure 28, the intensity of the prominent peaks in cellobiose was diminished. Over m/z = 100, cellobiose had some weak peaks but they were absent in maltose.

Table 18. Summary of Major Negative Ion Peaks in the SIMS Spectra of Cellobiose and Maltose

m/z	Cellobiose	Maltose	
53			C_3OH^-
55			$C_3OH_3^-$
57			$C_3OH_5^-$ or $C_2O_2H^-$
59			$C_3OH_7^-$ or $C_2O_2H_3^-$
69			$C_4OH_5^-$ or $C_3O_2H^-$
71			$C_4OH_7^-$ or $C_3O_2H_3^-$
73		-	$C_4OH_9^-$ or $C_3O_2H_5^-$
75		-	$C_3O_2H_7^-$
83		-	$C_4O_2H_3^-$ or $C_5OH_7^-$
85		-	$C_4O_2H_5^-$ $C_5OH_9^-$ or $C_3O_3H^-$
87			$C_4O_2H_7^-$ or $C_3O_3H_3^-$
89			$C_4O_2H_9^-$ C_6OH^- or $C_3O_3H_5^-$
97		-	$C_5O_2H_5^-$ or $C_4O_3H^-$
99		-	$C_5O_2H_7^-$ or $C_4O_3H_3^-$
101		-	$C_5O_2H_9^-$ or $C_4O_3H_5^-$
111		-	$C_6O_2H_7^-$ or $C_5O_3H_3^-$
113		-	$C_6O_2H_9^-$ $C_5O_3H_5^-$ or $C_4O_4H^-$
115		-	$C_6O_2H_{11}^-$ $C_5O_3H_7^-$ or $C_4O_4H_3^-$
117		-	$C_5O_3H_9^-$ or $C_4O_4H_5^-$
119		-	$C_5O_3H_{11}^-$ or $C_4O_4H_7^-$

Table 18 (cont'd). Summary of Major Negative Ion Peaks in the SIMS Spectra of Cellobiose and Maltose

m/z	Cellobiose	Maltose	
125		-	$C_6O_3H_5^-$ or $C_5O_4H^-$
127		-	$C_6O_3H_7^-$ or $C_5O_4H_3^-$
129		-	$C_6O_3H_9^-$ or $C_5O_4H_5^-$
131		-	$C_6O_3H_{11}^-$ or $C_5O_4H_7^-$
141		-	$C_6O_4H_5^-$ or $C_5O_5H^-$
143		-	$C_6O_4H_7^-$ or $C_5O_5H_3^-$
159		-	$C_6O_5H_7^-$
161		-	$C_6O_5H_9^-$
179		-	$C_6O_6H_{11}^-$

Mannan And Glucan

ESCA Analysis ESCA spectra of mannan and glucan are shown in Figure 29. The atom percentages in mannan and glucan are shown below in Table 19.

Table 19. Atom % in Mannan and Glucan

	carbon %	oxygen %	nitrogen %
mannan	56.62	41.60	1.77
glucan	56.56	43.44	none

A small amount of nitrogen was found in mannan (Figure 29(a)), probably coming from protein contamination in the mannan sample. Three peaks were shown on the carbon high resolution spectra of both mannan (Figure 30(a)) and glucan (Figure 30(b)). However, two peaks were on the oxygen high

resolution spectrum of mannan (Figure 31(a)) , one peak was on the oxygen high resolution spectrum of glucan (Figure 31(b)). The small peak seen on mannan oxygen high resolution spectrum may be from protein contamination. Peak assignments are listed in Table 20.

Table 20. Carbon and Oxygen Peak Assignment of Mannan and Glucan

	raw data (eV)	charge corrected data (eV)	functional group assignment
mannan	276.97	285.00	**C**-H, C-C
	278.78	286.81	**C**-O-H
	280.58	288.61	O-**C**-O
	525.15	533.18	C-**O**-H
glucan	277.17	285.00	**C**-H, C-C
	278.78	286.61	**C**-O-H
	280.34	288.17	O-**C**-O
	525.16	532.99	C-**O**-H

SIMS Analysis The mannan positive ion spectrum (Figure 32) did not have as many high mass (m/z > 100) peaks as in its negative ion spectrum (Figure 34). The main peaks above m/z = 50 were m/z = 55, 57, 69, 73, 81, 83, 85, 97, 99, 109 and 127. The same pattern was followed by the glucan positive ion spectrum, Figure 33, with its prominent peaks above m/z = 50 at m/z=53, 55, 57, 69, 71, 73, 81, 85 and 97. Above m/z = 100, there were some low intensity peaks at m/z = 101, 103, 105, 107, 109, 111, 113, 115, 125, 127, 129 and 145. Peak

assignments are listed in Table 21.

Table 21. Summary of Major Positive Ion Peaks in the SIMS Spectra of Mannan, Glucan, Mannose and Glucose

m/z	Mannan	Glucan	Mannose	Glucose	
53					C_3OH^+
55					$C_3OH_3^+$
57					$C_2O_2H^+$
59					$C_2O_2H_3^+$
61					$C_2O_2H_5^+$
65				-	C_4OH^+
67					$C_4OH_3^+$
69					$C_3O_2H^+$
71					$C_3O_2H_3^+$
73					$C_3O_2H_5^+$
77				-	C_5OH^+
79				-	$C_5OH_3^+$
81					$C_4O_2H^+$
83					$C_4O_2H_3^+$
85					$C_4O_2H_5^+$
87					$C_3O_3H_3^+$
89	-		-		$C_3O_3H_5^+$
91					$C_3O_3H_7^+$
95	-		-	-	$C_5O_2H_3^+$
97					$C_5O_2H_5^+$ or $C_4O_3H^+$
99			-		$C_5O_2H_7^+$ or $C_4O_3H_3^+$
101					$C_4O_3H_5^+$ or $C_5O_2H_9^+$
103					$C_4O_3H_7^+$ or $C_5O_2H_{11}^+$
109			-		$C_6O_2H_5^+$ or $C_5O_3H^+$
111			-		$C_5O_3H_3^+$

Table 21 (cont'd). Summary of Major Positive Ion Peaks in the SIMS Spectra of Mannan, Glucan, Mannose and Glucose

m/z	Mannan	Glucan	Mannose	Glucose	
113			-		$C_5O_3H_5^+$
115	-				$C_5O_3H_7^+$
125	-		-		$C_6O_3H_5^+$ or $C_5O_4H^+$
127					$C_6O_3H_7^+$ or $C_5O_4H_3^+$
133	-	-	-		$C_5O_4H_9^+$
145	-				$C_6O_4H_9^+$ or $C_5O_5H_5^+$

In the mannan negative ion spectrum (Figure 34), the most prominent ions above m/z = 50 were at m/z = 59, 71, 79, 87, 97, 99, 101, 111, 113, 125, 139 and 161. More peaks were introduced above m/z = 100, like m/z = 109, 115, 119, 123, 127, 129, 137, 141, 143, 151, 153, 155, 159, 165, 167, 177, 179, 181 and 221. Peak assignments are given in Table 22. In the glucan negative ion spectrum (Figure 35), some high peaks above m/z = 50 were at m/z = 59, 69, 71, 73, 85, 87, 97, 99, 101, 111, 113, 119, 125, 127, 129, 141, 161, 179 and 221. See Table 22 for peak assignments.

Table 22. Summary of Major Negative Ion Peaks in the SIMS Spectra of Mannan, Glucan, Mannose and Glucose

m/z	Mannan	Glucan	Mannose	Glucose	
53					C_3OH^-
55					$C_3OH_3^-$
57					$C_2O_2H^-$
59					$C_2O_2H_3^-$
63		-	-	-	$C_2O_2H_7^-$

Table 22 (cont'd). Summary of Major Negative Ion Peaks in the SIMS Spectra of Mannan, Glucan, Mannose and Glucose

m/z	Mannan	Glucan	Mannose	Glucose	
67				-	$C_4OH_3^-$
69					$C_3O_2H^-$
71					$C_3O_2H_3^-$
73					$C_3O_2H_5^-$
79		-	-	-	$C_5OH_3^-$
81		-	-	-	$C_4O_2H^-$
83					$C_4O_2H_3^-$
85					$C_4O_2H_5^-$
87					$C_3O_3H_3^-$
89					$C_3O_3H_5^-$
95		-			$C_5O_2H_3^-$
97					$C_5O_2H_5^-$
99					$C_4O_3H_3^-$
101					$C_4O_3H_5^-$
103			-		$C_4O_3H_7^-$
109			-	-	$C_5O_3H^-$
111					$C_5O_3H_3^-$
113					$C_5O_3H_5^-$
115					$C_5O_3H_7^-$
117			-		$C_4O_4H_5^-$
119					$C_4O_4H_7^-$
121		-	-	-	$C_6O_3H^-$
123			-	-	$C_6O_3H_3^-$
125					$C_6O_3H_5^-$
127					$C_5O_4H_3^-$
129					$C_5O_4H_5^-$
131			-		$C_5O_4H_7^-$

Table 22 (cont'd). Summary of Major Negative Ion Peaks in the SIMS Spectra of Mannan, Glucan, Mannose and Glucose

m/z	Mannan	Glucan	Mannose	Glucose	
137		-	-	-	$C_6O_4H^-$
139			-	-	$C_6O_4H_3^-$
141					$C_6O_4H_5^-$
143					$C_6O_4H_7^-$
145		-	-	-	$C_6O_4H_9^-$
149		-	-		$C_5O_5H_9^-$
153			-	-	$C_6O_5H^-$
155		-	-	-	$C_6O_5H_3^-$
159					$C_6O_5H_7^-$
161					$C_6O_5H_9^-$
177		-	-		$C_6O_6H_9^-$
179					$C_6O_6H_{11}^-$
181		-	-	-	$C_6O_6H_{13}^-$

Discussions

For both the positive ion and negative ion spectra, cellobiose had more informative than maltose. Apparently, cellobiose had more fragments than maltose among any mass region. Peaks at m/z = 109, 127 and 145 in the positive ion spectrum of cellobiose, and m/z = 101, 143 and 161 in the negative ion spectrum of cellobiose were pyranose rings with losing some H_2O on side chains.

The glucan and mannan positive ion spectra showed more high mass fragments than their monomer glucose (Figure 9) and mannose (Figure 10), see Table 21. As shown in Figure 34 and Figure 35, there were more high mass (m/z > 100) fragments in

the negative ion spectra of mannan and glucan than in the negative ion spectra of mannose and glucose (Figure 12 and Figure 13). This was expected since mannan and glucan are polymers of mannose and glucose. Spectra of mannan and glucan exhibited no strong and distinctive peaks above m/z = 150.

The differences in SIMS spectra of stereoisomers, such as glucose, mannose and galactose, cellobiose and maltose, mannan and glucan, may be caused by several reasons: the difference in the stability of the pyranose ring, the difference in how easily the ions can eliminate side chains, the difference in ability of ions to delocalize charge, the difference in crystalline structure of saccharides, and the way saccharide molecules orient on the surface of the glass substrate [26].

Protein

Bovine serum albumin was used in this experiment as a model protein. ESCA and SIMS analyses were applied to bulk film of bovine serum albumin and bovine serum albumin adsorbed to PET. The adsorbed protein was investigated to explore the usefulness of static SIMS to provide fundamental information from such system. Glutamic acid was also used in this experiment, to help interpret protein spectra.

Glutamic Acid

Glutamic acid, $C_5H_9NO_4$. The structure is shown below:

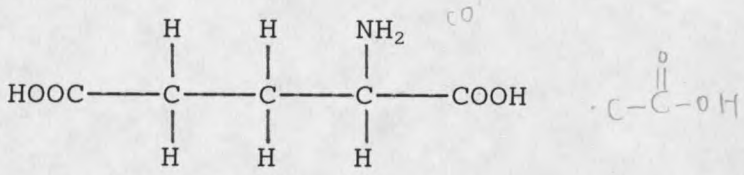

ESCA Analysis Figure 36 shows ESCA spectrum of glutamic acid. A ratio of C : N : O = 51.47 : 10.10 : 38.43 in ESCA analysis, approximates 5.1 : 1 : 3.8, which is very close to what appears in its chemical formula, which is 5 : 1 : 4.

Three peaks appeared on the carbon high resolution spectrum (Figure 37), and two peaks appeared on oxygen high resolution spectrum (Figure 38). The peak assignments are shown in Table 23.

Table 23. Carbon and Oxygen Peak Assignments of Glutamic Acid

	raw data (eV)	charge corrected data (eV)	function group assignment
carbon peak	276.82	285.00	**C**-H, C-C
	278.05	286.23	**C**-N
	280.39	288.57	O-**C**=O
oxygen peak	523.39	531.57	O-C=**O**
	525.01	533.19	**O**-C=O

SIMS Analysis In the positive ion spectrum, some nitrogen-containing species were introduced at m/z = 28, 42, 44, 46, 54, 56, 58, 70, 72, 74, 82, 84, 86, 102, 114, 130 and 148 (Figure 39). Other prominent peaks were at m/z = 55, 69, 75, 79, 85, 95 and 97. The peak assignments are shown in

Table 24.

Table 24. Summary of Major Positive Ion Peaks in the SIMS Spectrum of Glutamic Acid

m/z		m/z	
17	NH_3^+	69	$C_3O_2H^+$
27	$C_2H_3^+$	70	$C_2O_2N^+$ or $C_3O_2H_2^+$
28	$C_2H_4^+$ or NCH_2^+ CO^+	71	$C_3O_2H_3^+$
29	COH^+	72	$C_2O_2H_2N^+$ or $C_3O_2H_4^+$
39	$C_3H_3^+$	74	$C_2O_2H_4N^+$
41	C_2OH^+	82	$C_3O_2N^+$ or $C_4O_2H_2^+$
42	$C_2NH_4^+$ or $C_2OH_2^+$	83	$C_4O_2H_3^+$
43	$C_2OH_3^+$	84	$C_3O_2H_2N^+$
44	$C_2H_4-NH_2^+$	85	$C_4O_2H_5^+$
45	$COOH^+$	86	$C_3O_2H_4N^+$
46	$COH_2-NH_2^+$	87	$C_4O_2H_7^+$
53	C_3OH^+	95	$C_5O_2H_3^+$
54	$C_3H_4N^+$	97	$C_5O_2H_5^+$
55	$C_3OH_3^+$	102	$C_4O_2H_8N^+$
56	$C_3H_6N^+$	104	$C_4O_2NH_{10}^+$
57	$HOOC-C^+$	114	$C_5O_2NH_8^+$
58	$OOC-CH_2^+$	130	$C_5O_3NH_8^+$
59	$HOOC-CH_2^+$	148	$C_5O_4NH_{10}^+$

In the negative ion spectrum, some even m/z value peaks were introduced at m/z = 26, 28, 38, 40, 42, 44, 46, 52, 54, 56, 58, 72, 74, 80, 82, 84, 86, 98, 100, 102, 128 and 146 (Figure 40). These ions might correspond to nitrogen-containing species. Also there are some prominent ions at m/z = 59, 71, 85 and 97. Peak assignments are listed in Table 25.

Table 25. Summary of Major Negative Ion peaks in the SIMS Spectrum of Glutamic Acid

m/z		m/z	
25	$C\text{-}CH^-$	60	$C_2O_2H_4^-$ or $CO_2H_2N^-$
26	CN^-	69	$C_3O_2H^-$
27	$C_2H_3^-$	71	$C_3O_2H_3^-$
28	$C_2H_4^-$ or NCH_2^- CO^-	72	$C_3O_2H_4^-$ or $C_2O_2NH_2^-$
35	Cl^-	73	$HOOC\text{-}CH_2\text{-}CH_2^-$
38	C_2N^-	74	$C_2O_2NH_4^-$
39	$C_3H_3^-$	80	$C_4ONH_2^-$
40	$C_2NH_2^-$	81	$C_4O_2H^-$
41	C_2OH^-	82	$C_4ONH_4^-$ or $C_4O_2H_2^-$
42	OCN^-	83	$C_4O_2H_3^-$
43	$C_2OH_3^-$	84	$C_4ONH_6^-$ or $C_4O_2H_4^-$
44	COO^- or $C_2H_4\text{-}NH_2^-$	85	$C_4O_2H_5^-$
45	$COOH^-$	86	$C_4O_2H_6^-$ or $C_3O_2NH_4^-$
46	$COOH_2^-$ or $COH_2\text{-}NH_2^-$	87	$C_4O_2H_7^-$
52	$C_3H_2N^-$	97	$C_5O_2H_5^-$
54	$C_3H_4N^-$	98	$C_4O_2NH_4^-$
55	$C_3OH_3^-$	99	$C_5O_2H_7^-$
56	$C_3H_6N^-$	100	$C_4O_2NH_6^-$
57	$C_2O_2H^-$	102	$C_4O_2NH_8^-$
58	$C_2O_2H_2^-$ or $C_2OH_4N^-$	128	$M\text{-}H\text{-}H_2O$: $C_5H_6O_3^-$
59	$HOOC\text{-}CH_2^-$	146	M-H: $C_5H_8NO_4^-$

Bulk Film of Bovine Serum Albumin

ESCA Analysis Carbon, oxygen, sulfur and nitrogen were found in albumin with a percentage of 65.91%, 18.06%, 1.16% and 14.87% respectively (see Figure 41).

Figure 42 shows the carbon high resolution peaks for a bulk film of albumin, and Figure 43 shows the oxygen high resolution peaks for this sample. The peak assignments are listed in Table 26.

Table 26. Carbon and Oxygen Peak Assignments of Albumin Bulk Film

	raw data (eV)	charged corrected data (eV)	function group assignment
carbon peak	276.61	285.00	**C**-H, C-C
	277.98	286.37	**C**-O
	279.82	288.21	**C**=O
oxygen peak	523.29	531.68	C-**O**
	525.00	533.39	C-**O**-C=O

SIMS Analysis Figure 44 shows the positive ion SIMS spectrum of a thick film of bovine serum albumin, from m/z = 0 - 300. Peaks have been identified using the protocol developed by David Mantus, (see Table 3-5) and are shown in Table 27 below. Low mass peaks at m/z = 15, 18 and 23 are CH_3^+, NH_4^+ and Na^+, respectively. Only those amino acids included in his study have been marked.

Peak identification of negative ion spectrum of bulk film of albumin (Figure 45) has also based on work of Mantus, see Tables 3-5. Major peaks of amino acid residues in the proteins are shown in Table 28.

Table 27. Summary of Major Positive Ion Peaks in the SIMS Spectrum of Albumin Bulk Film

m/z	I	$I-H_2$	others	m/z	I	$I-H_2$	others
28		$Gly-H_2$		82			His
30	Gly			84		$Leu-H_2$	Lys, Glu
42		$Ala-H_2$		86	Leu		
44	Ala			88			Asp
56			Glu	91			Phe
60	Ser			97			Arg
68		$Pro-H_2$		102	Glu		
70	Pro	$Val-H_2$	Arg	107			Try
72	Val		Asp	110	His		
77			Phe, Trp	120	Phe		
81			His	136	Tyr		

Table 28. Summary of Major Negative Ion Peaks in the SIMS Spectrum of Albumin Bulk Film

m/z	AA		m/z	AA	
26		CN^-	97	Glu	$C_5H_5O_2^-$
42		OCN^-	100	Val	$CH(CH_3)_2-CH_2-C(NH)O^-$
58	Gly	$CH_3-C(NH)O^-$	101	Gly	$NHCOH-CH_2-C(NH)O^-$
59	Glu	$C_2H_3O_2^-$	114	Leu	$CH_2CH(CH_3)_2-CH_2-C(NH)O^-$
66	Pro	$C_4H_4N^-$ 	115	Ala Val	$NHCOH-CH(CH_3)-C(NH)O^-$ $CH(CH_3)_2-CH(NH_2)-C(NH)O^-$
71	Glu	$C_3H_3O_2^-$	119	Tyr	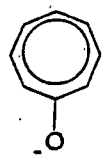
72	Ala	$CH_3-CH_2-C(NH)O^-$	128	Glu	$C_5H_6O_4^-$
73	Gly	$NH_2-CH_2-C(NH)O^-$	129	Leu	$CH_2CH(CH_3)_2-CH(NH_2)-C(NH)O^-$

Table 28 (cont'd). Summary of Major Negative Ion Peaks in the SIMS Spectrum of Albumin Bulk Film

m/z	AA		m/z	AA	
80	Glu	$C_4H_2NO^-$	157	Leu	$CH_2CH(CH_3)-CH(NHCOH)-C(NH)O^-$
87	Ala	$NH_2-CH(CH_3)-C(NH)O^-$			

Bovine Serum Albumin Adsorbed to PET

ESCA Analysis Carbon, oxygen and nitrogen were found in adsorbed albumin (Figure 46) with a percentage of 64.07%, 23.71% and 5.72% respectively. Sodium (4.19%) was also present in the spectrum, this may be due to contamination on the exposed PET surface or from PBS.

Figure 47 shows the carbon high resolution peaks for adsorbed albumin, and Figure 48 shows the oxygen high resolution peaks for this sample. The peak assignments are listed in Table 29.

Table 29. Carbon and Oxygen Peak Assignment of Adsorbed Albumin

	raw data (eV)	charge corrected data (eV)	function group assignment
carbon peak	276.74	285.00	C-H, C-C
	278.32	286.58	C-O
	280.57	288.83	C=O
oxygen peak	523.54	531.80	C-O
	525.33	533.59	C-O-C=O

SIMS Analysis Unfortunately, the positive ion spectrum of adsorbed albumin on PET had poor signal intensity (Figure 49). A few amino acid peaks were identified and are summarized in Table 30.

Table 30. Summary of Major Positive Ion Peaks in the SIMS Spectrum of Adsorbed Albumin

m/z	I	I-H_2	others	m/z	I	I-H_2	others
28		Gly-H_2		70	Pro	Val-H_2	Arg
30		Gly		77			Phe, Trp
42		Ala-H_2		84		Leu-H_2	Lys, Glu
44	Ala			86	Leu		
56			Glu				

Figure 50 showed the negative ion SIMS spectra of adsorbed albumin. The peak pattern was almost the same as the peak pattern of albumin bulk film, but the intensity was much lower. Major peaks indicative of various amino acid residues in the proteins are summarized in Table 31.

Table 31. Summary of Major Negative Ion Peaks in the SIMS Spectrum of Adsorbed Albumin

m/z	AA		m/z	AA	
26		CN^-	87	Ala	NH_2-$CH(CH_3)$-$C(NH)O^-$
42		OCN^-	97	Glu	$C_5H_5O_2^-$
58	Gly	CH_3-$C(NH)O^-$	100	Val	$CH(CH_3)_2$-CH_2-$C(NH)O^-$
59	Glu	$C_2H_3O_2^-$	101	Gly	NHCOH-CH_2-$C(NH)O^-$

Table 31 (cont'd). Summary of Major Negative Ion Peaks in the SIMS Spectrum of Adsorbed Albumin

m/z	AA		m/z	AA	
66	Pro	$C_4H_4N^-$ 	115	Ala	$NHCOH-CH(CH_3)-C(NH)O^-$
				Val	$CH(CH_3)_2-CH(NH_2)-C(NH)O^-$
71	Glu	$C_3H_3O_2^-$	119	Tyr	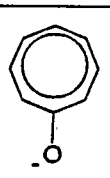
72	Ala	$CH_3-CH_2-C(NH)O^-$	128	Glu	$C_5H_6O_4^-$
73	Gly	$NH_2-CH_2-C(NH)O^-$	129	Leu	$CH_2CH(CH_3)_2-CH(NH_2)-C(NH)O^-$
80	Glu	$C_4H_2NO^-$	157	Leu	$CH_2CH(CH_3)_2-CH(NHCOH)-C(NH)O^-$

Discussions

The positive ion spectra of many amino acids are dominated by the immonium ion (I). This ion has the generic structure $H_2N^+=CH-R$. The R group distinguishes the particular amino acid (see Table 2), and the immonium ion peak will be found at m/z = [R+29]. This is the only important positive ion in the spectra of amino acids [13]. In the positive ion spectrum of glutamic acid, the immonium ion was observable as a prominent peak at m/z = 102 (Figure 39). The most significant peak at m/z = 84 was due to the loss of neutral H_2O from the immonium ion, giving an ion with the formula $C_4H_6NO^+$ and a possible cyclic structure.

The negative ion spectrum of glutamic acid contained a

strong peak at m/z = 146 from the $(M-H)^-$ ion. The peak at m/z = 128 was due to the loss of H_2O from the $(M-H)^-$ ion. Peaks at m/z = 59, 71, 80 and 97, from ions with the likely formula $C_2O_2H_3^-$, $C_3O_2H_3^-$, $C_4H_2NO^-$ and $C_5O_2H_5^-$, respectively, were observed in the spectrum. These peaks made a major contribution to the negative ion SIMS spectra of albumin and cell wall antigens.

It is readily apparent that many more peaks are present in both positive and negative spectra of albumin than can be assigned. Many of the odd mass peaks, which are usually associated with hydrocarbon ions, may be due to either contamination or long chain fatty acids (0.006%) that often aggregate with albumin. While the albumin used here is labeled fatty acid free, any residue of fatty acid would be highly surface active and concentrate at the protein vacuum interface. Other peaks may originate from various biomolecules found in small quantities in the protein.

The main difference between the albumin bulk film and the adsorbed albumin spectra was the relative intensities of the peaks arising from the amino acids. The source of this difference may be the different interactions between albumin molecules and the substrate surfaces. And also, in the spectra of adsorbed albumin, some peaks arising from PET were observed. The positive ion spectrum of adsorbed albumin contains a peak at m/z = 105 from PET fragment [27]

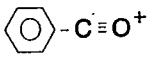

The PET $(M+H)^+$ ion peak was also observable as a weak peak at m/z = 193 in the positive ion spectrum of adsorbed albumin

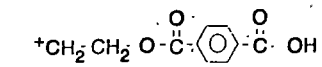

More peaks arising from PET were seen in the negative ion spectrum of adsorbed albumin. Peaks at m/z = 76, 105, 121 and 165 were believed to have the structures

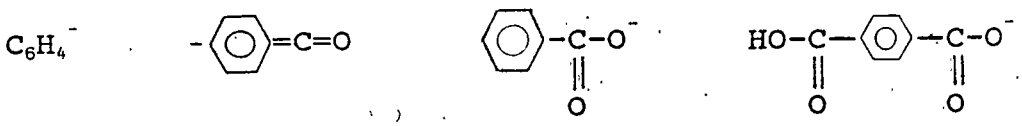

(76D) (121D) (105D) (165D)

respectively. The $(M-H)^-$ ion peak of PET was also observed at m/z = 191 [28].

C. albicans Cell Wall Antigens

Two purified *C. albicans* cell wall antigens (AgH9 and AgC6) [20] and crude *C. albicans* cell wall antigen [21] were analyzed by ESCA and SIMS.

ESCA Analysis

The atom percentages of carbon, nitrogen and oxygen in AgH9, AgC6 and crude antigens are listed in Table 32. A small amount of Ca_2O_3 and Si was found in the ESCA spectra of *C. albicans* cell wall AgH9 and AgC6 (Figure 51(a) and (b)), probably due to either sample contamination or the glass

substrate.

Table 32. Atom % of AgH9, AgC6 And Crude Antigens

	Carbon	Oxygen	Nitrogen
AgH9	61.72	31.48	3.88
AgC6	63.46	29.91	3.21
crude antigen	65.14	20.42	14.43

Four carbon peaks were shown on the carbon high resolution region in AgH9, AgC6 and crude antigen (Figure 52). AgH9 and AgC6 had the same peak ratio. Peak assignments are listed in Table 33.

Table 33. Carbon and Oxygen Peak Assignments of *C. albicans* Cell Wall AgH9, AgC6 And Crude Antigens

	raw data (eV)	charge corrected data (eV)	function group assignment
carbon peak	276.66 (AgH9) 276.72 (AgC9) 276.66 (crude)	285.00	**C**-H
	278.15 (AgH9) 278.25 (AgC6) 278.09 (crude)	286.49 (AgH9) 286.53 (AgC6) 286.43 (crude)	**C**-O
	279.70 (AgH9) 279.83 (AgC6) 279.79 (crude)	288.04 (AgH9) 288.11 (AgC6) 288.13 (crude)	**C**=O **C**-N
	280.84 (AgH9) 280.97 (AgC6) 280.78 (crude)	289.18 (AgH9) 289.25 (AgC6) 289.12 (crude)	O-**C**=O
oxygen peak	523.15 (AgH9) 523.10 (AgC6) 523.21 (crude)	531.49 (AgH9) 531.38 (AgC6) 531.55 (crude)	C=**O**
	524.53 (AgH9) 524.57 (AgC6) 524.61 (crude)	532.87 (AgH9) 532.85 (AgC6) 532.95 (crude)	C-**O**

Most carbon and oxygen in saccharides are singled bonded, so the decrease in C-O bond in crude antigen means crude antigen has less saccharide than purified antigens. Two oxygen peaks were presented on the oxygen high resolution region (Figure 53). Table 33 lists the peak assignments. In crude antigen, the decrease of C-O means the decrease of saccharides, therefore, it has more nitrogen.

SIMS Analysis

The positive ion spectra of cell wall AgH9 and AgC6 looked the same (Figure 54 and Figure 55). They were similar to the positive ion spectrum of mannose (Figure 10). From m/z = 50 to 100, the positive ion spectra of the purified antigens and of mannose had a similar peak pattern. They both had strong peaks at m/z = 53, 55, 57, 67, 69, 71, 77, 79, 81 and 91. Above m/z = 100, both the purified antigens and the mannose had higher mass fragments, but the ratios of the peak intensities were different. Overall, the cell wall purified antigens had higher intensity of high mass peaks than the mannose. That may mean the cell wall purified antigens samples have better ionization matrix and constituents with higher molecular weight. In the positive ion spectra for the cell wall purified antigens, several even m/z value peaks were observed at m/z = 58, 70, 86 and 128, which indicate nitrogen containing species. ESCA analysis also indicated there was a small amount of nitrogen in *C. albicans* cell wall purified antigens, see Figure 51. Table 34 shows major peak

assignments.

Table 34. Summary of Major Positive Ion Peaks in the SIMS Spectrum of *C. albicans* Cell Wall Purified Antigens

m/z		m/z	
27	$C_2H_3^+$	95	$C_5O_2H_3^+$
29	COH^+	97	$C_5O_2H_5^+$
39	$C_3H_3^+$	105	$C_4O_3H_9^+$
41	C_2OH^+	107	$C_6O_2H_3^+$
43	$C_2OH_3^+$	109	$C_6O_2H_5^+$
53	C_3OH^+	111	$C_5O_3H_3^+$
55	$C_3OH_3^+$	115	$C_4O_4H_3^+$ or $C_5O_3H_7^+$
57	$C_2O_2H^+$	117	$C_4O_4H_5^+$ or $C_5O_3H_9^+$
58	$C_2ONH_4^+$	119	$C_4O_4H_7^+$
59	$C_2O_2H_3^+$	121	$C_4O_4H_9^+$
65	C_4OH^+	123	$C_6O_3H_3^+$
67	$C_4OH_3^+$	125	$C_5O_4H^+$ or $C_6O_3H_5^+$
69	$C_3O_2H^+$	128	$C_5O_3NH_6^+$
70	$C_3ONH_4^+$	131	$C_5O_4H_7^+$
71	$C_3O_2H_3^+$	133	$C_5O_4H_9^+$
77	C_5OH^+	135	$C_5O_4H_{11}^+$
79	$C_5OH_3^+$	137	$C_6O_4H^+$
81	$C_4O_2H^+$	141	$C_6O_4H_5^+$
83	$C_4O_2H_3^+$	143	$C_6O_4H_7^+$
85	$C_4O_2H_5^+$	145	$C_6O_4H_9^+$
86	$C_3O_2NH_4^+$	147	$C_5O_5H_7^+$
91	$C_3O_3H_7^+$	149	$C_5O_5H_9^+$
93	$C_5O_2H^+$	153	$C_6O_5H^+$
159	$C_6O_5H_7^+$	165	$C_6O_5H_{13}^+$

All the major peaks presented in the positive ion spectra of purified antigens were observed in the positive ion spectrum of crude antigens (Figure 56). However, more fragments were involved in the spectrum of crude antigens.

The negative ion spectra for *C. albicans* cell wall AgH9 and AgC6 looked approximately identical (Figure 57 and Figure 58). However, they differed from the negative ion spectrum of mannose. Above m/z = 50, the spectrum of mannose contained an intense peak at m/z = 59 with a formula of $C_2O_2H_3^-$, and another intense peak at m/z = 71 with a formula of $C_3O_2H_3^-$. The spectra of purified antigens not only had these two strong peaks, but also had more intensive peaks at m/z = 80 and 97. Some even m/z value peaks were introduced in their negative ion spectra, indicating the nitrogen involvement, for example, m/z = 26, 42, 58, 64, 80 and 110. Table 35 summarizes major peak assignments.

All the major peaks appearing in the negative ion spectra of purified antigens were also observed in the crude antigens spectrum with a different peak intensity ratio (Figure 59).

Table 35. Summary of Major Negative Ion Peaks in the SIMS Spectrum of *C. albicans* Cell Wall Purified Antigens

m/z		m/z	
25	C_2H^-	96	$C_4O_2NH_2^-$
26	CN^-	97	$C_5O_2H_5^-$
35	Cl^-	99	$C_4O_3H_3^-$
41	C_2OH^-	101	$C_4O_3H_5^-$

Table 35 (cont'd). Summary of Major Negative Ion Peaks in the SIMS Spectrum of *C. albicans* Cell Wall Purified Antigens

m/z		m/z	
42	OCN^-	103	$C_4O_3H_7^-$
43	$C_2OH_3^-$	107	$C_6O_2H_3^-$
45	$C_2OH_5^-$	110	$C_5O_2NH_4^-$
55	$C_3OH_3^-$	111	$C_5O_3H_3^-$
57	$C_2O_2H^-$ or $C_3OH_5^-$	113	$C_4O_4H^-$ or $C_5O_3H_5^-$
58	$C_2ONH_4^-$	115	$C_4O_4H_3^-$ or $C_5O_3H_7^-$
59	$C_2O_2H_3^-$	119	$C_4O_4H_7^-$
64	$CO_2NH_6^-$	121	$C_4O_4H_9^-$
65	C_4OH^-	123	$C_6O_3H_3^-$
69	$C_3O_2H^-$	125	$C_6O_3H_5^-$
71	$C_3O_2H_3^-$	127	$C_6O_3H_7^-$
73	$C_3O_2H_5^-$	137	$C_6O_4H^-$
79	$C_2O_3H_7^-$	139	$C_6O_4H_3^-$
80	$C_4ONH_2^-$	141	$C_6O_4H_5^-$
81	$C_4O_2H^-$	153	$C_6O_5H^-$
83	$C_4O_2H_3^-$	161	$C_6O_5H_9^-$
85	$C_3O_3H^-$ or $C_4O_2H_5^-$	179	$C_6O_6H_{11}^-$
87	$C_3O_3H_3^-$ or $C_4O_2H_7^-$	191	$C_7O_6H_{11}^-$

Discussions

It has been shown that AgH9 and AgC6 contain mannose and glucose, with mannose/glucose ratio of 3 : 1 and 11 : 1, respectively [20]. Mannose was observed in the positive ion spectra of AgH9 and AgC6. However, there was no strong indication of glucose peaks in either spectra. This may be due to several reasons. The amount of mannose is larger than

the amount of glucose in the samples. Mannose may have better ionization matrix effect than glucose. Mannose positive ions may be easier to get off the substrate surface than glucose positive ions. Also, quadrupole SIMS may not be sensitive enough to tell the hidden glucose peaks in the mannose-dominated positive ion spectrum.

Pronase was used in the antigen isolation procedure [20]. So no protein should be detected in purified AgH9 or AgC6 after protease treatment. However, the negative ion spectra of AgH9 and AgC6 exhibited strong, distinctive peaks indicative of the amino acids involvement. Significant peaks at m/z = 26 and 42, from ions CN^- and OCN^-, respectively, in the negative ion spectra of cell wall antigens were observed in the spectra of all the amino acids [13]. Single, strong peaks at m/z = 59, 71, 80 and 97 were also seen in the negative ion spectra of glutamic acid (Figure 40), bulk film of albumin (Figure 45) and adsorbed albumin (Figure 50). ESCA analysis also confirmed the nitrogen involvement (Table 32 and Figure 51). The amino acids in the AgH9 and AgC6 may be from residual mannoprotein or residual pronase.

That the mannose was seen in the positive ion spectrum of cell wall purified antigens and the amino acids were seen in the negative ion spectra might be caused by several reasons. In the positive ion spectrua, mannose might have a better ionization matrix effect than other components. Therefore, mannose produced more positive ions. However, in the negative

ion spectra, amino acids might have a better ionization matrix effect than other compounds, so amino acids produced more negative ions. Also, mannose positive ions may be more stable, while amino acid negative ions may be more stable. Another reason might be the low sensitivity of quadrupole SIMS. It is not sensitive enough to tell the hidden amino acid peaks in the positive ion spectrum and the hidden mannose peaks in the negative ion spectrum.

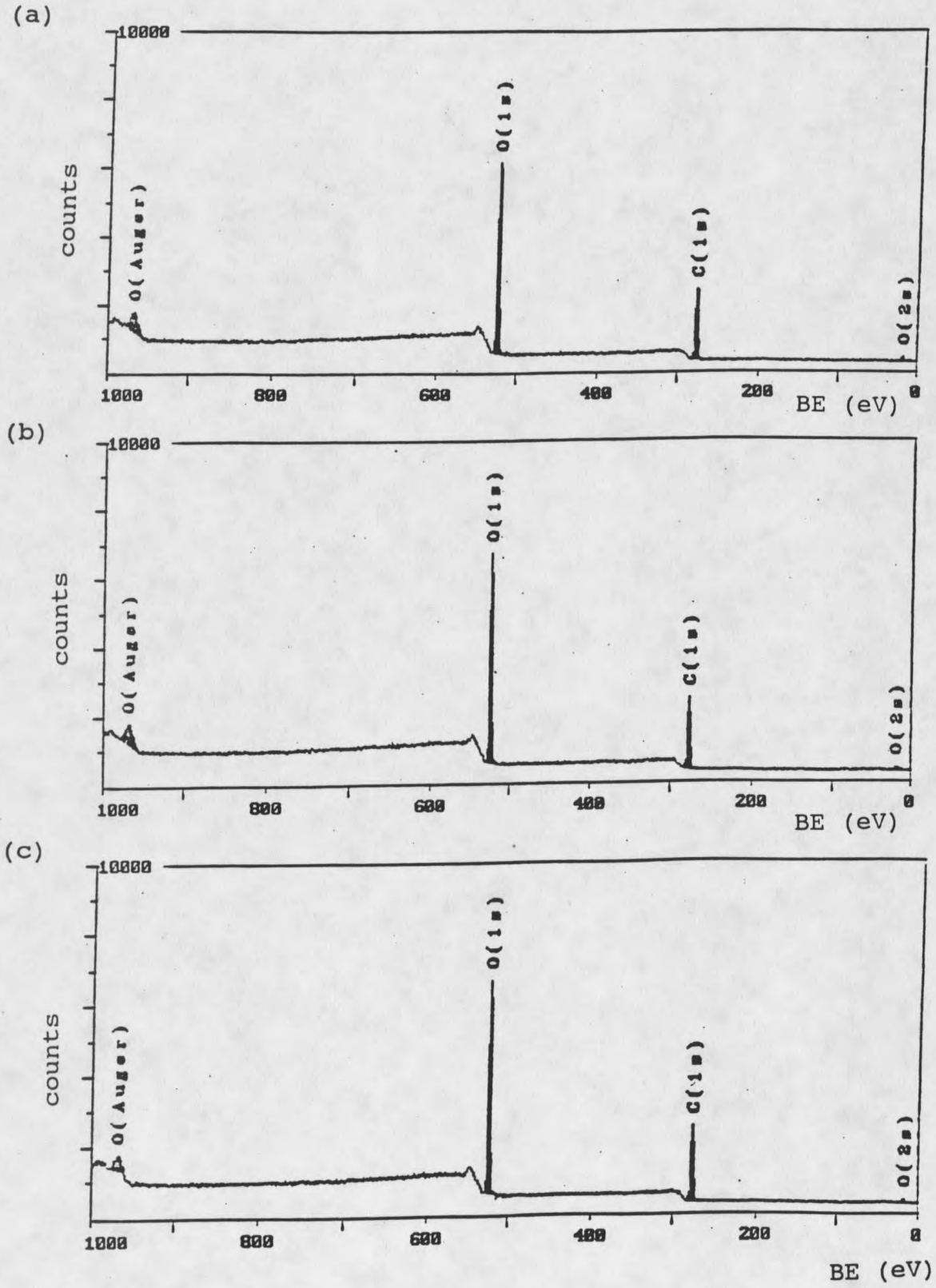

Figure 6. ESCA spectra of (a) glucose, (b) mannose and (c) galactose

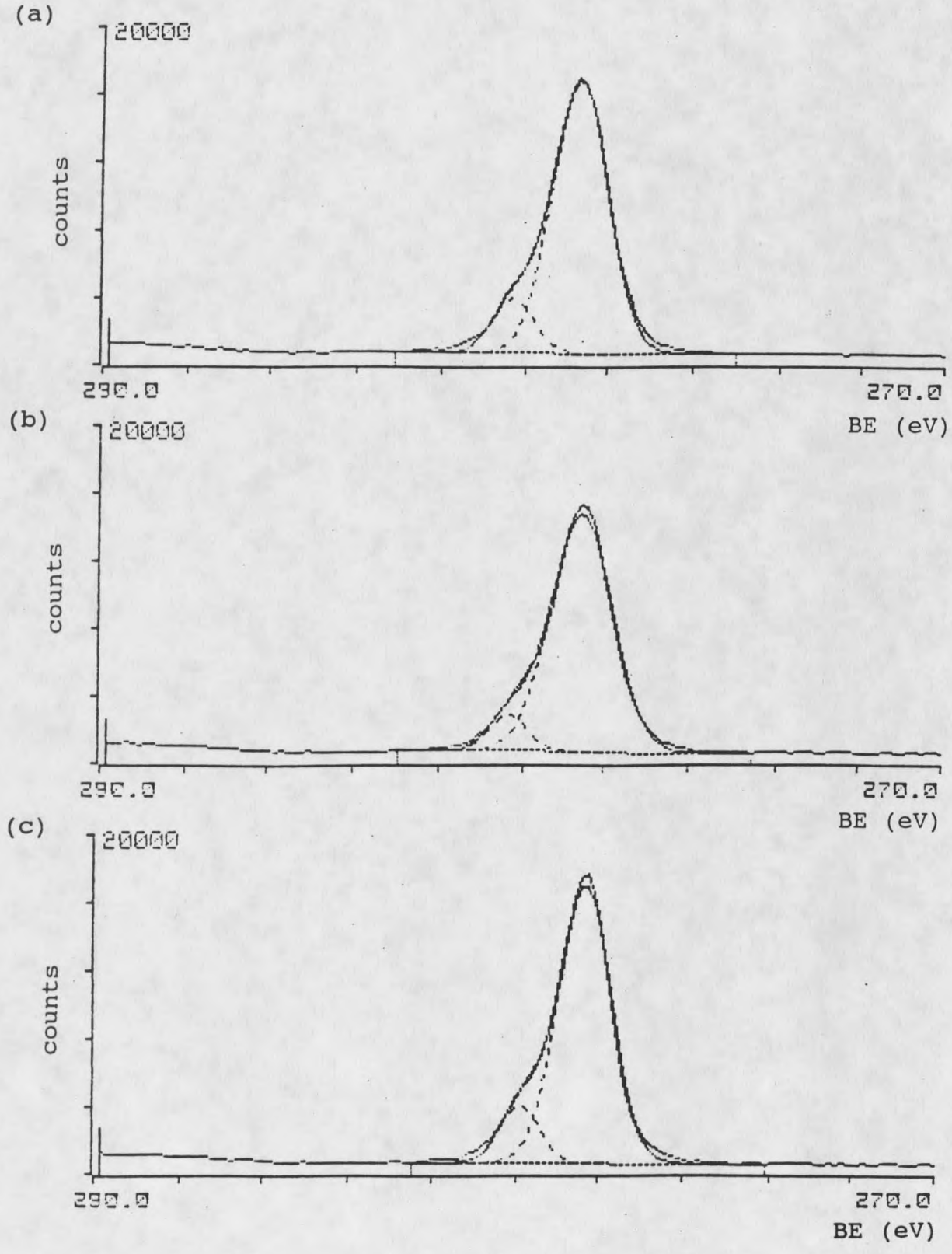

Figure 7. Carbon high resolution peak of (a) glucose, (b) mannose and (c) galactose

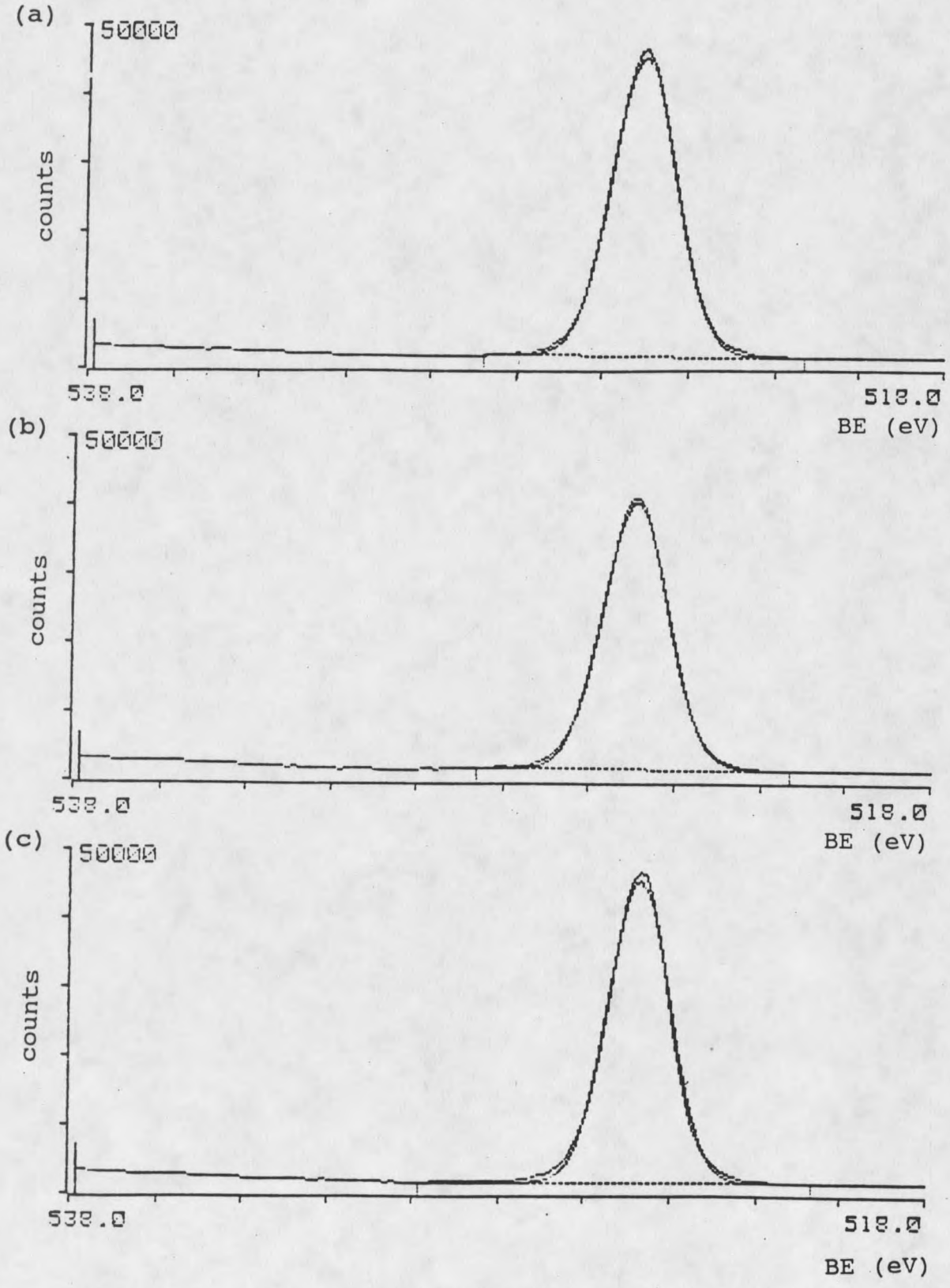

Figure 8. Oxygen high resolution peak of (a) glucose, (b) mannose and (c) galactose

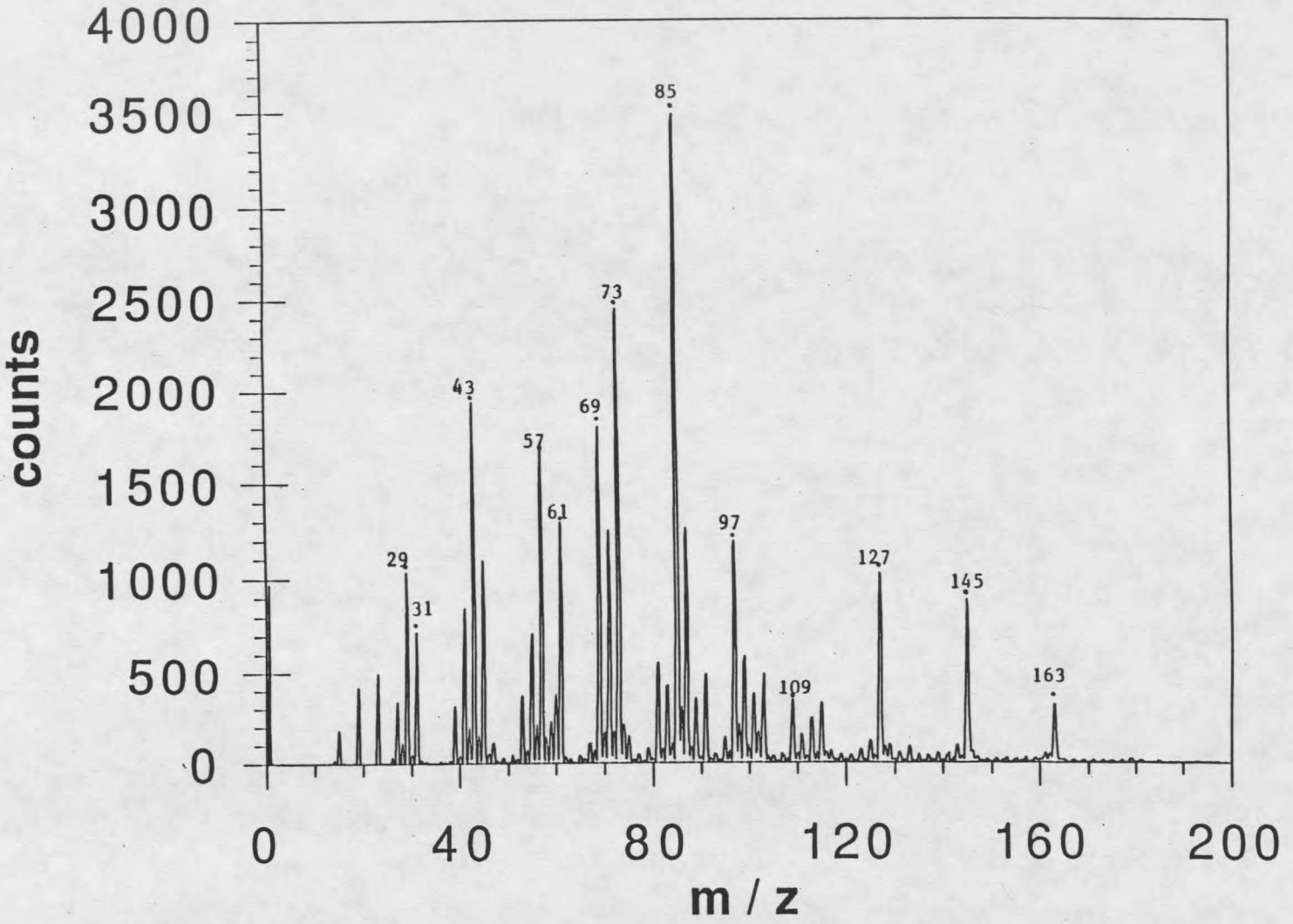

Figure 9. Positive ion static SIMS spectrum of glucose

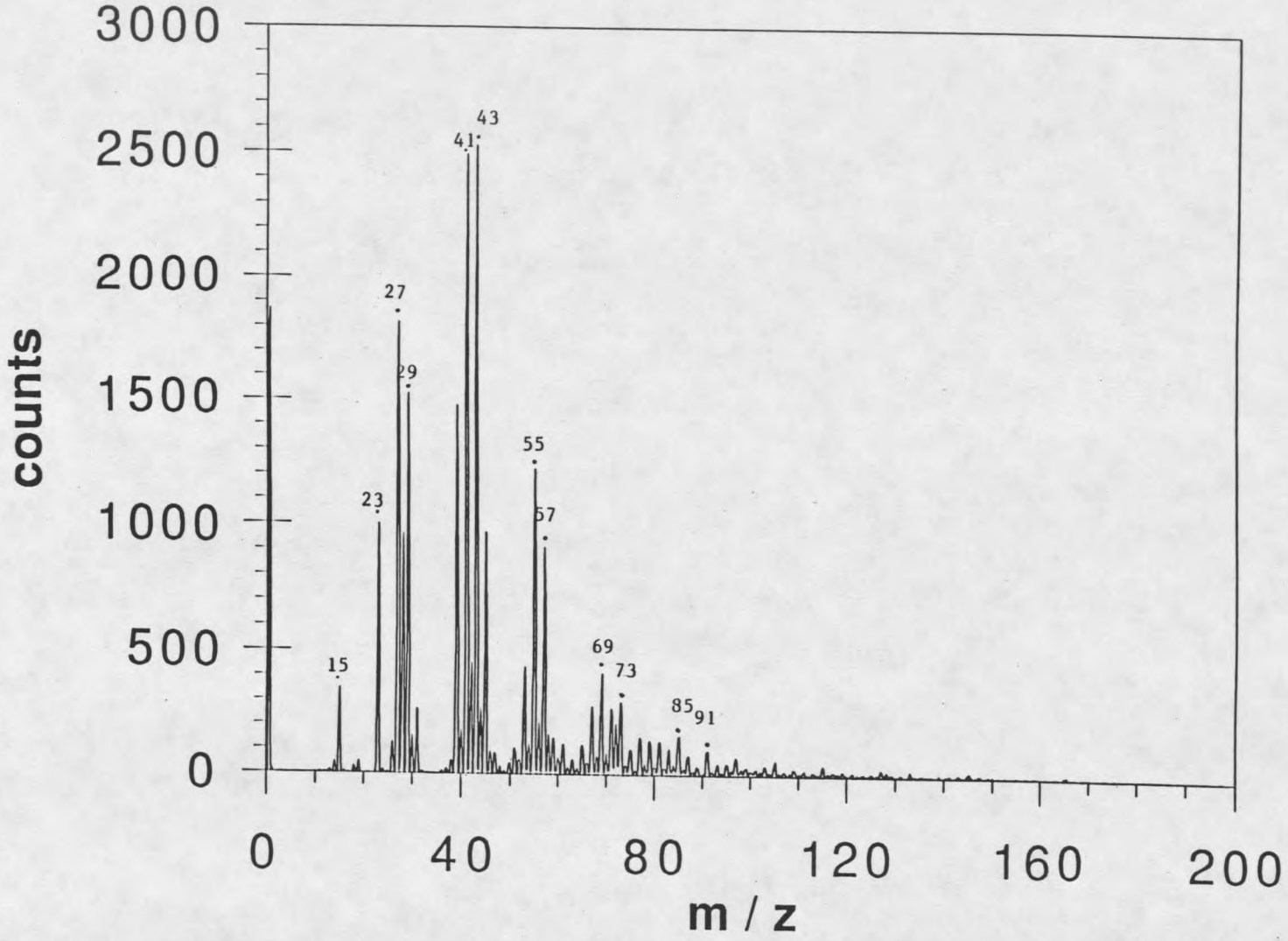

Figure 10. Positive ion static SIMS spectrum of mannose

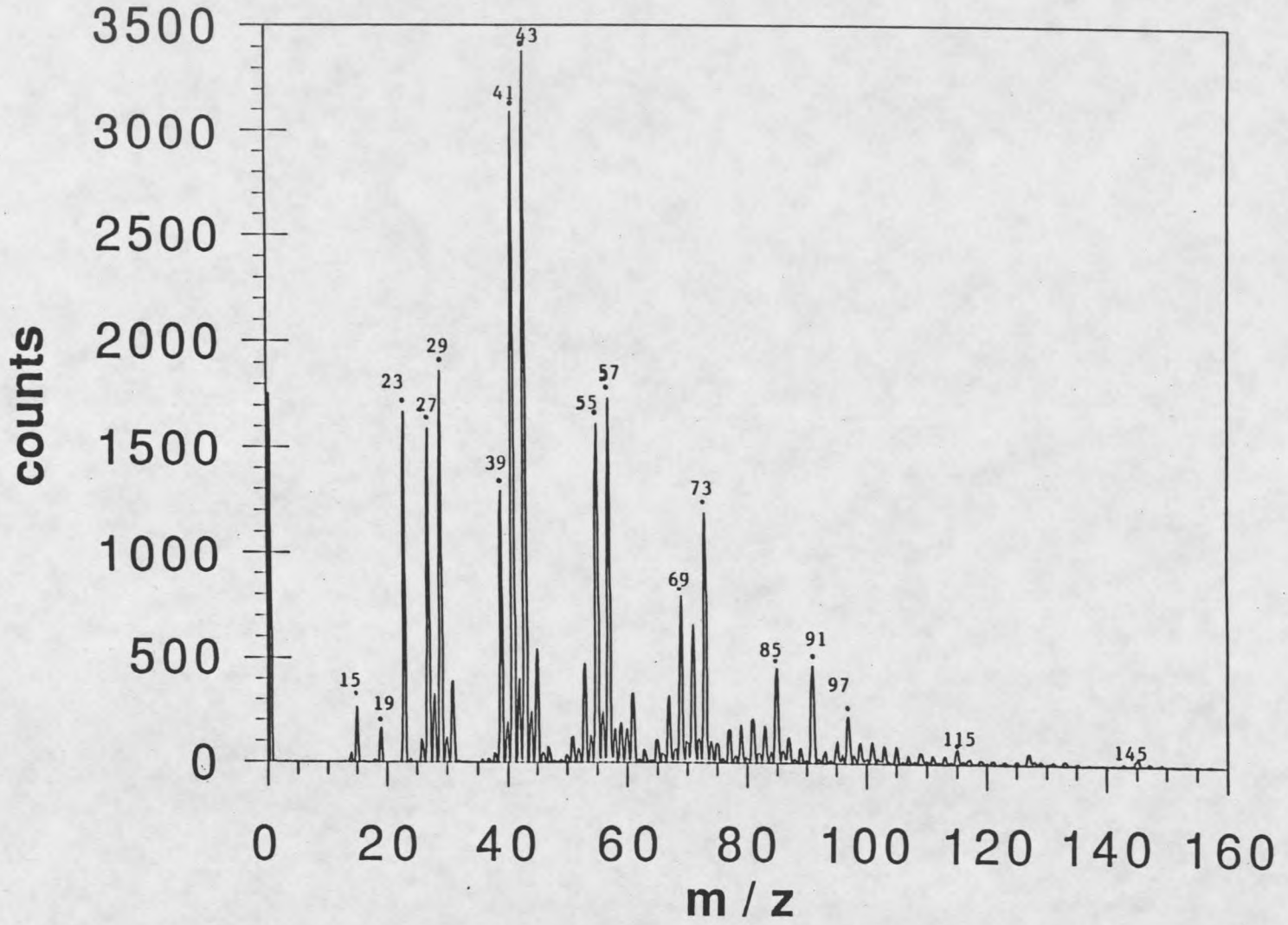

Figure 11. Positive ion static SIMS spectrum of galactose

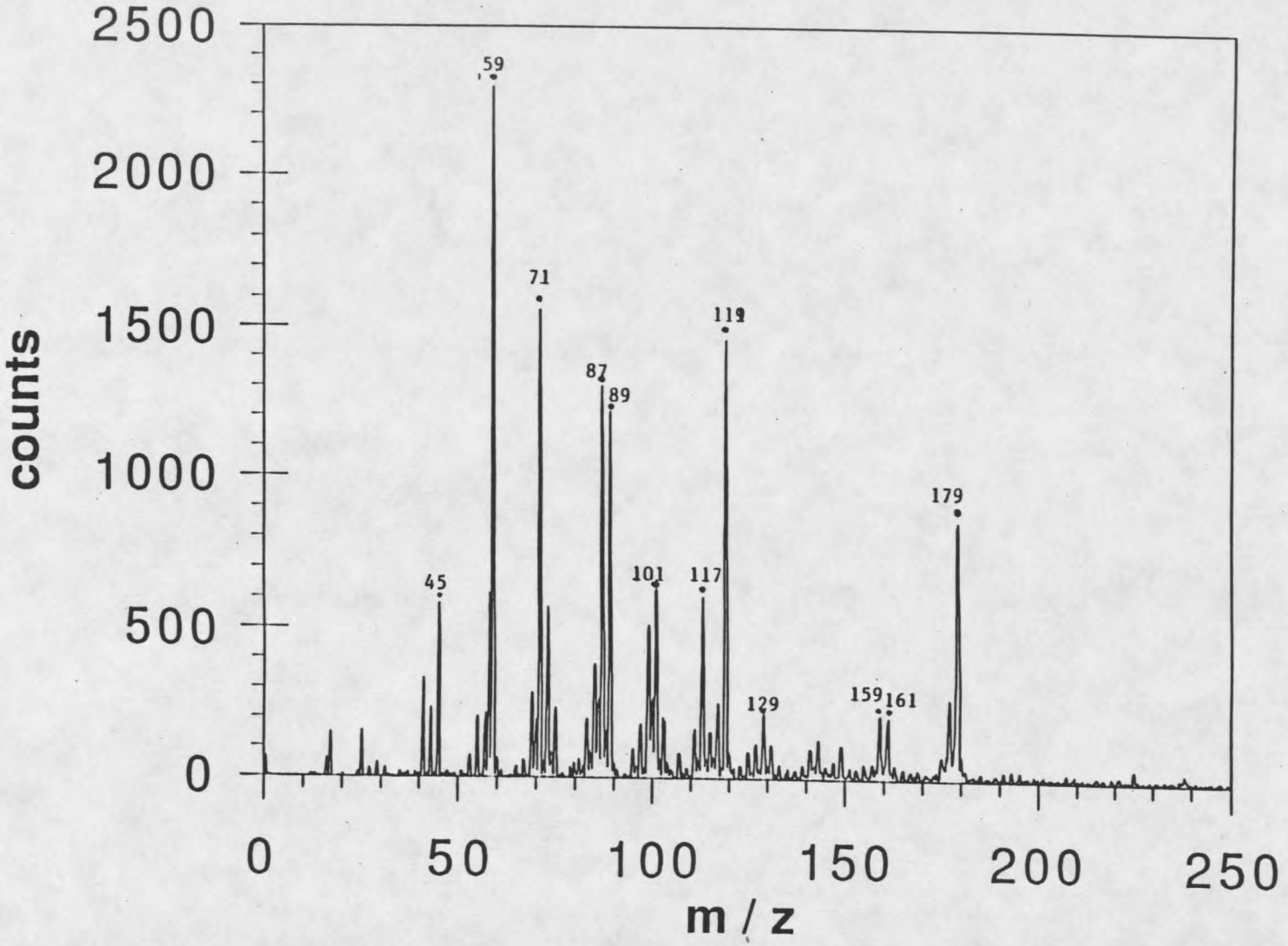

Figure 12. Negative ion static SIMS spectrum of glucose

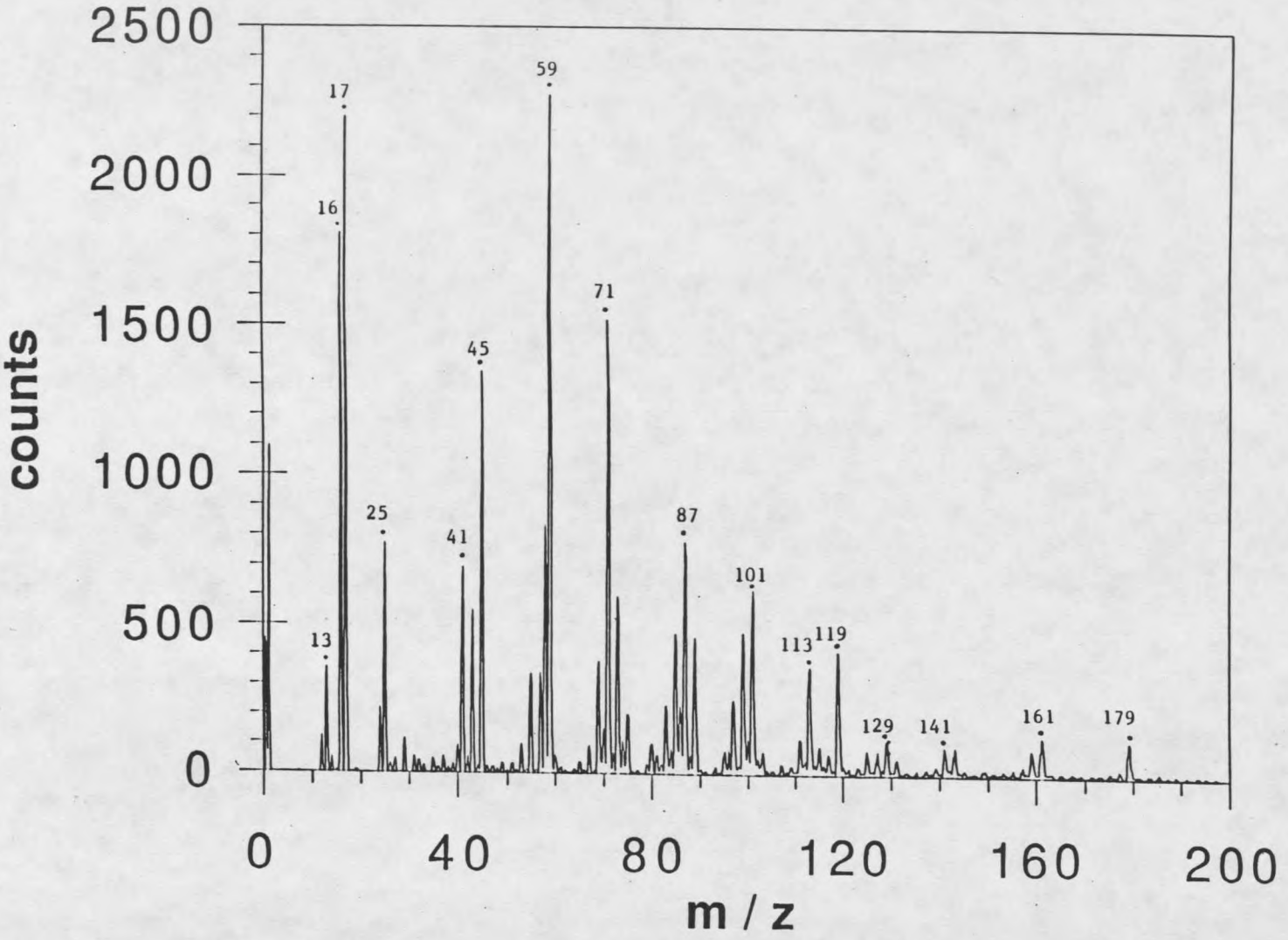

Figure 13. Negative ion static SIMS spectrum of mannose

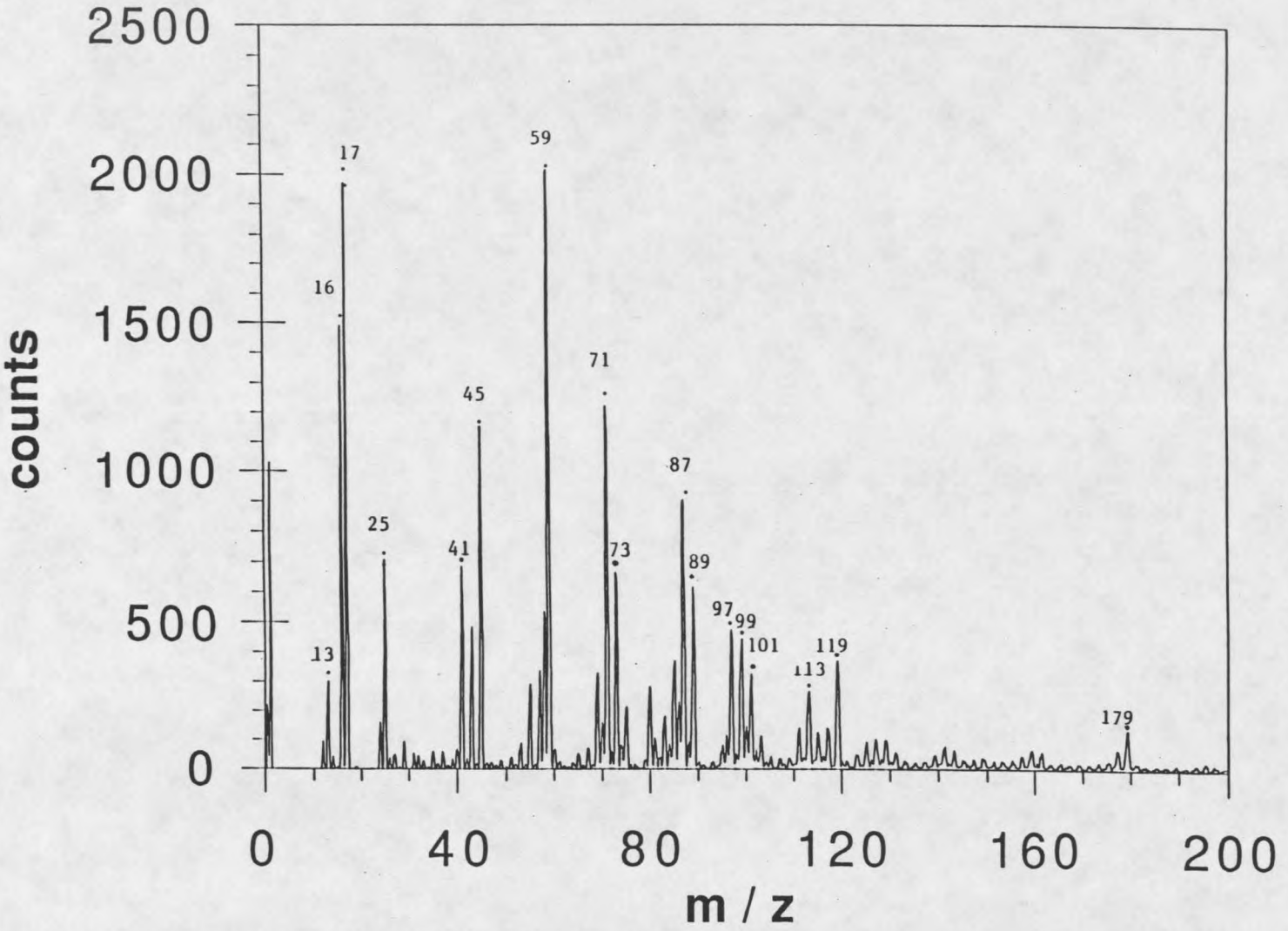

Figure 14. Negative ion static SIMS spectrum of galactose

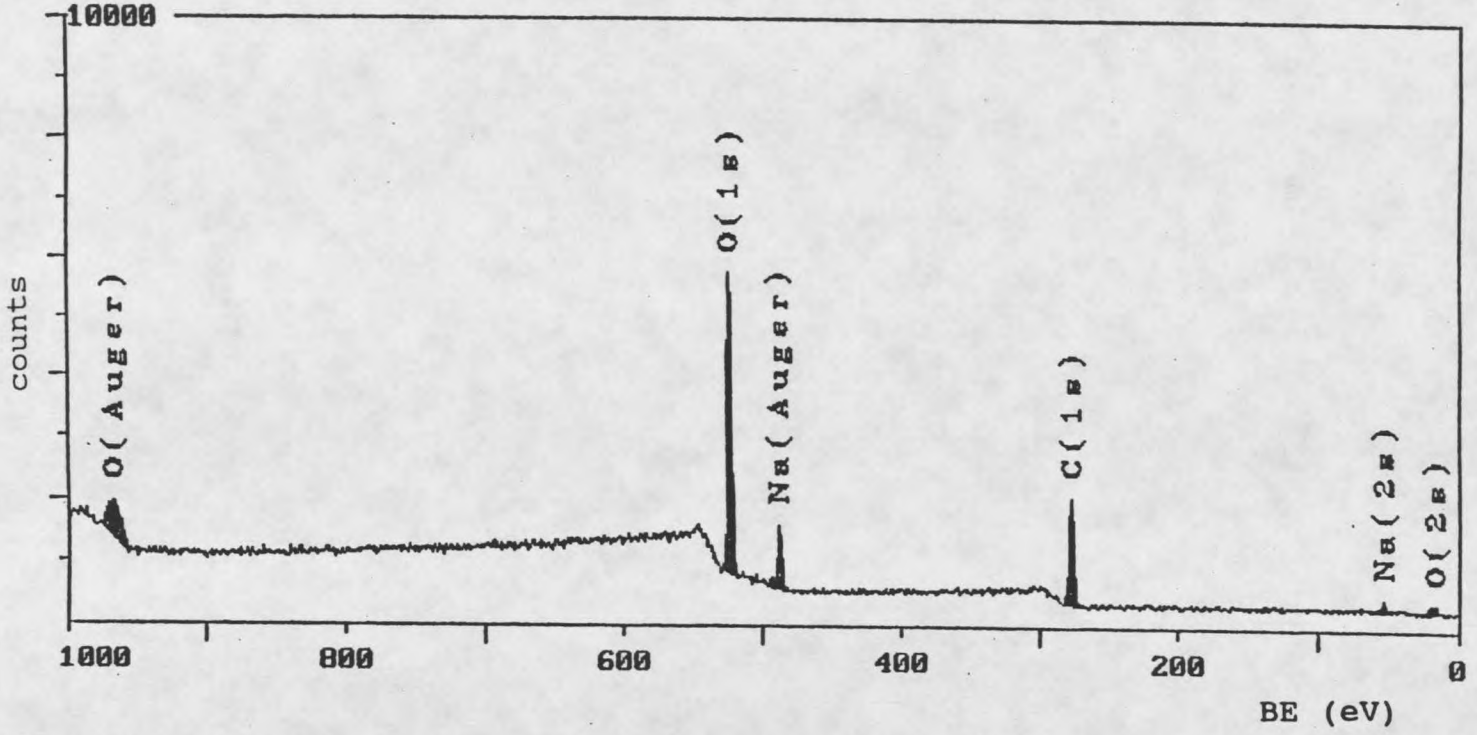

Figure 15. ESCA spectrum of glucuronic acid

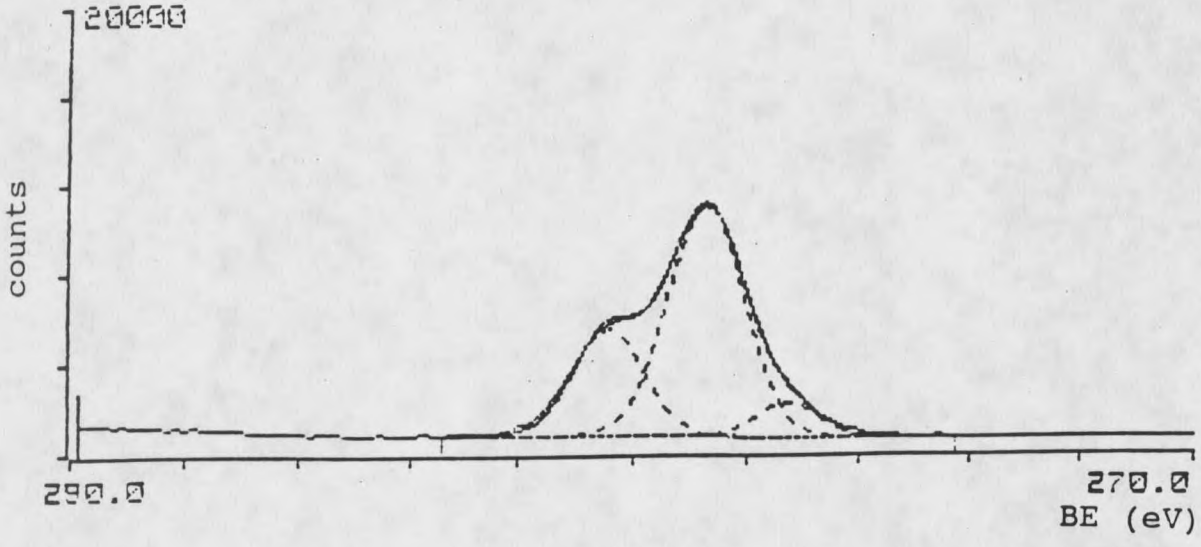

Figure 16. Carbon high resolution peak of glucuronic acid

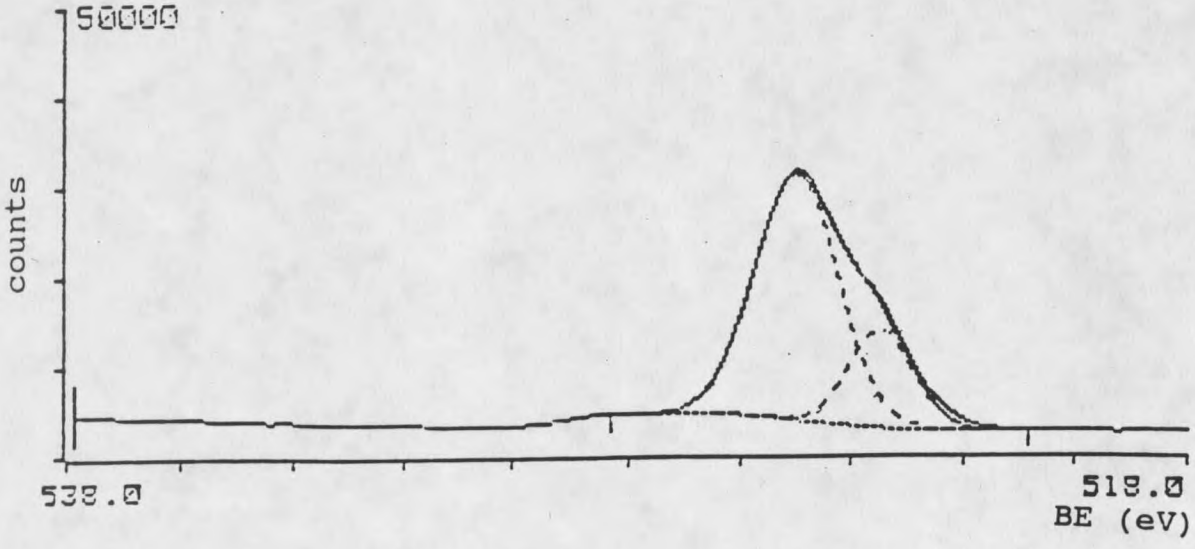

Figure 17. Oxygen high resolution peak of glucuronic acid

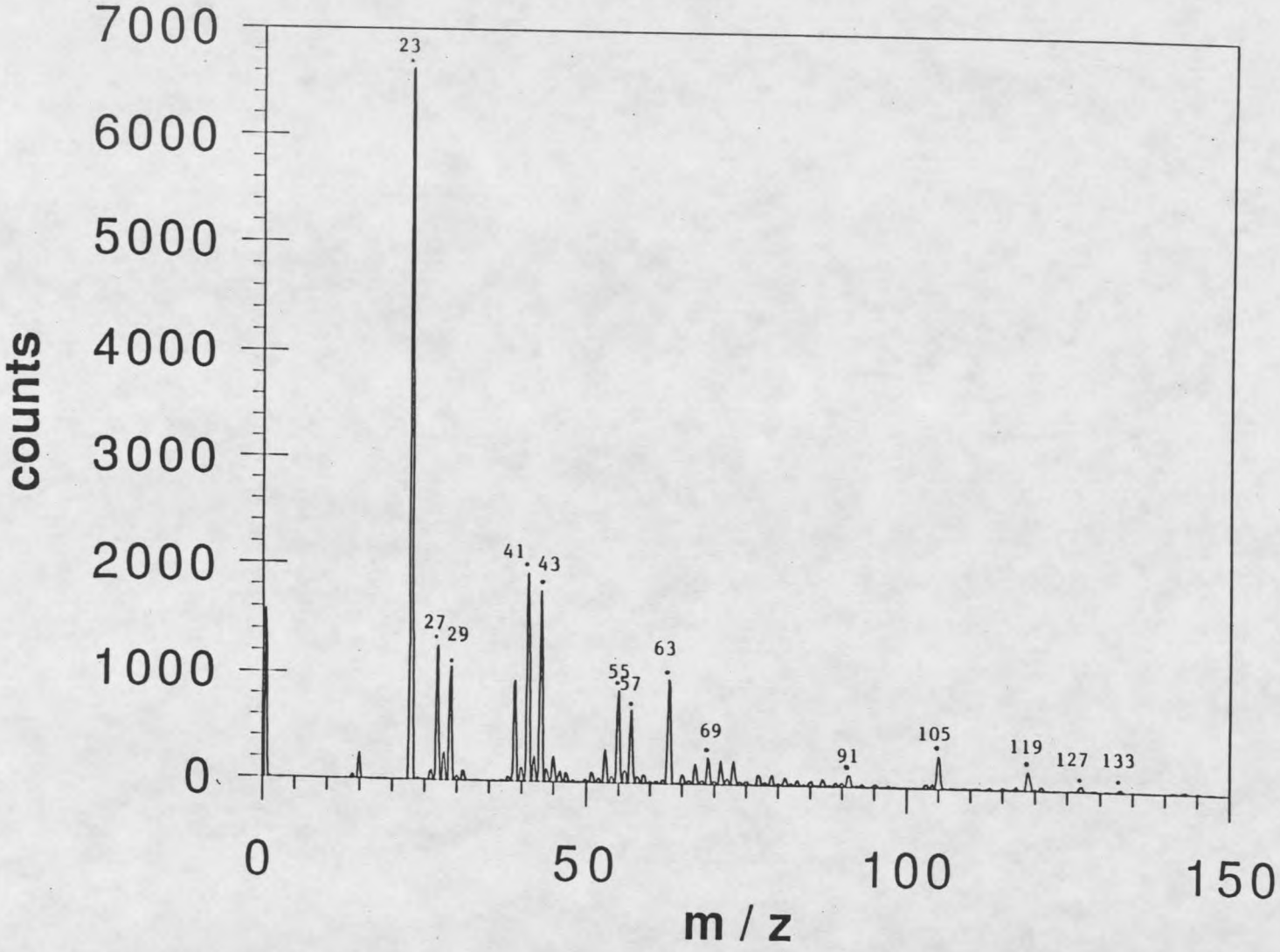

Figure 18. Positive ion static SIMS spectrum of glucuronic acid

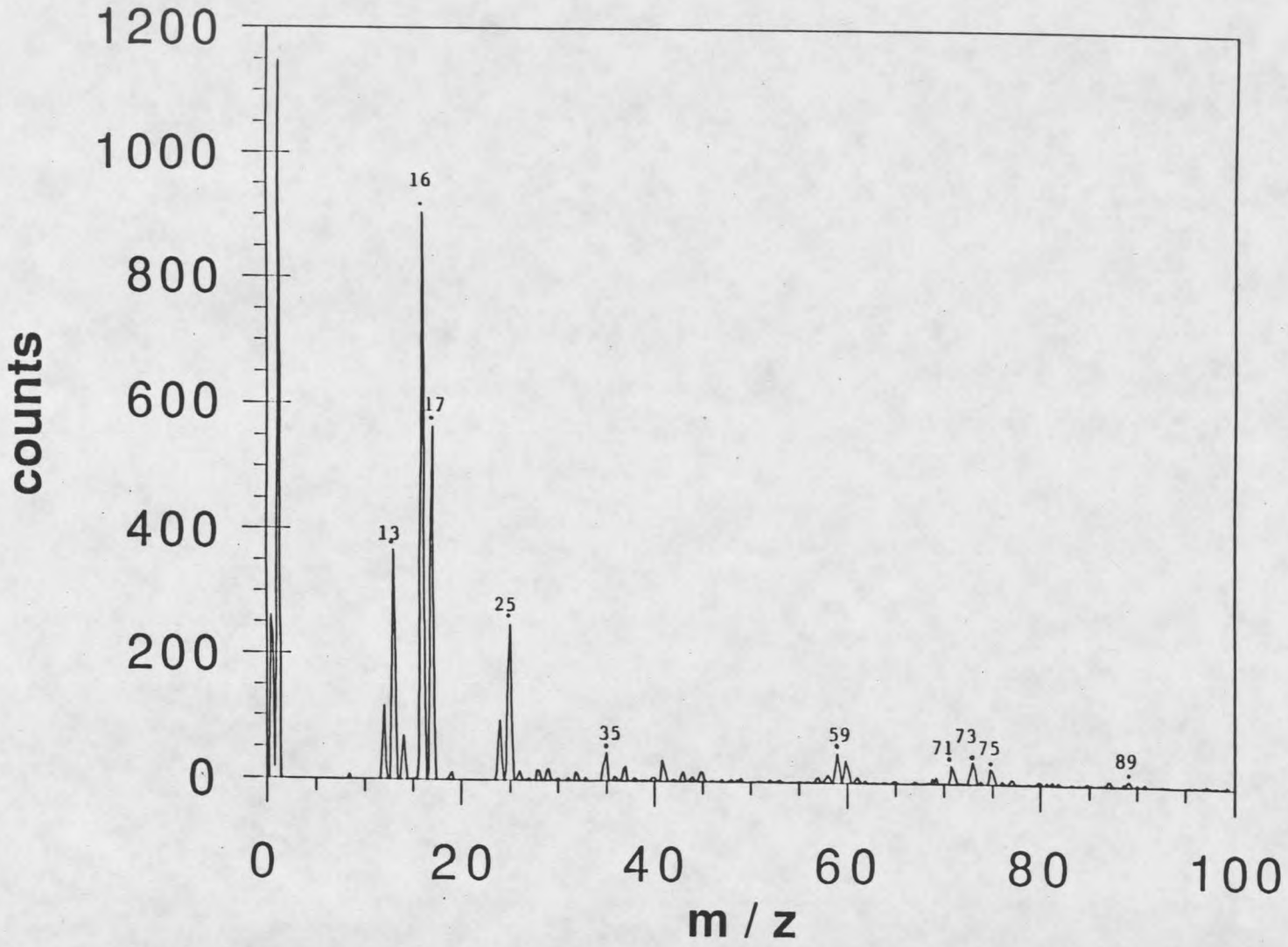

Figure 19. Negative ion static SIMS spectrum of glucuronic acid

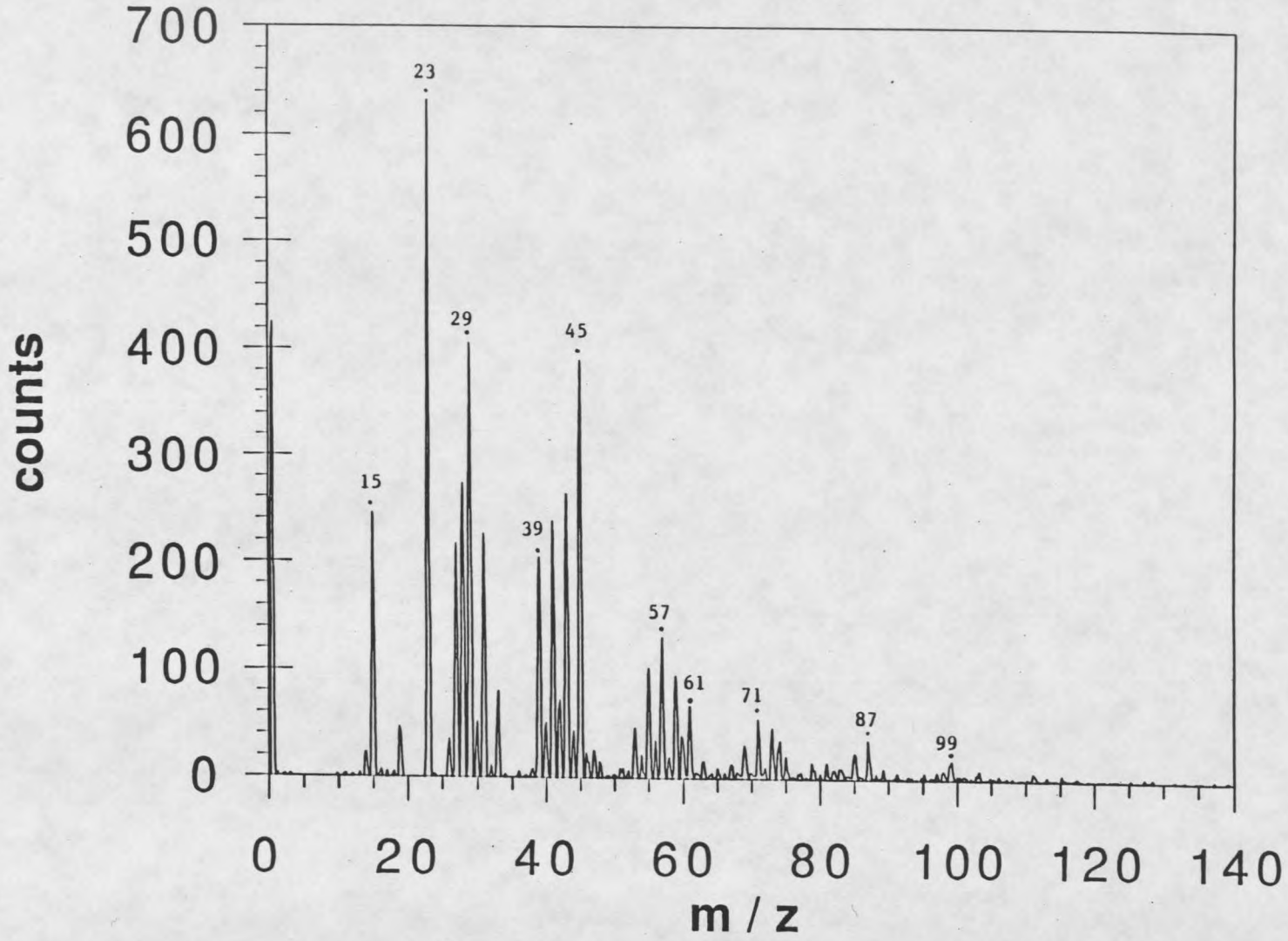

Figure 20. Positive ion static SIMS spectrum of methyl α-D-mannopyranoside

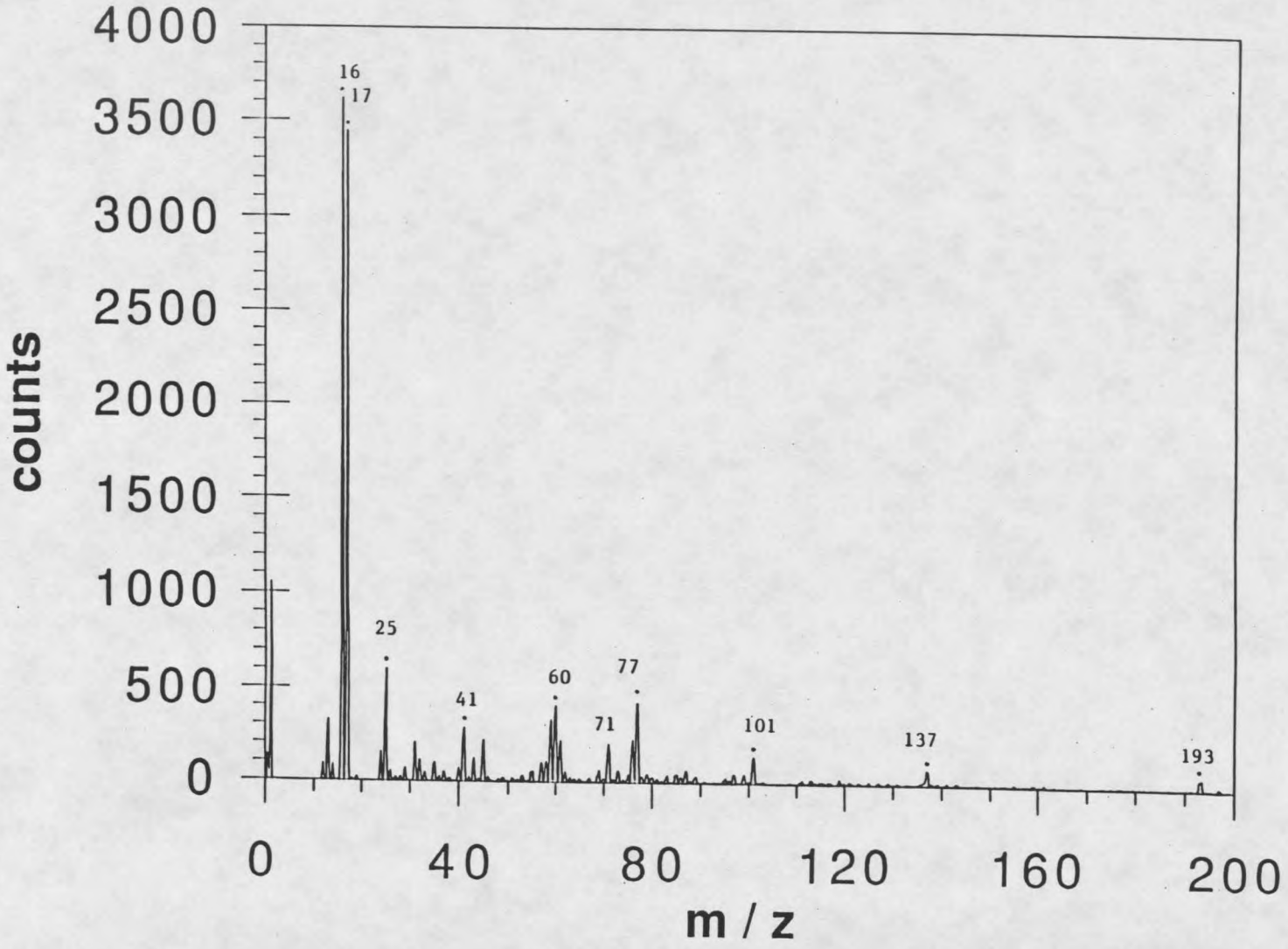

Figure 21. Negative ion static SIMS spectrum of methyl α-D-mannopyranoside

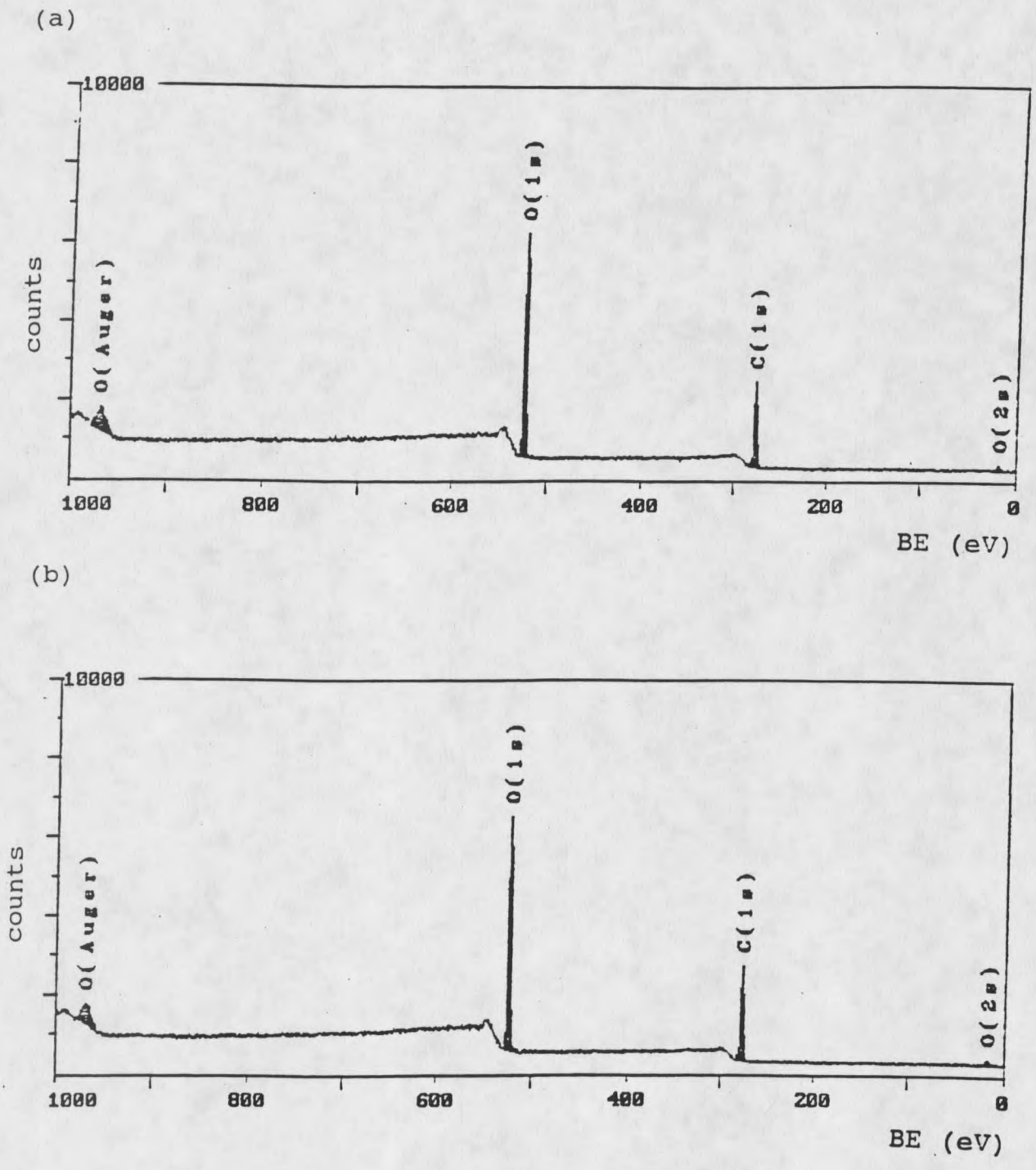

Figure 22. ESCA spectra of (a) cellobiose and (b) maltose

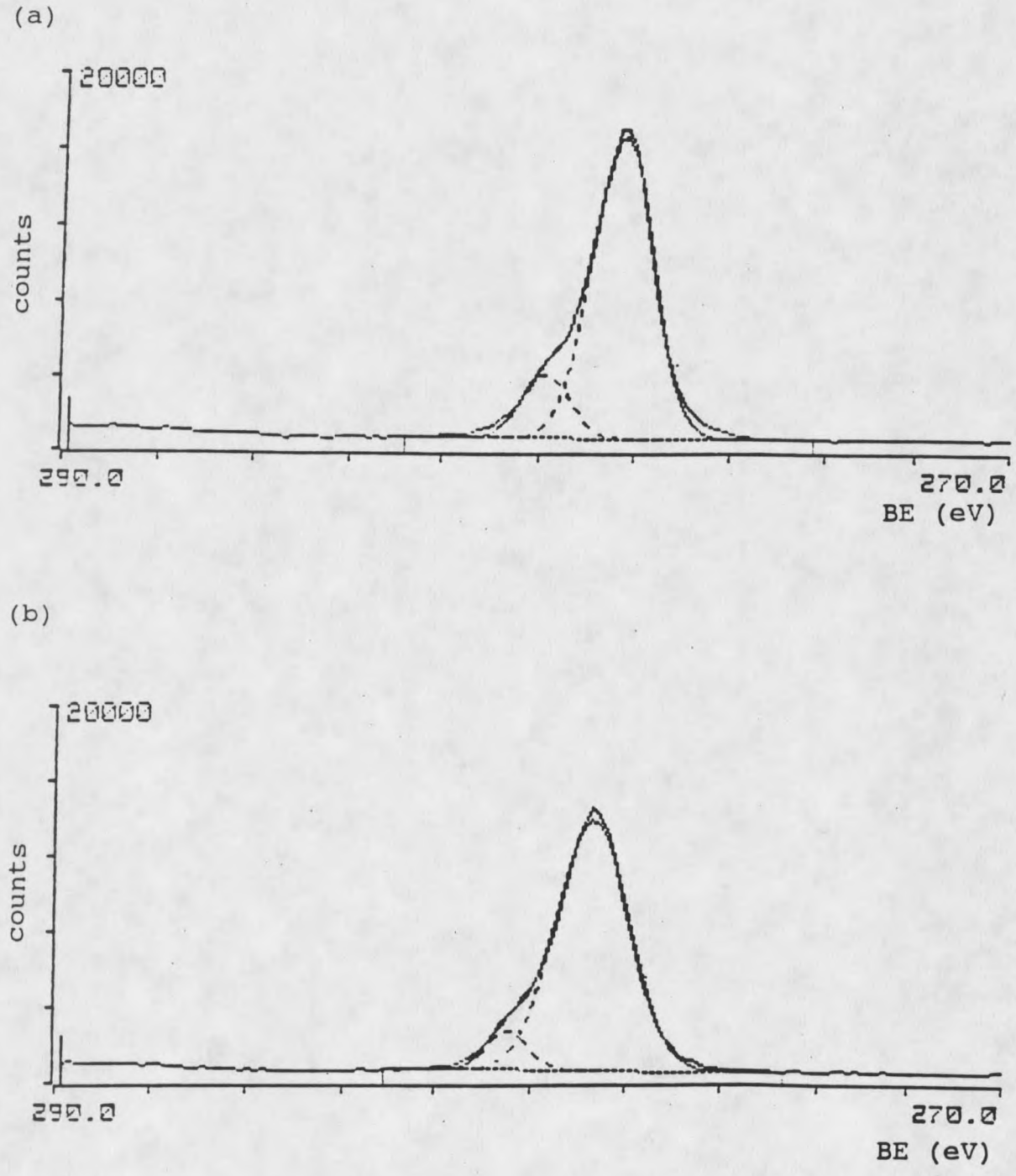

Figure 23. Carbon high resolution peak of (a) cellobiose and (b) maltose

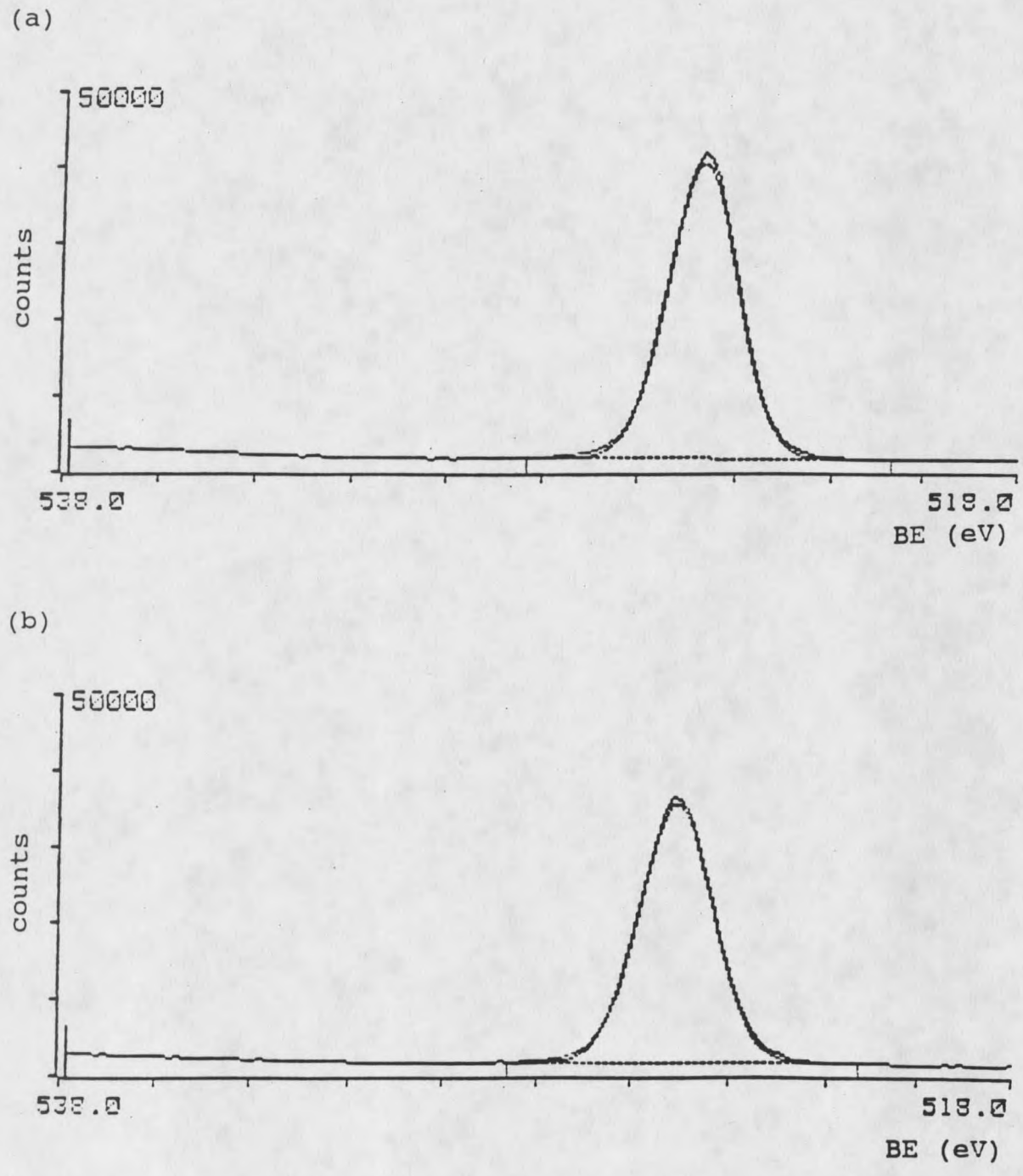

Figure 24. Oxygen high resolution peak of (a) cellobiose and (b) maltose

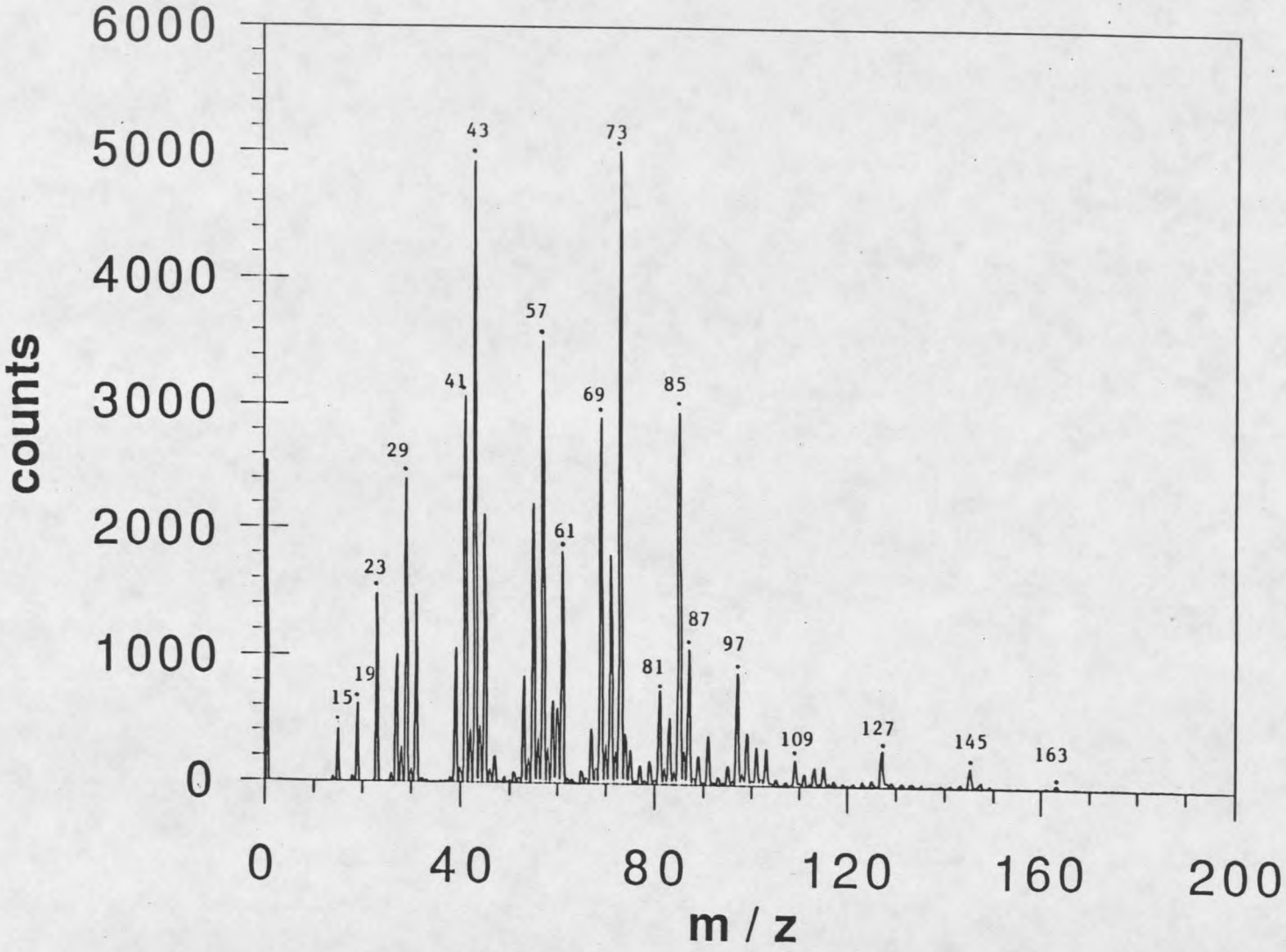

Figure 25. Positive ion static SIMS spectrum of cellobiose

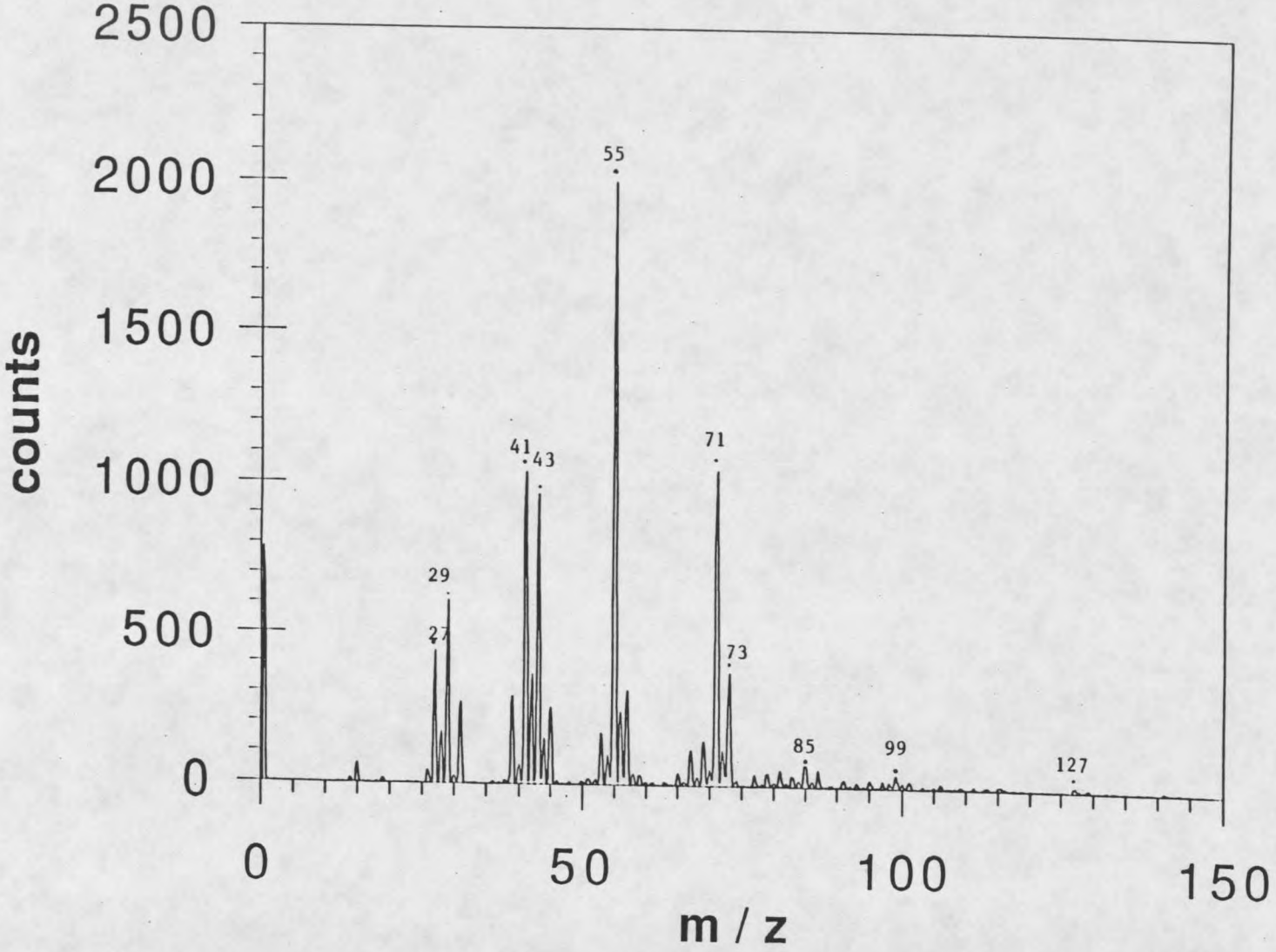

Figure 26. Positive ion static SIMS spectrum of maltose

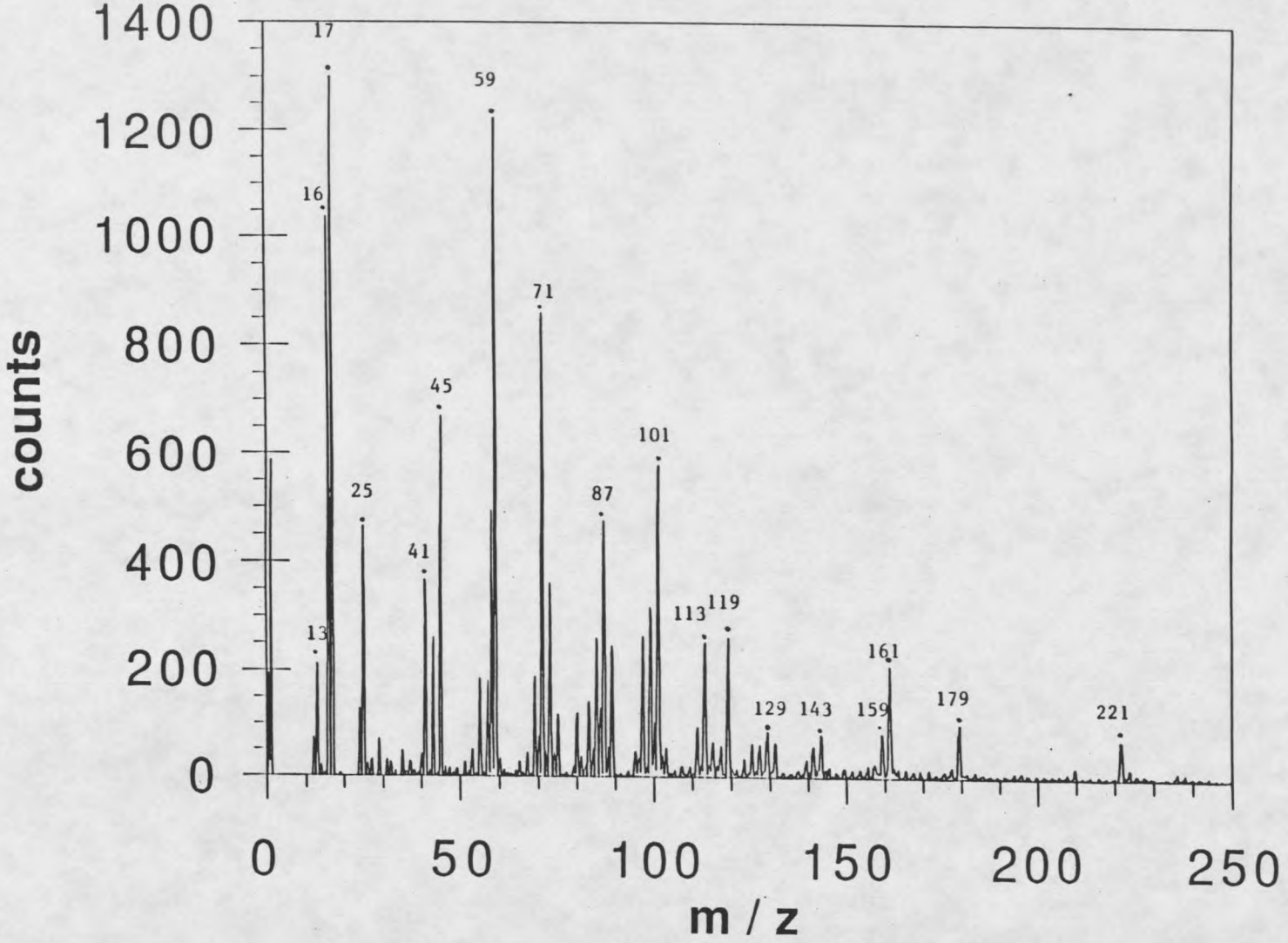

Figure 27. Negative ion static SIMS spectrum of cellobiose

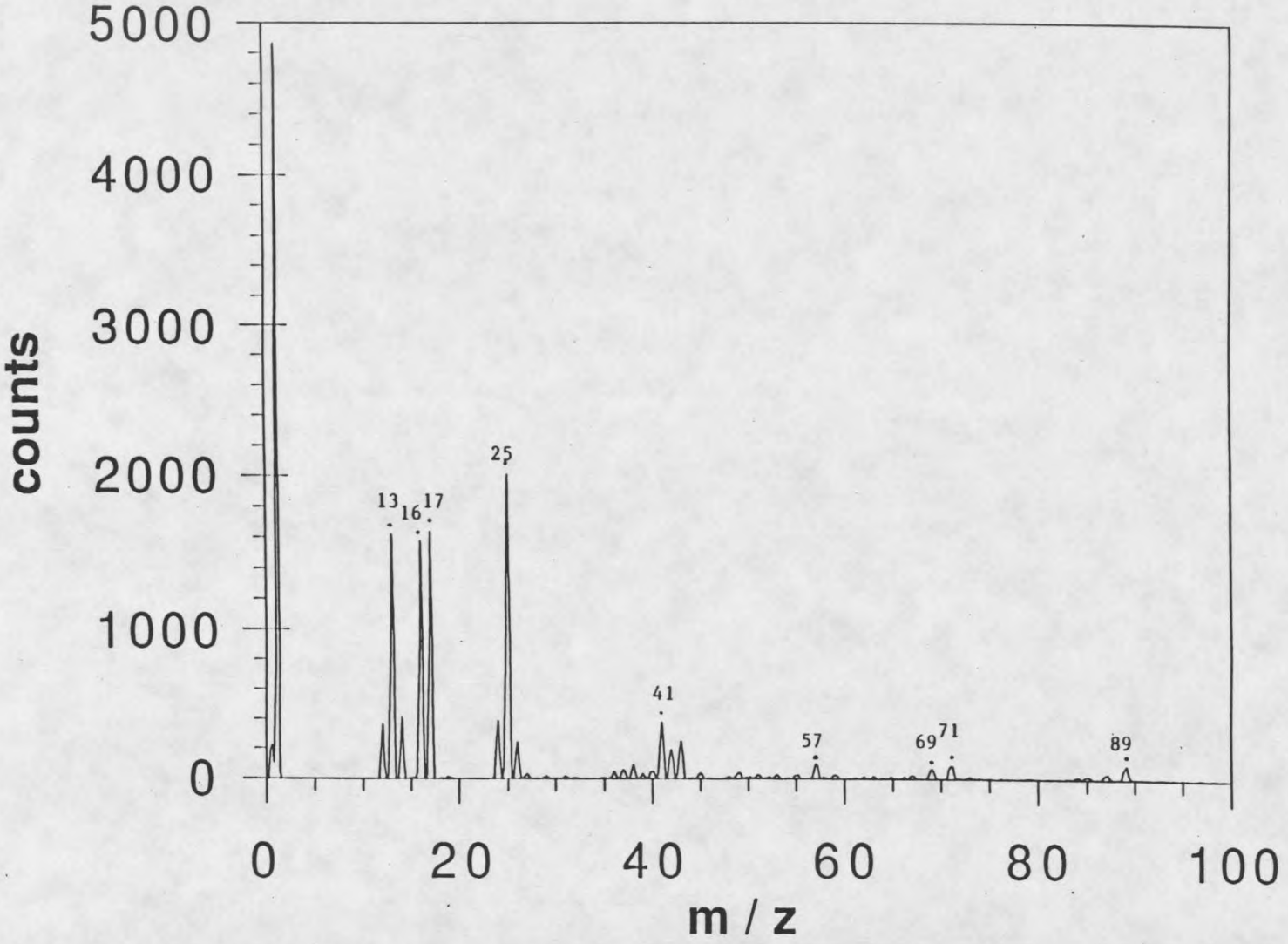

Figure 28. Negative ion static SIMS spectrum of maltose

(a)

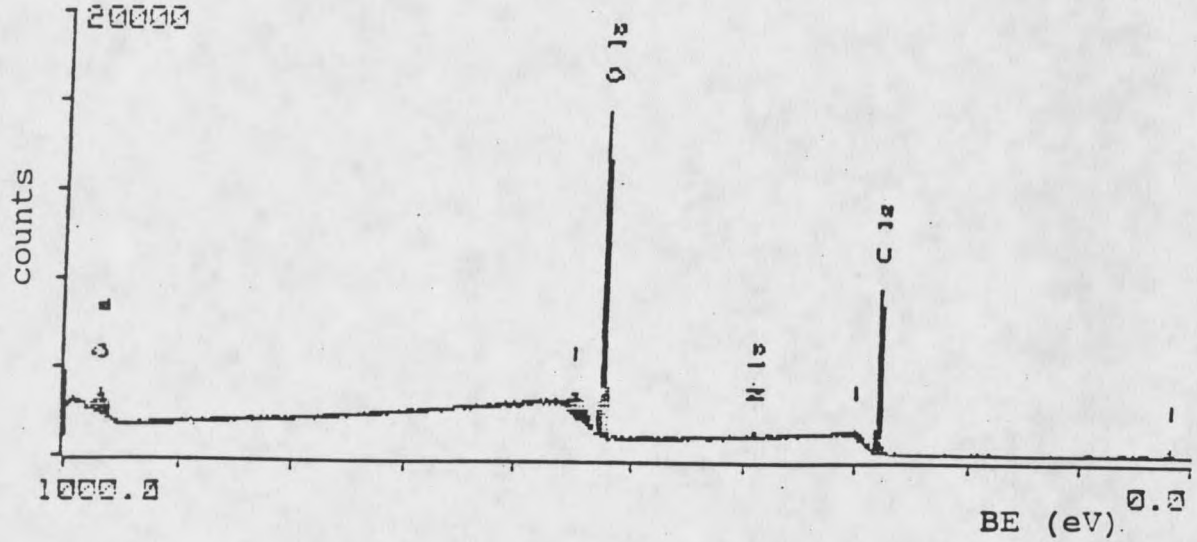

(b)

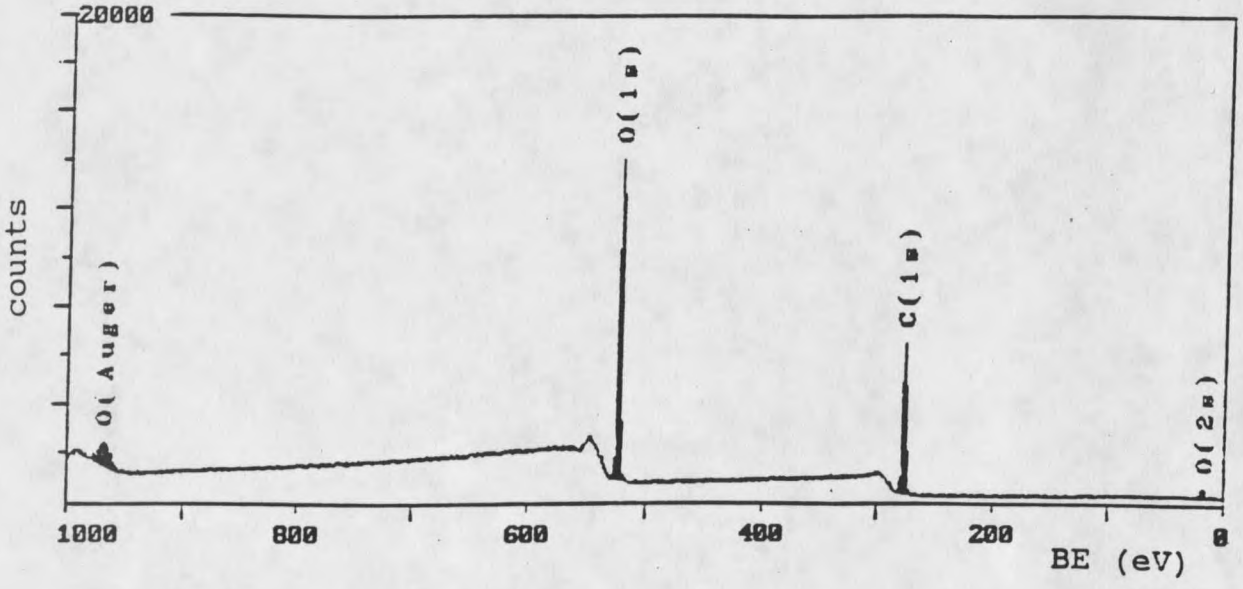

Figure 29. ESCA data of (a) mannan and (b) glucan

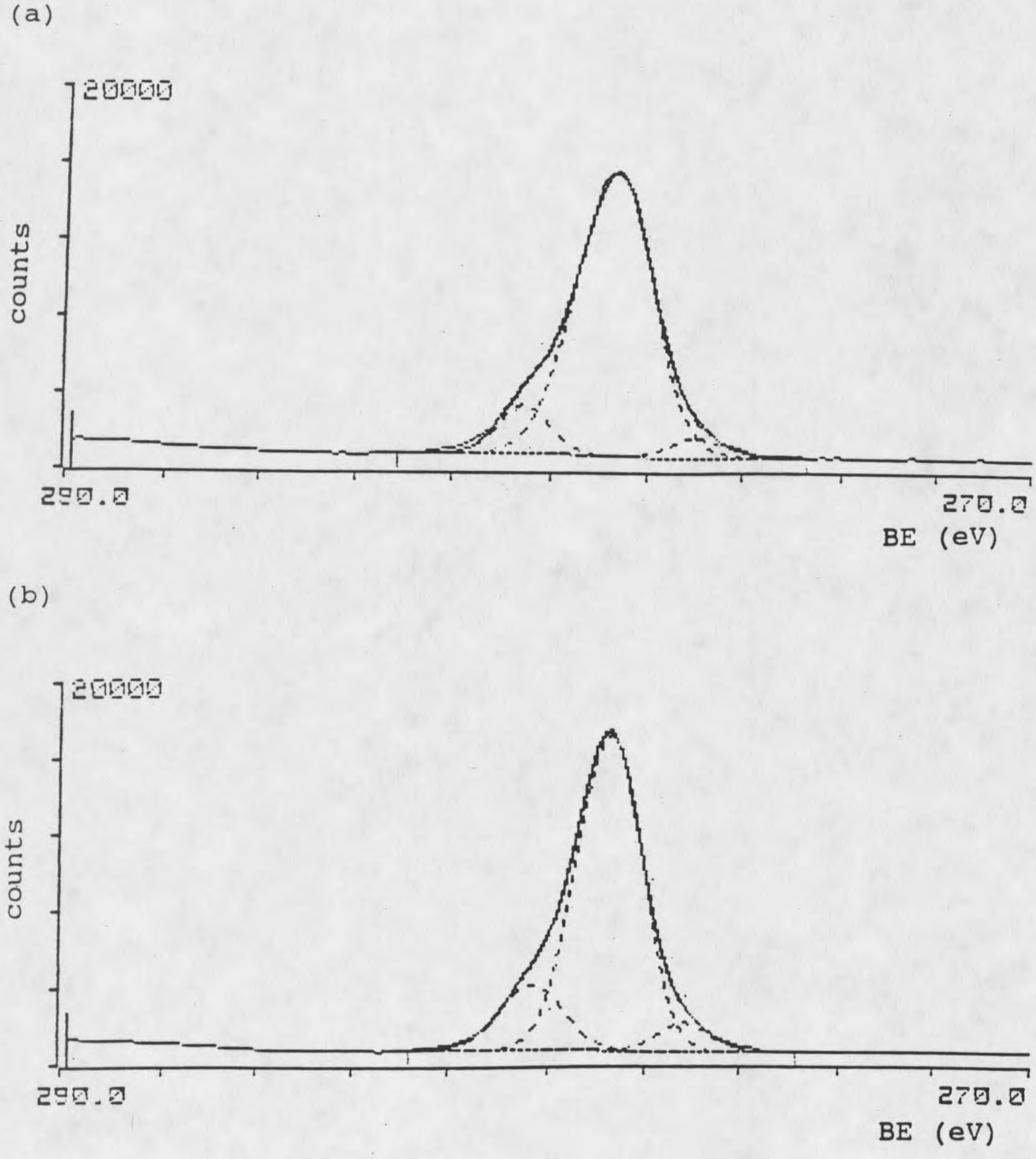

Figure 30. Carbon high resolution peak of (a) mannan and (b) glucan

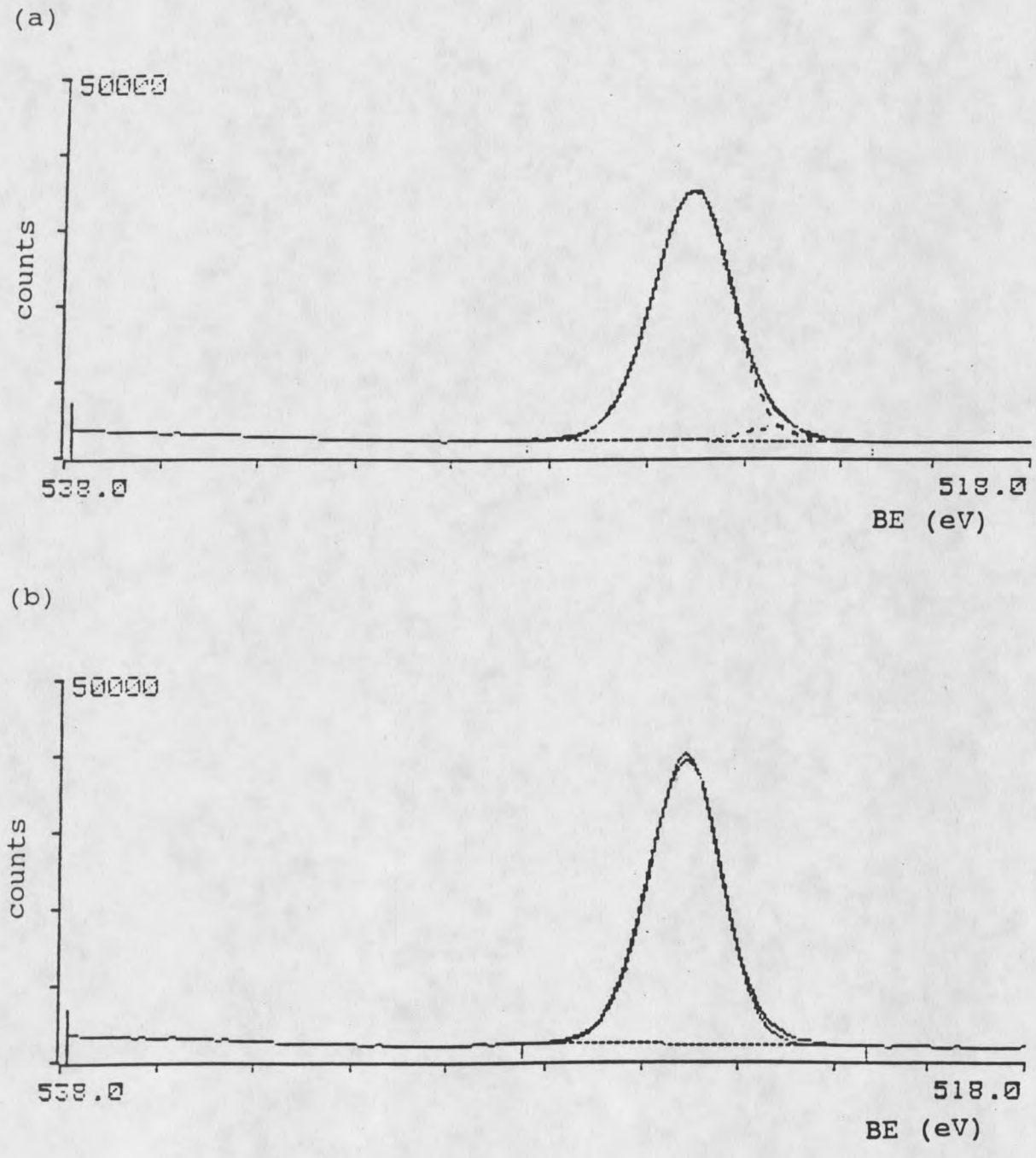

Figure 31. Oxygen high resolution peak of (a) mannan and (b) glucan

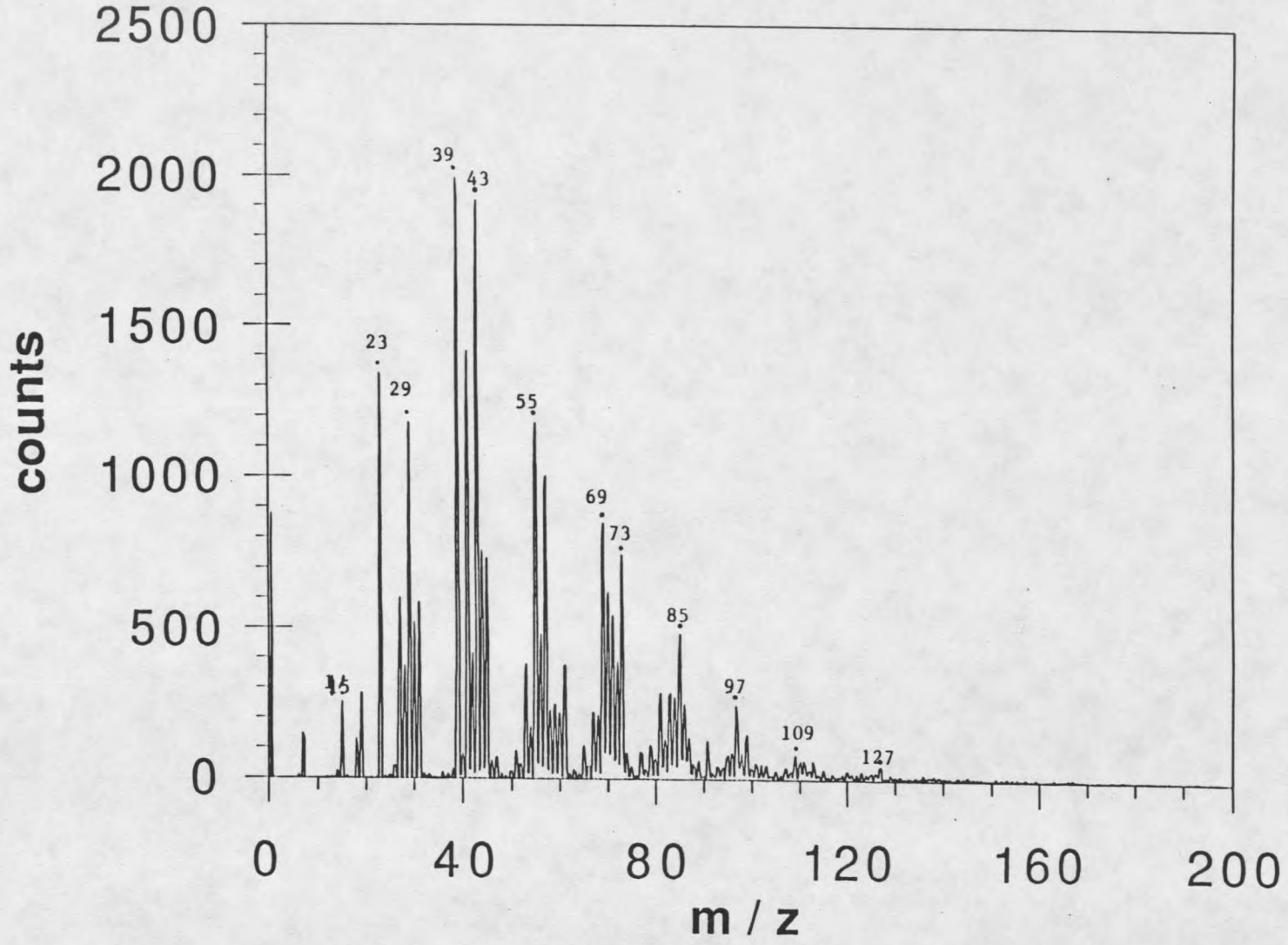

Figure 32. Positive ion static SIMS spectrum of mannan

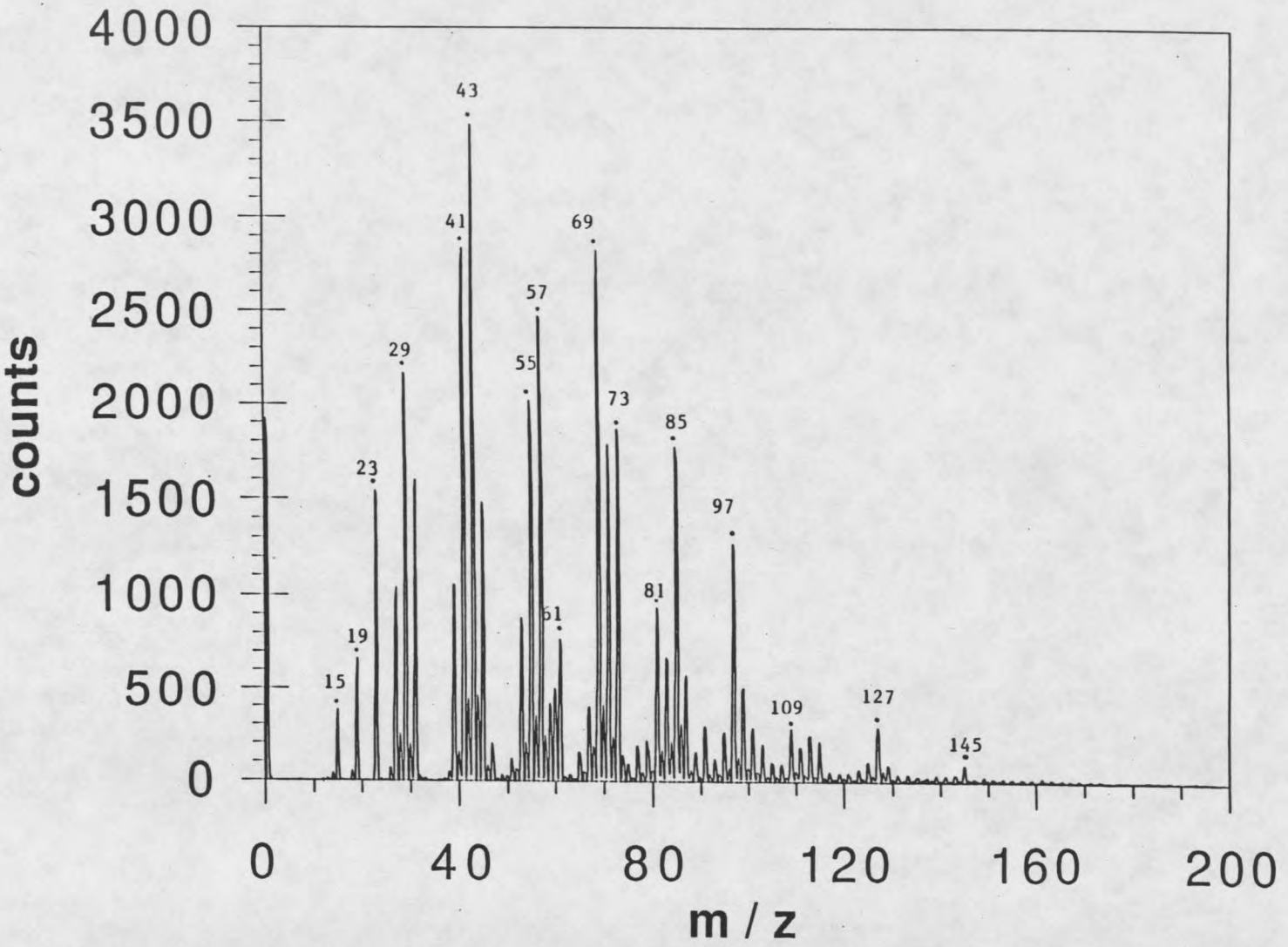

Figure 33. Positive ion static SIMS spectrum of glucan

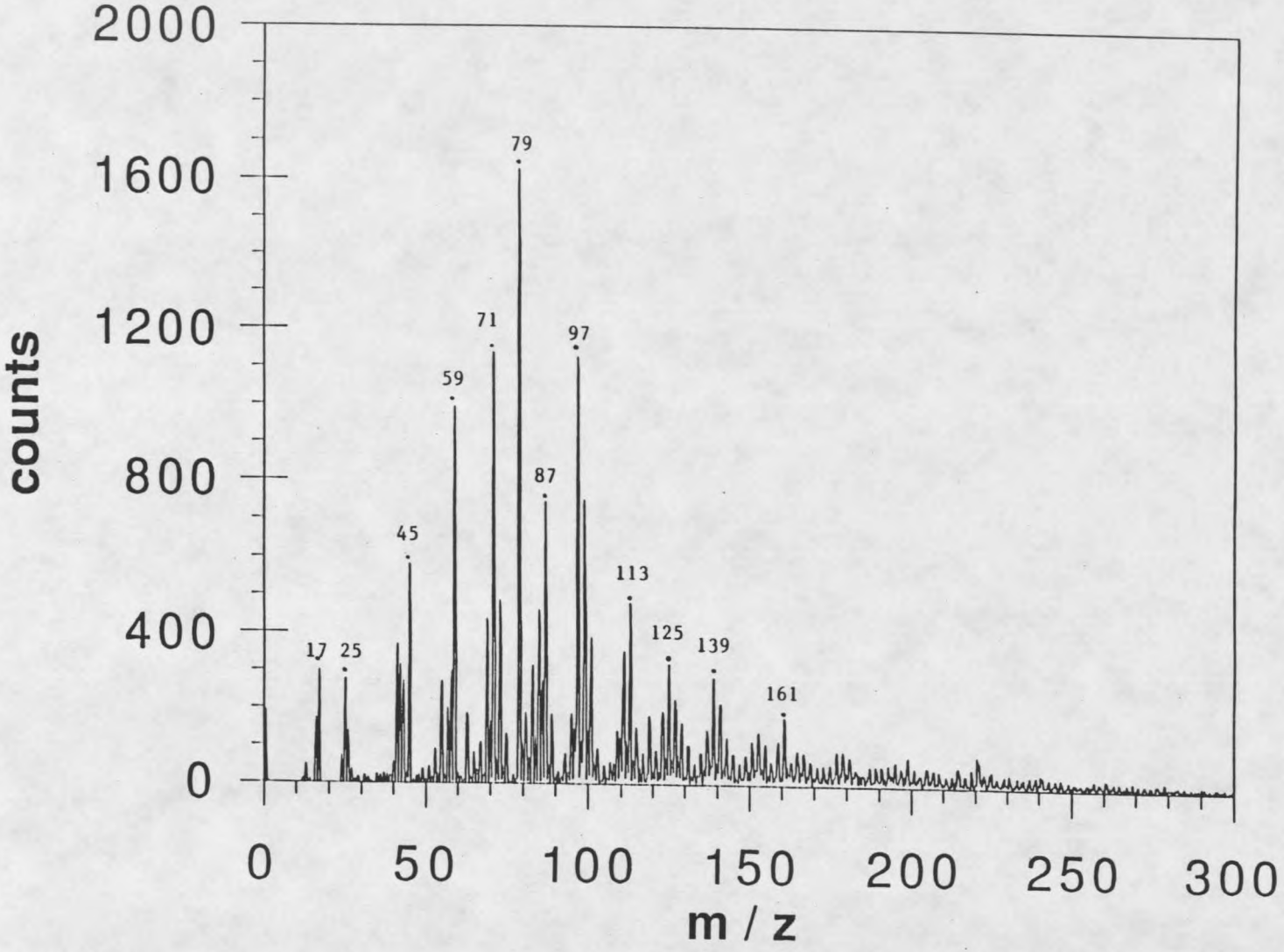

Figure 34. Negative ion static SIMS spectrum of mannan

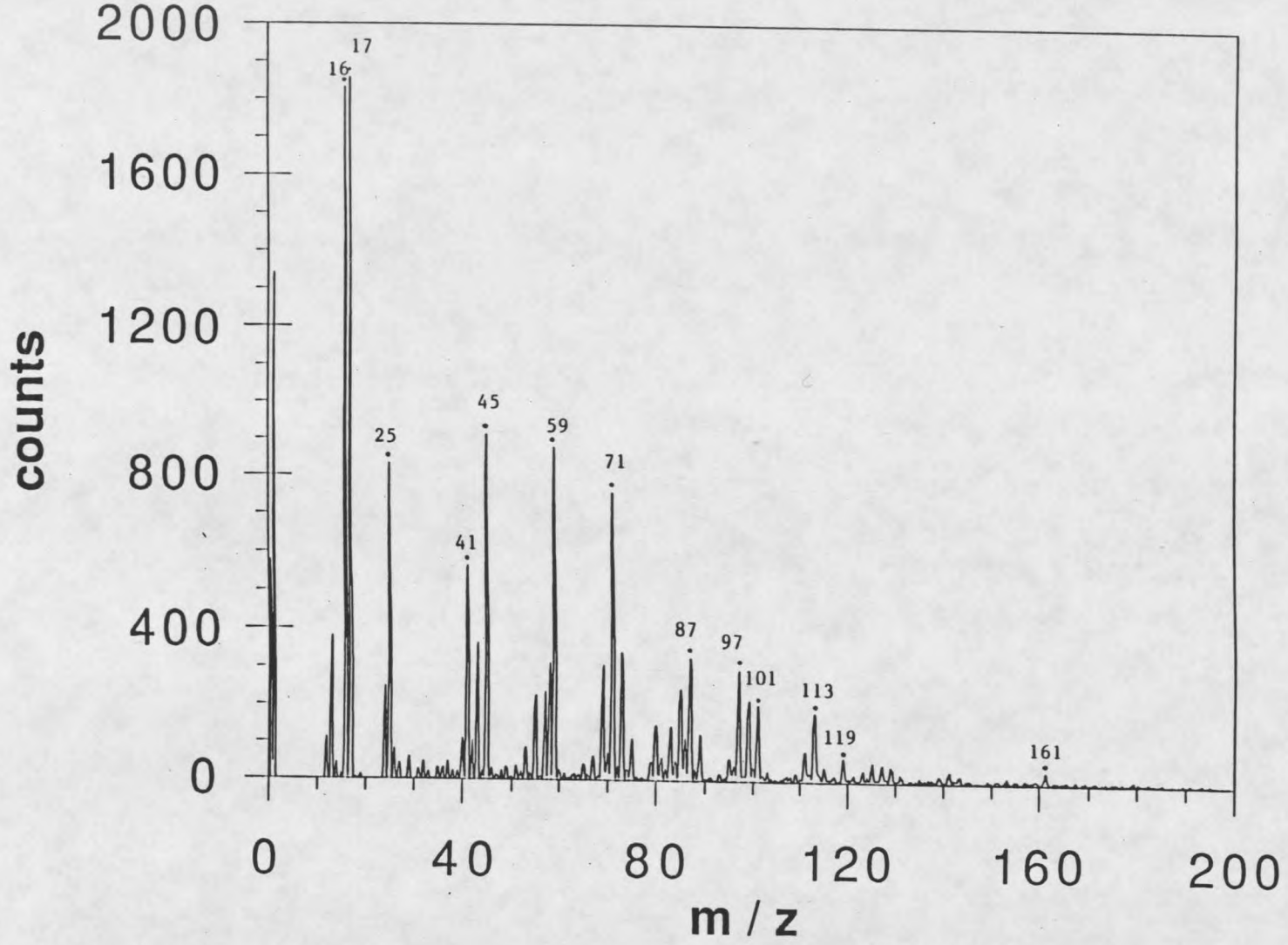

Figure 35. Negative ion static SIMS spectrum of glucan

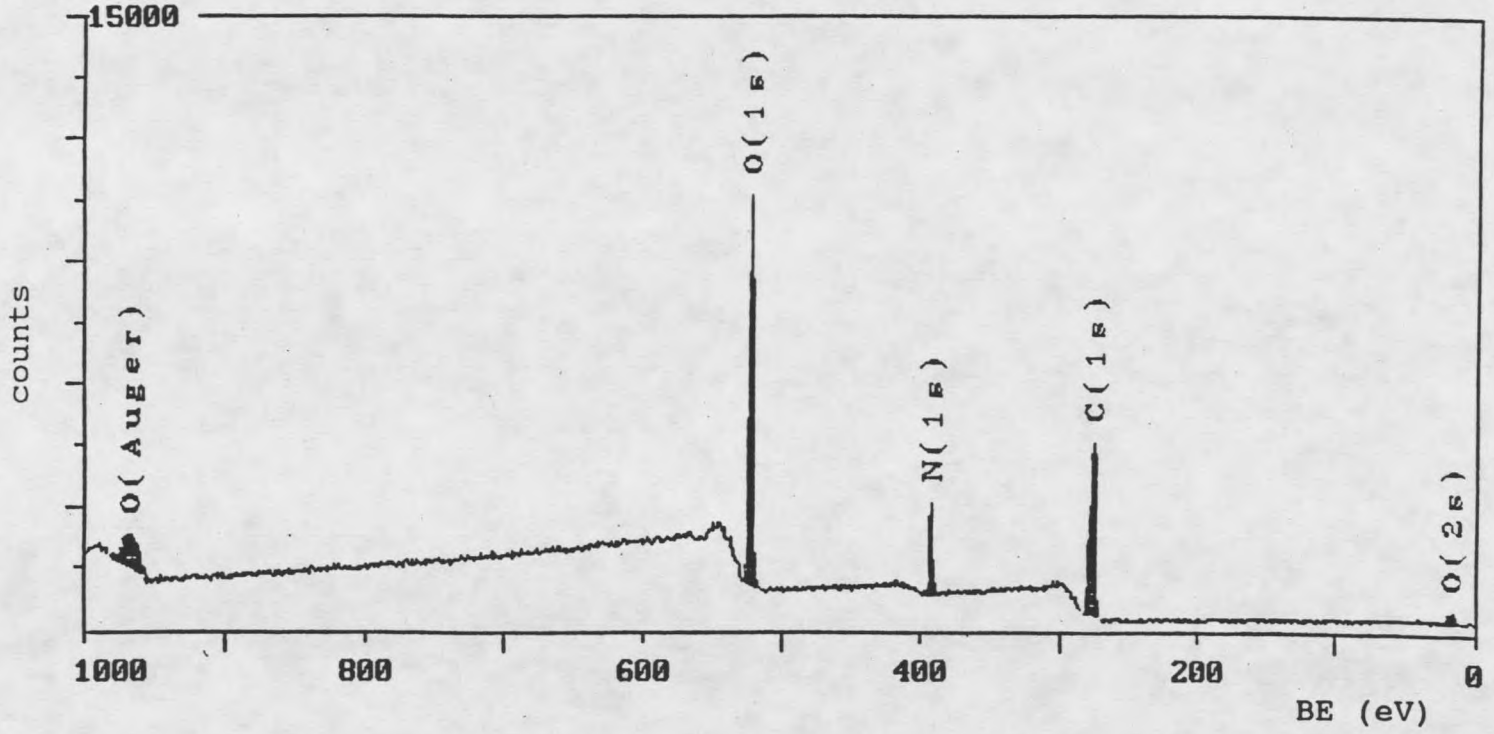

Figure 36. ESCA spectrum of glutamic acid

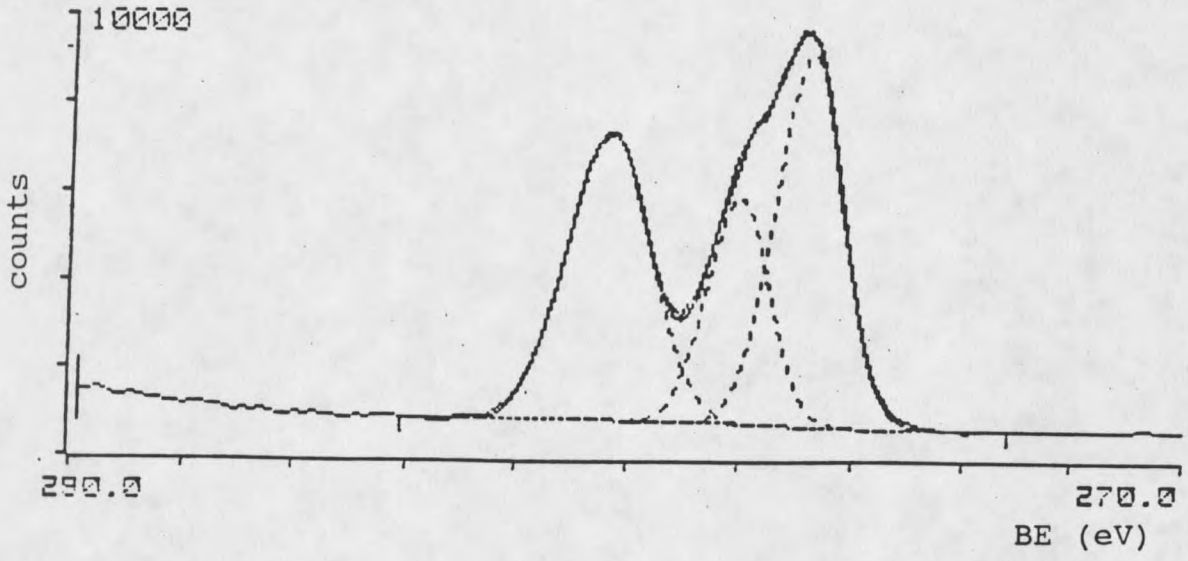

Figure 37. Carbon high resolution peak of glutamic acid

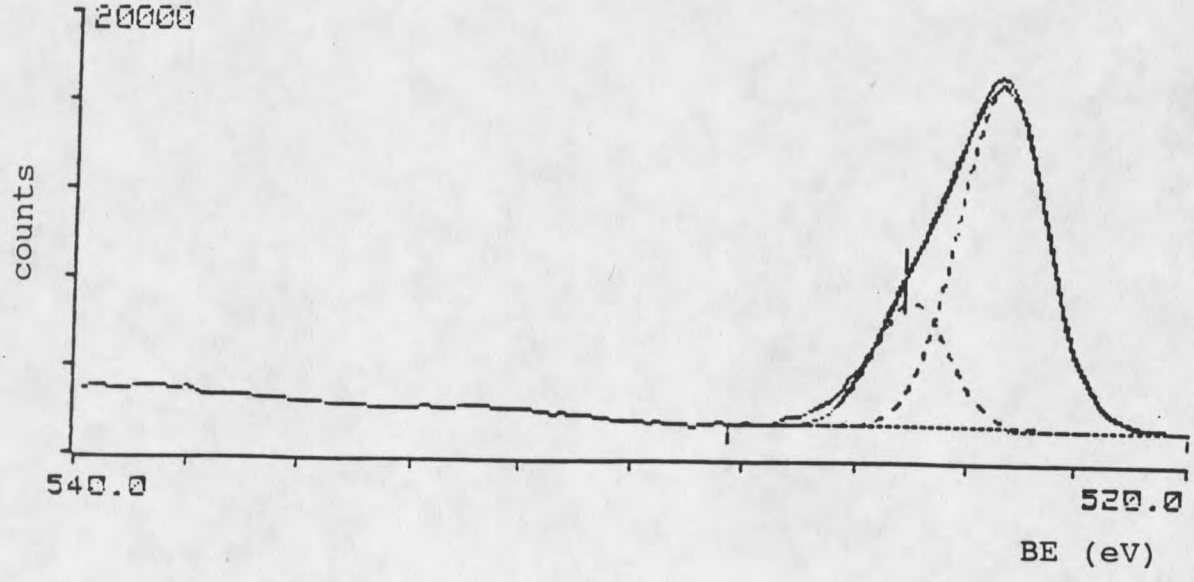

Figure 38. Oxygen high resolution peak of glutamic acid

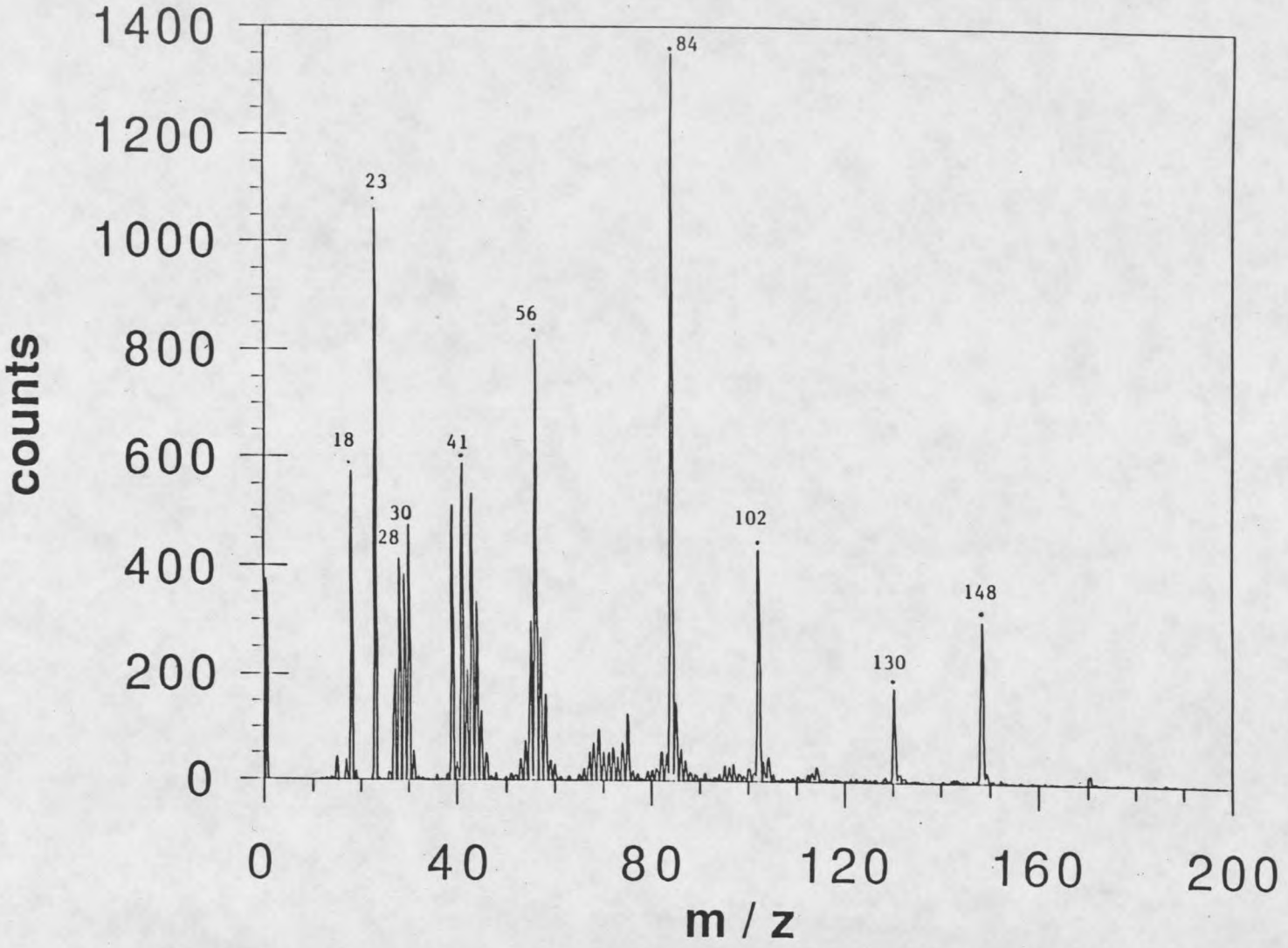

Figure 39. Positive ion static SIMS spectrum of glutamic acid

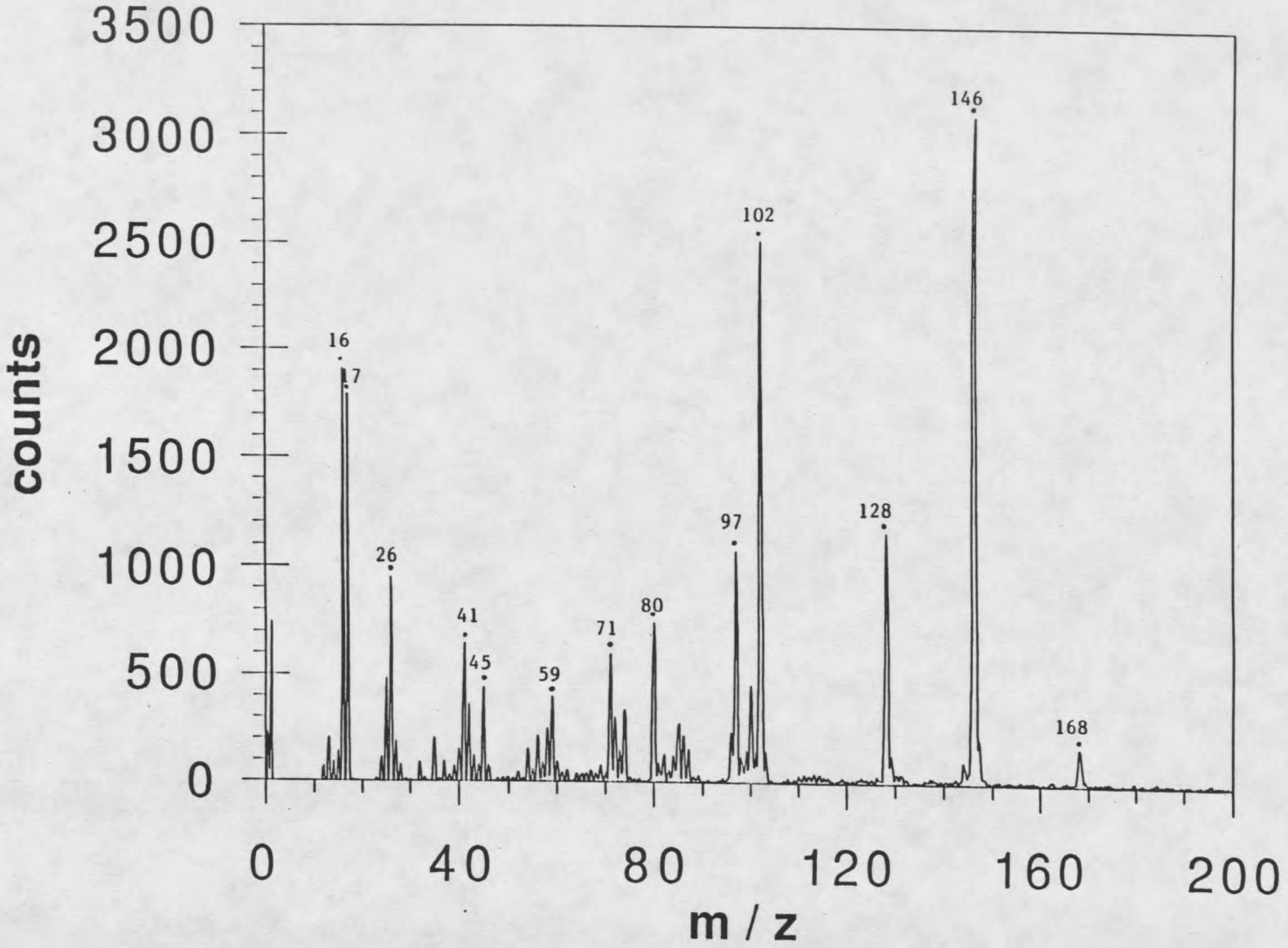

Figure 40. Negative ion static SIMS spectrum of glutamic acid

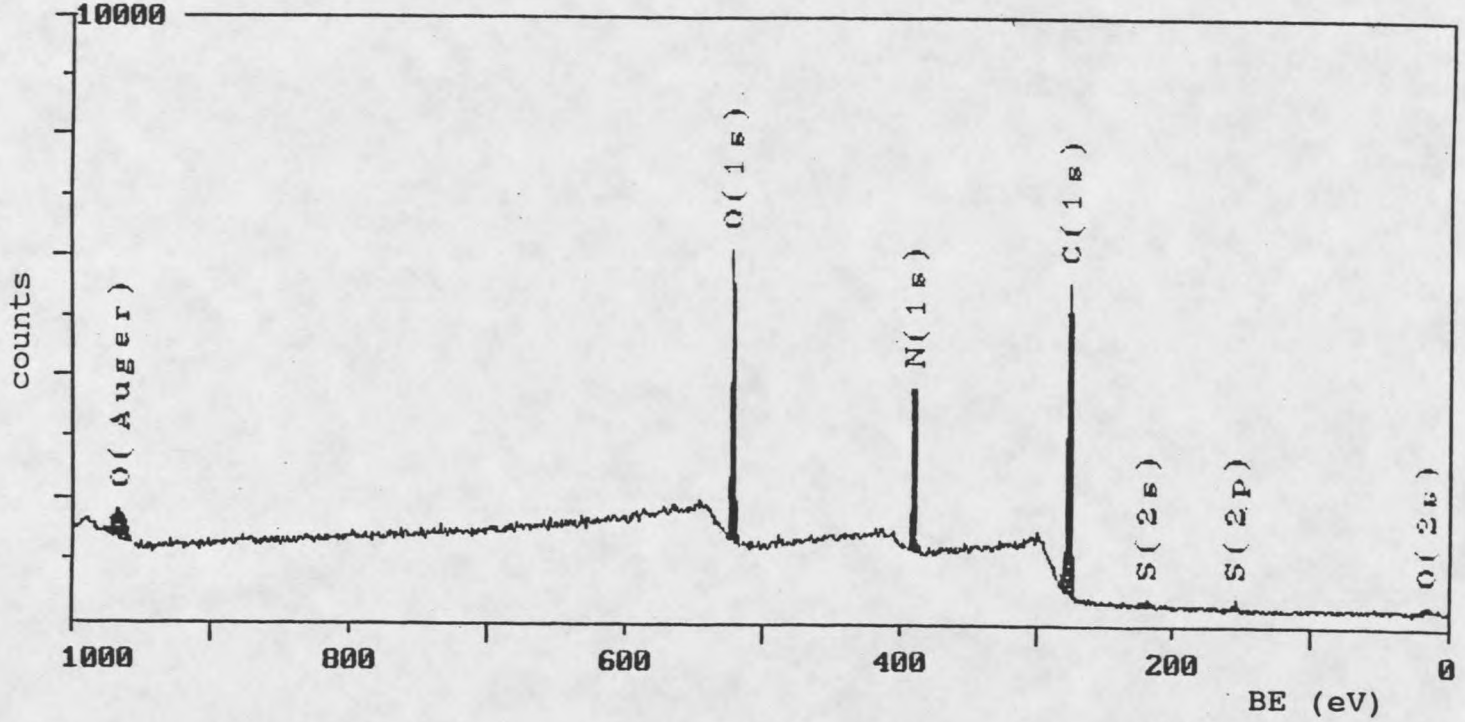

Figure 41. ESCA spectrum of albumin bulk film

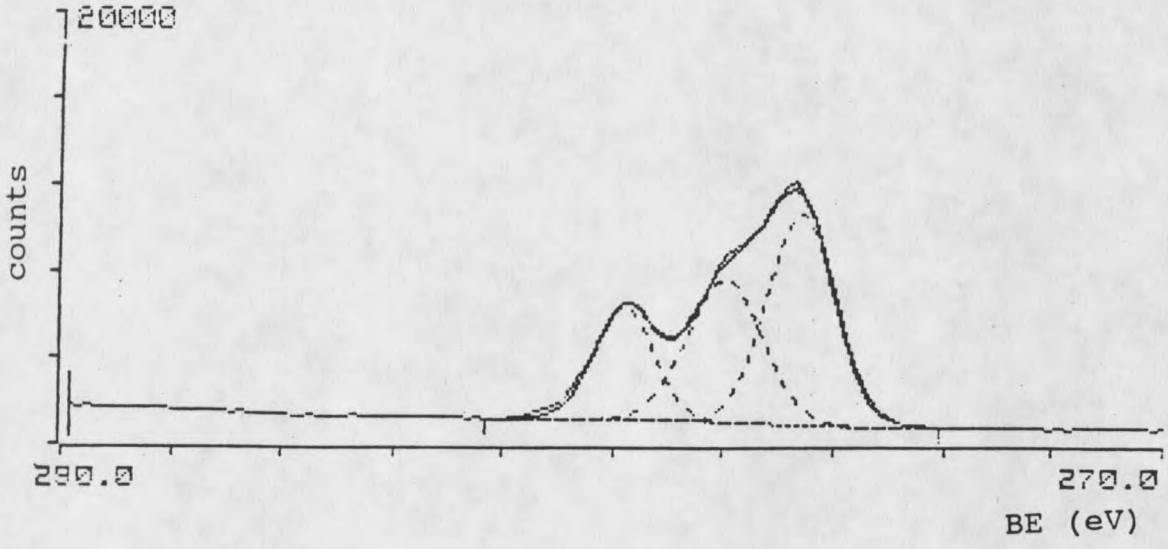

Figure 42. Carbon high resolution peak of albumin bulk film

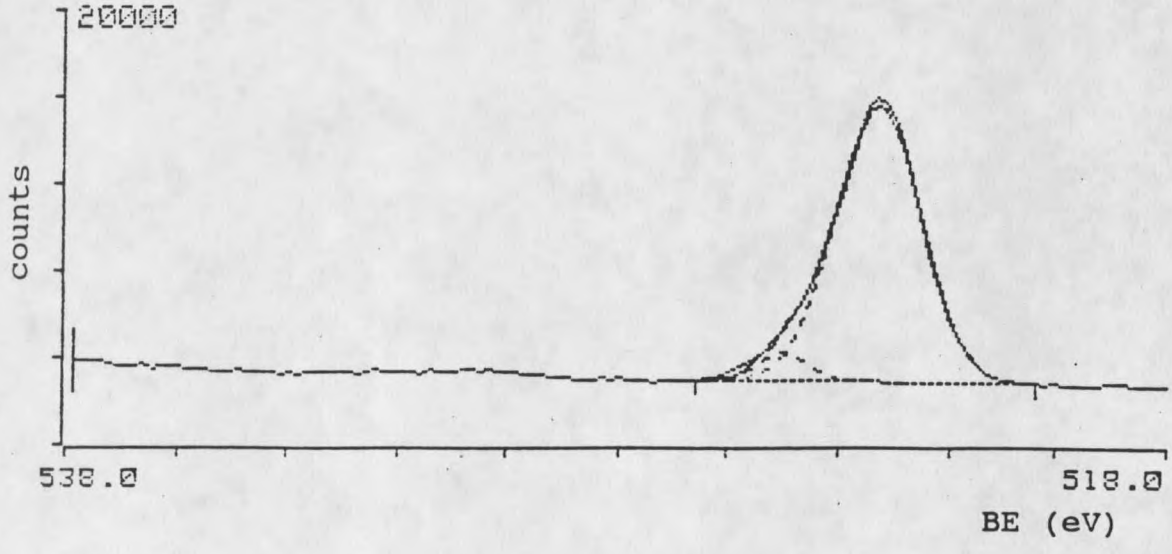

Figure 43. Oxygen high resolution peak of albumin bulk film

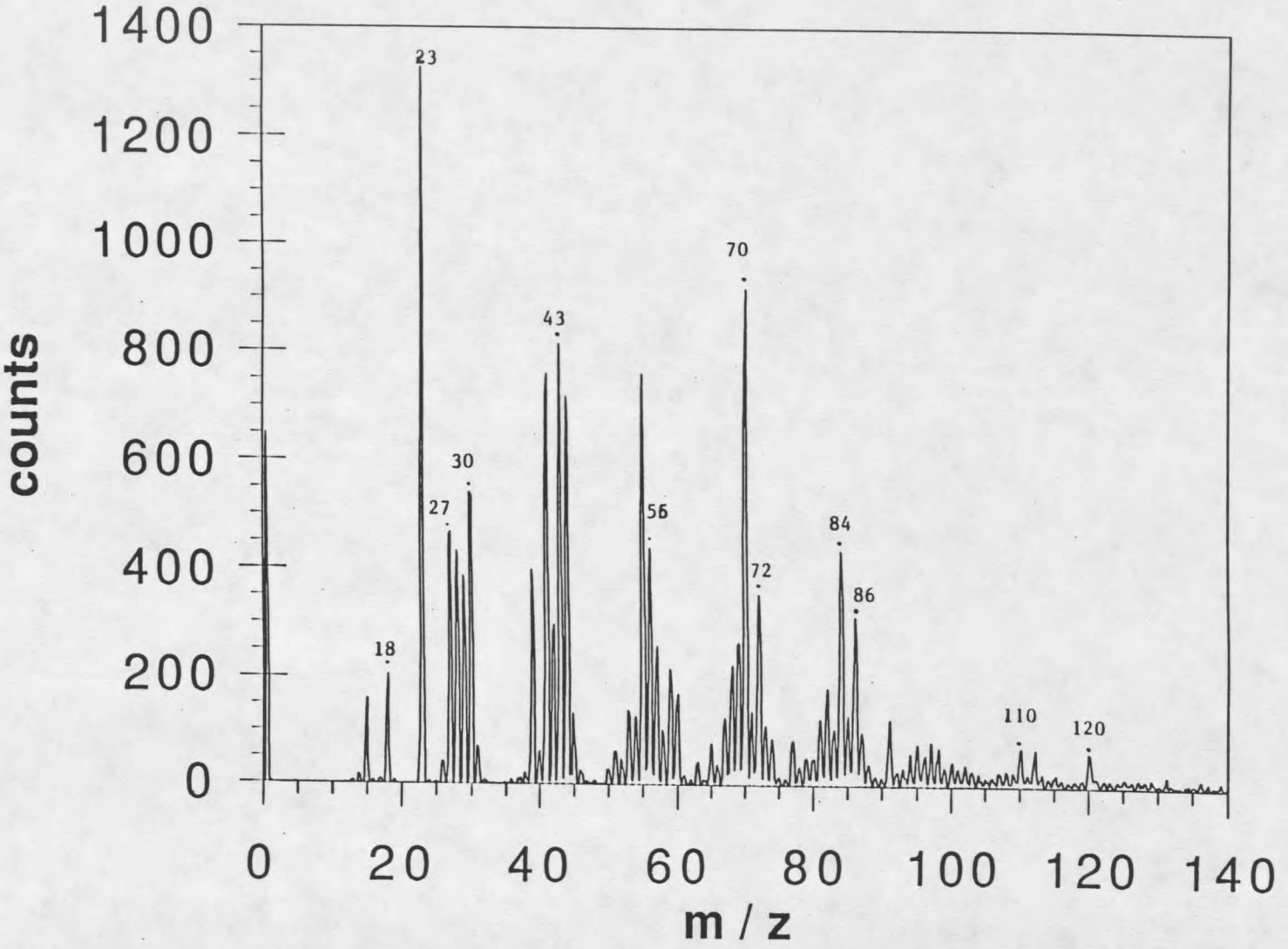

Figure 44. Positive ion static SIMS spectrum of albumin bulk film

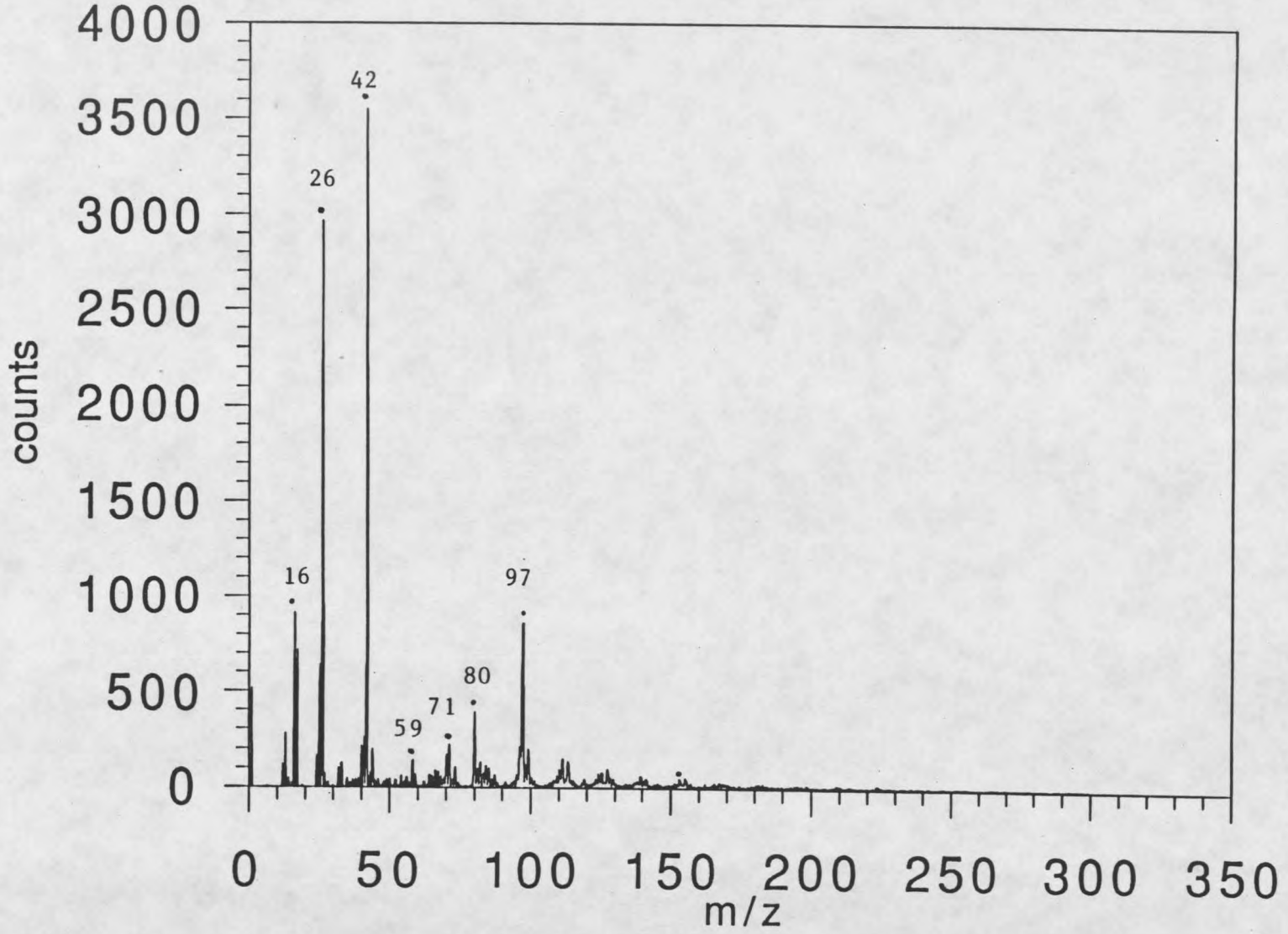

Figure 45. Negative ion static SIMS spectrum of albumin bulk film

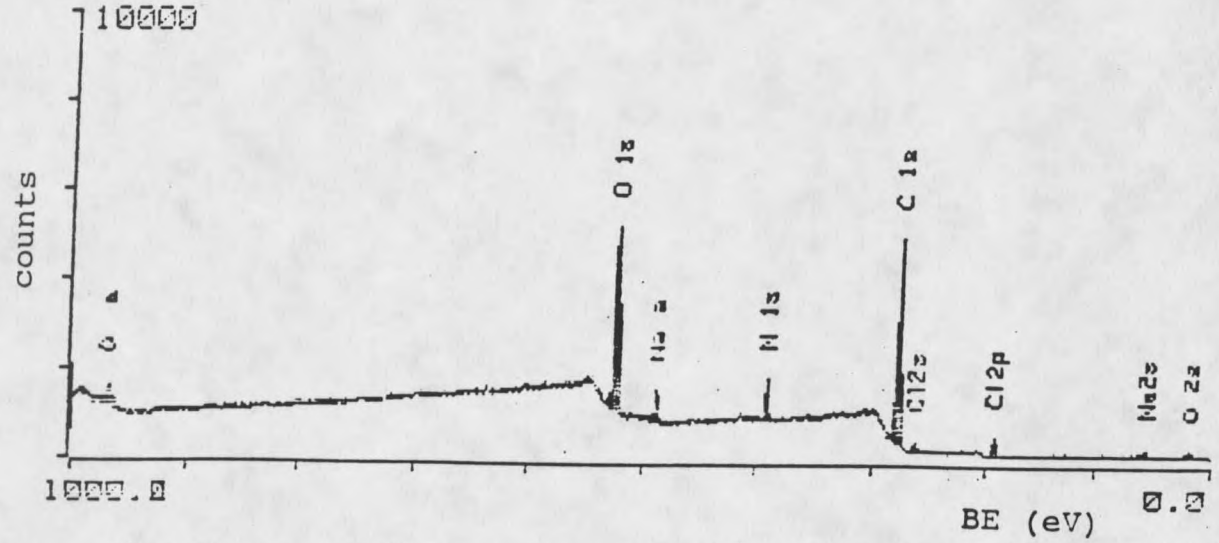

Figure 46. ESCA spectrum of adsorbed albumin

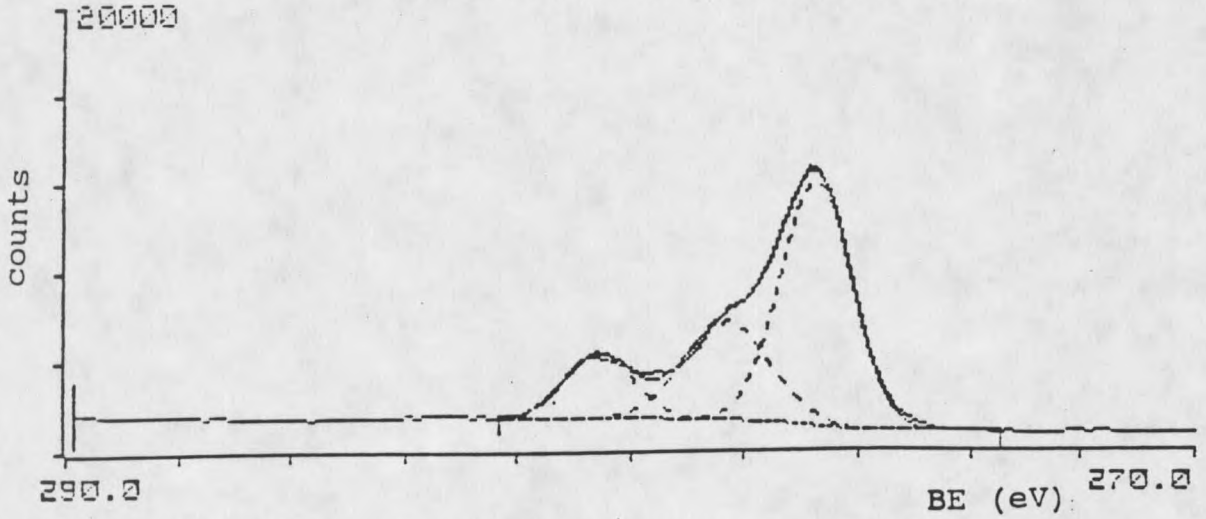

Figure 47. Carbon high resolution peak of adsorbed albumin

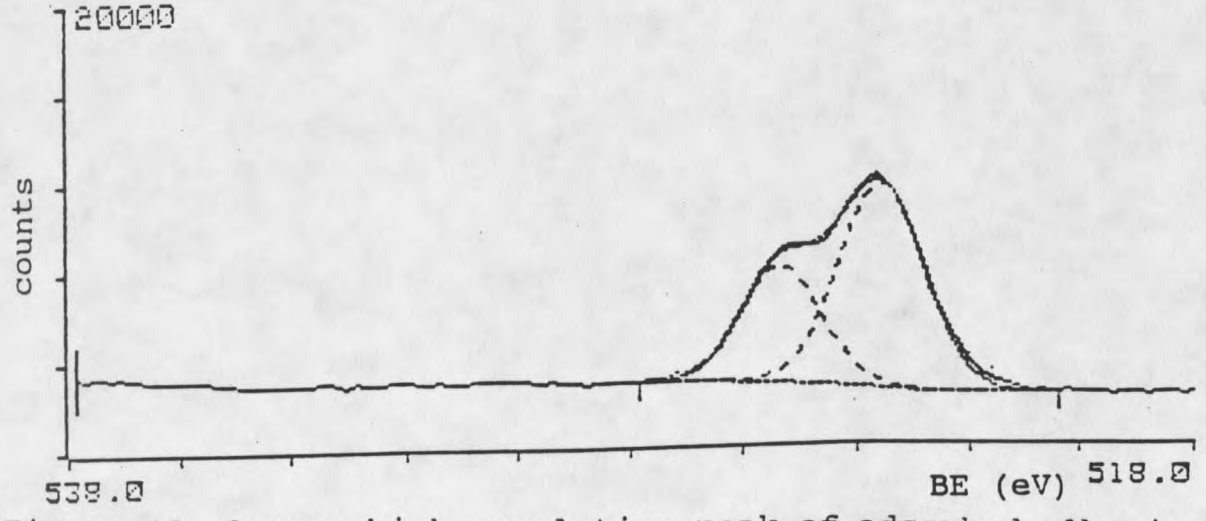

Figure 48. Oxygen high resolution peak of adsorbed albumin

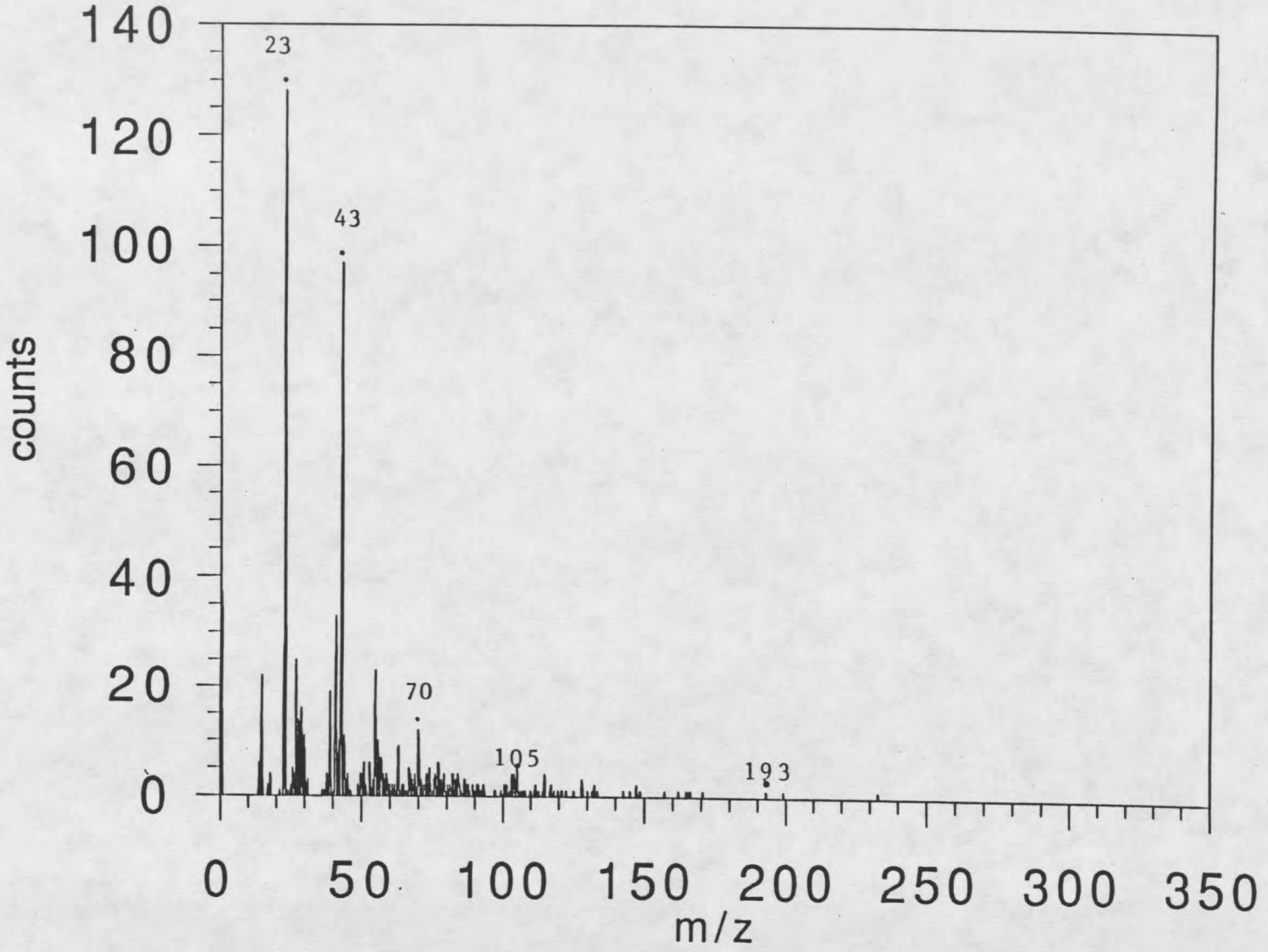

Figure 49. Positive ion static SIMS spectrum of adsorbed albumin

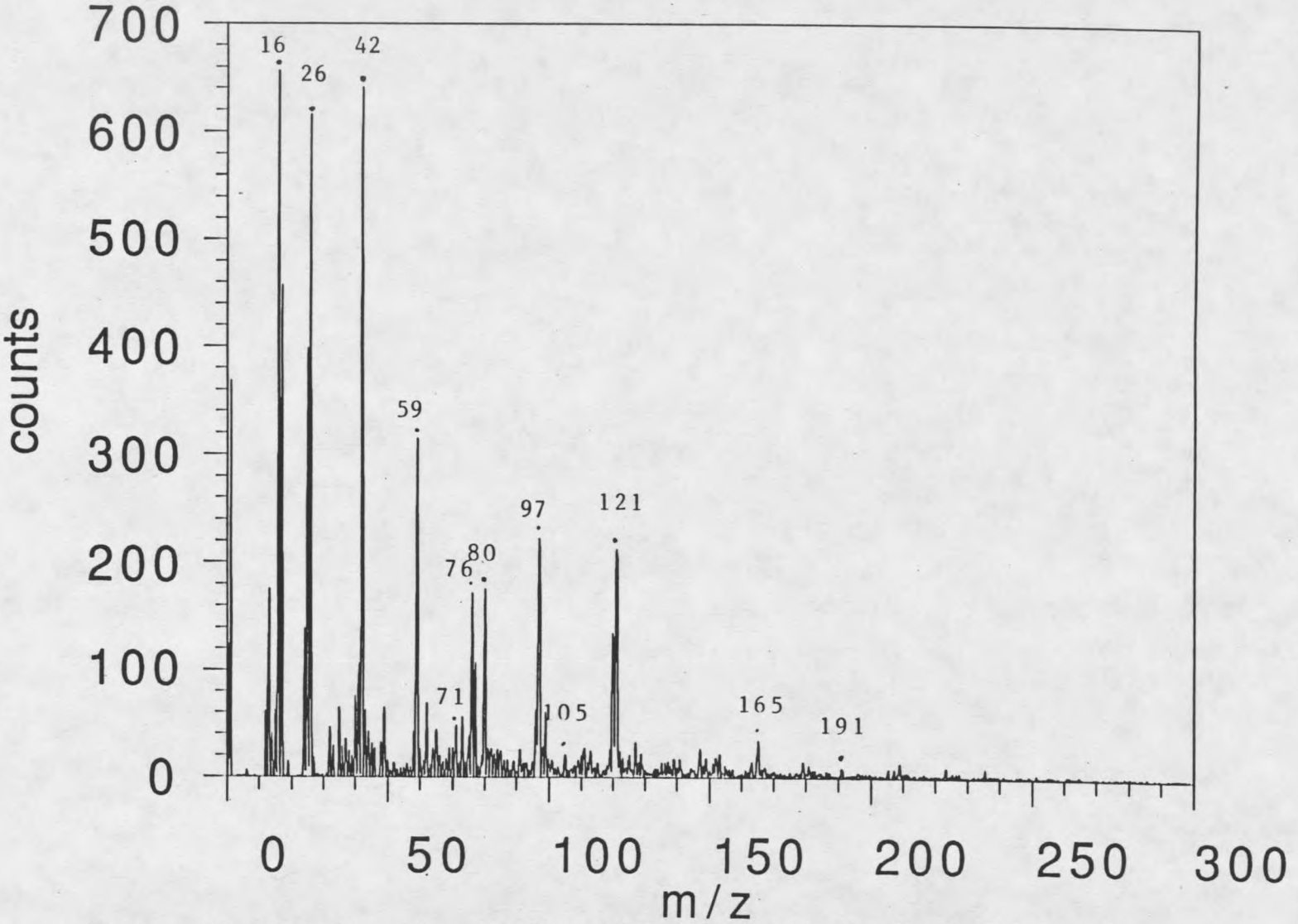

Figure 50. Negative ion static SIMS spectrum of adsorbed albumin

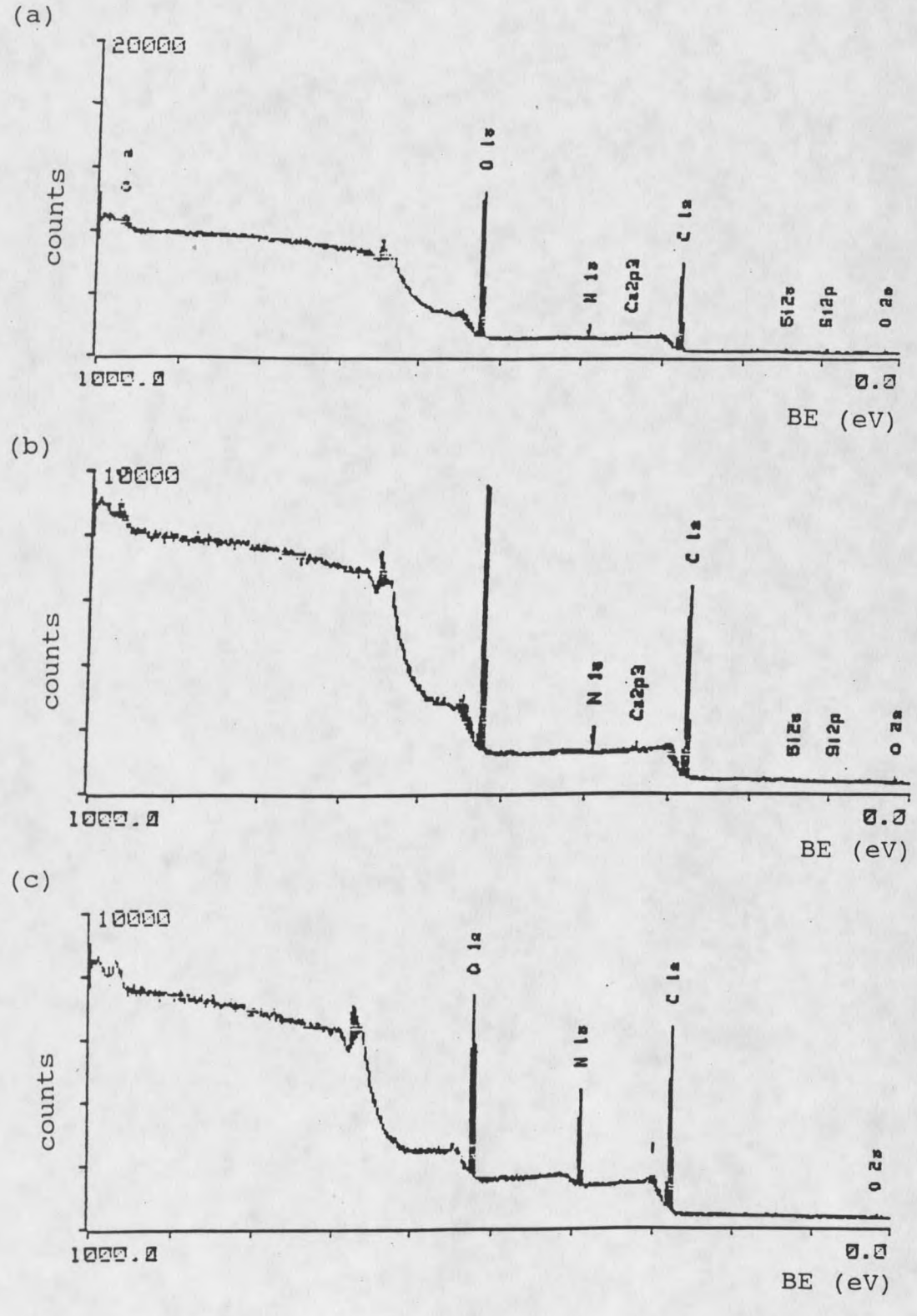

Figure 51. ESCA spectrum of (a) AgH9, (b) AgC6 and (c) crude antigen

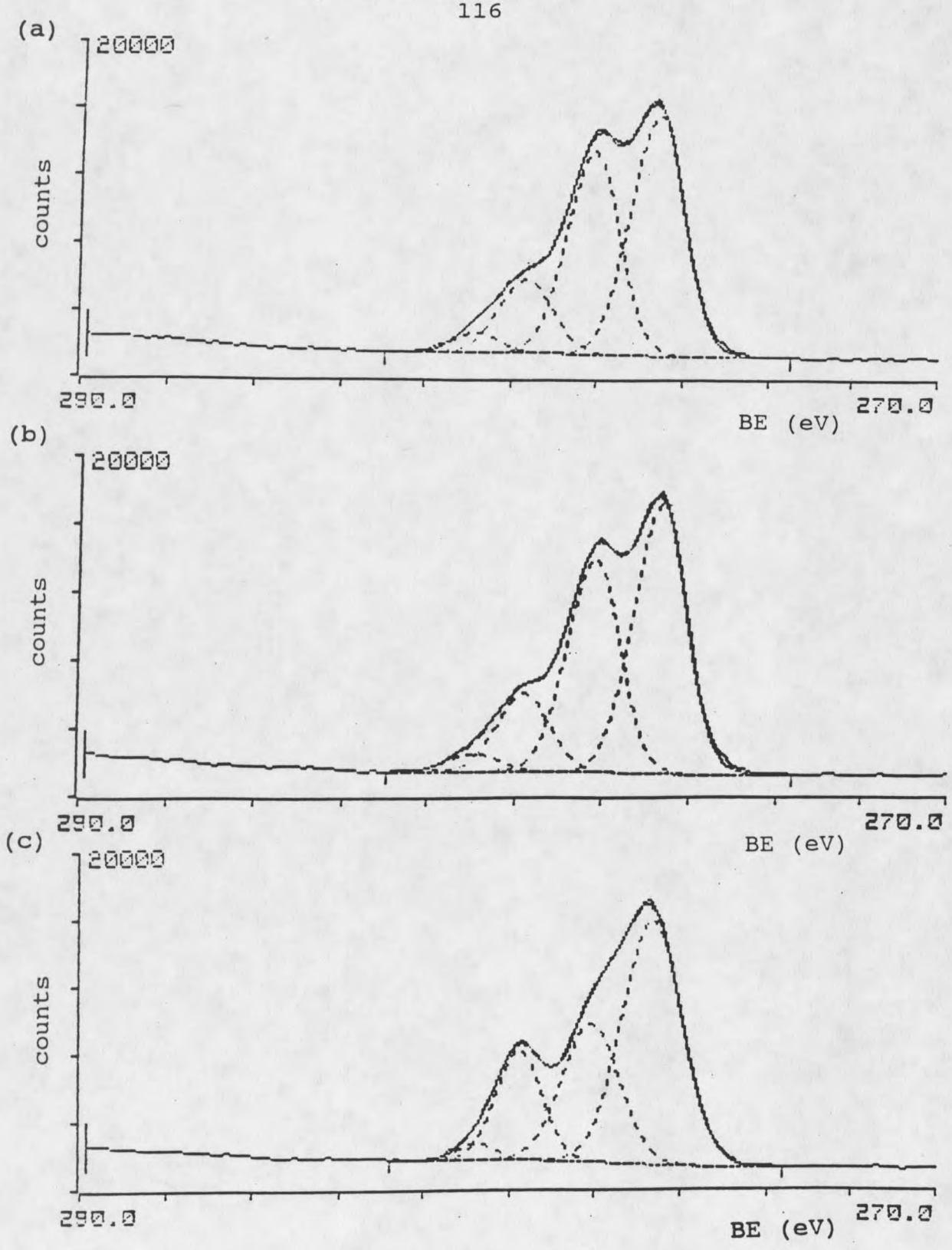

Figure 52. Carbon high resolution peak of (a) AgH9, (b) AgC6 and (c) crude antigen

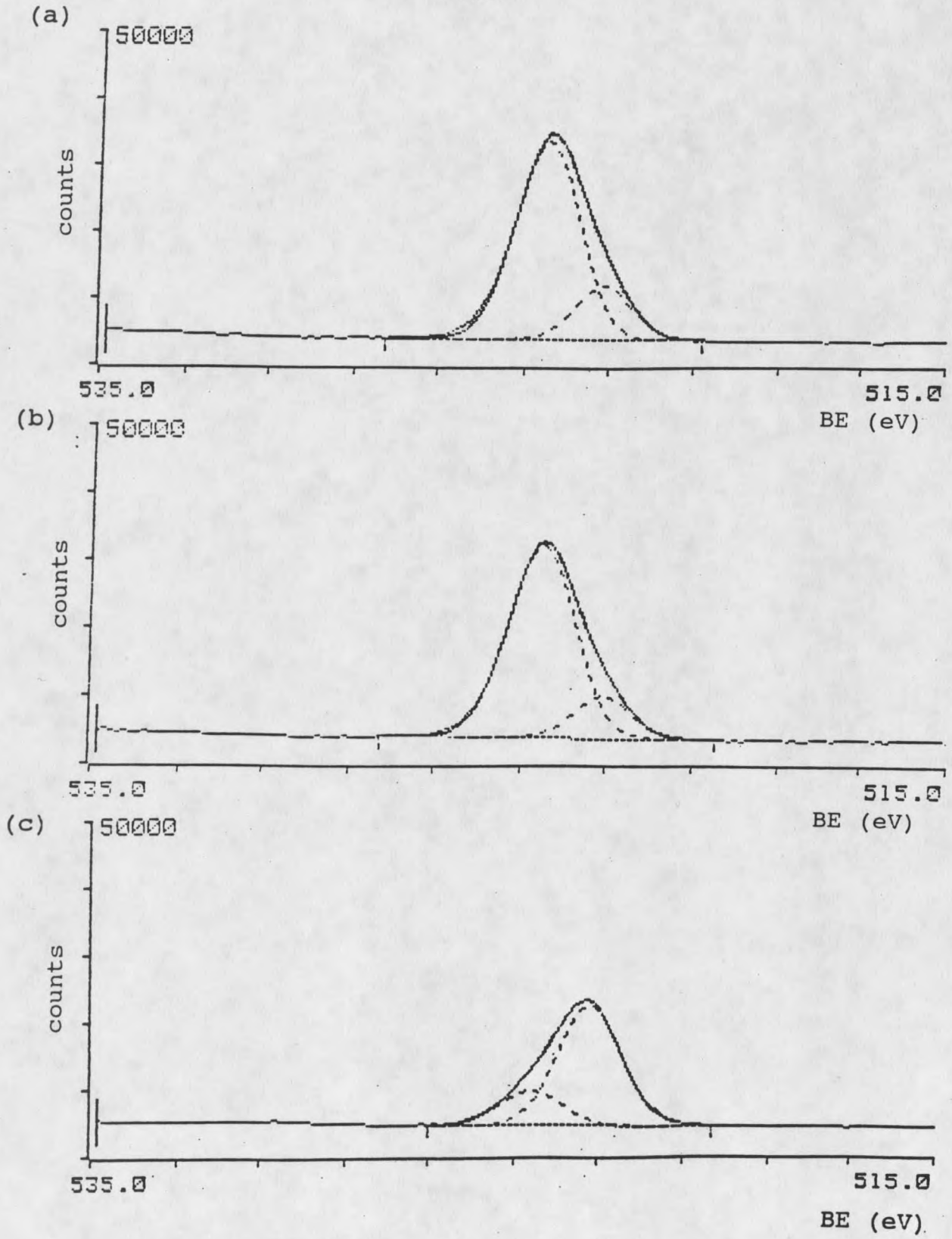

Figure 53. Oxygen high resolution peak of (a) AgH9, (b) AgC6 and (c) crude antigen

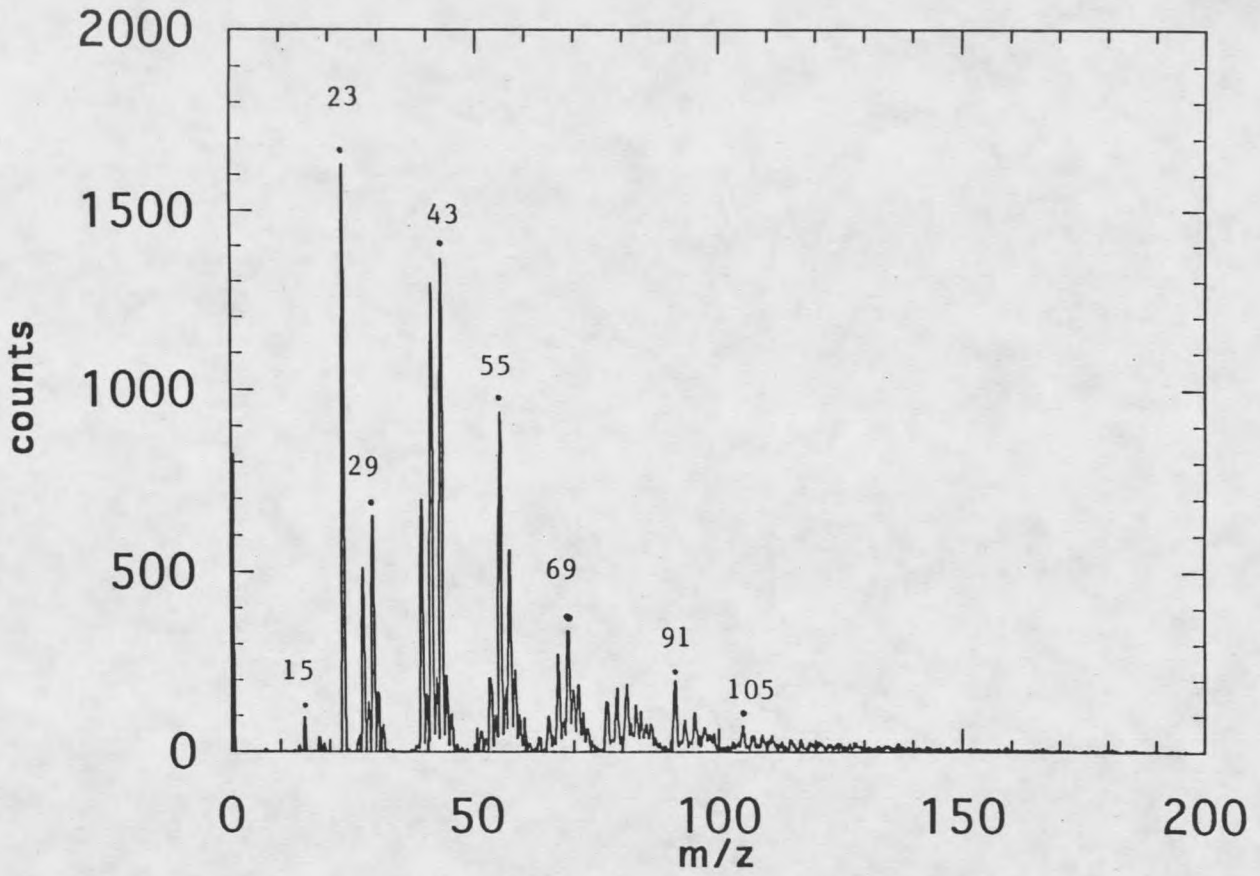

Figure 54. Positive ion static SIMS spectrum of *C. albicans* cell wall AgH9

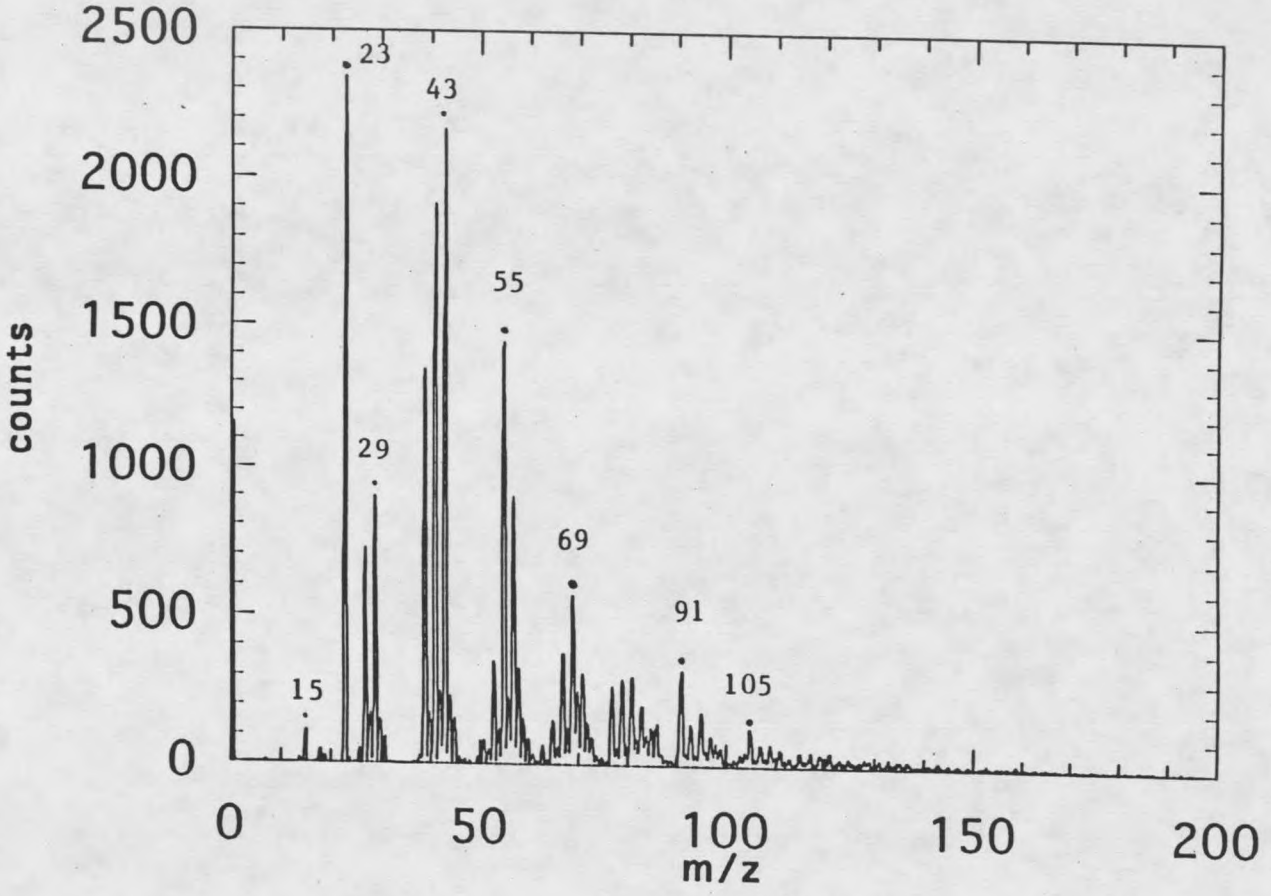

Figure 55. Positive ion static SIMS spectrum of *C. albicans* cell wall AgC6

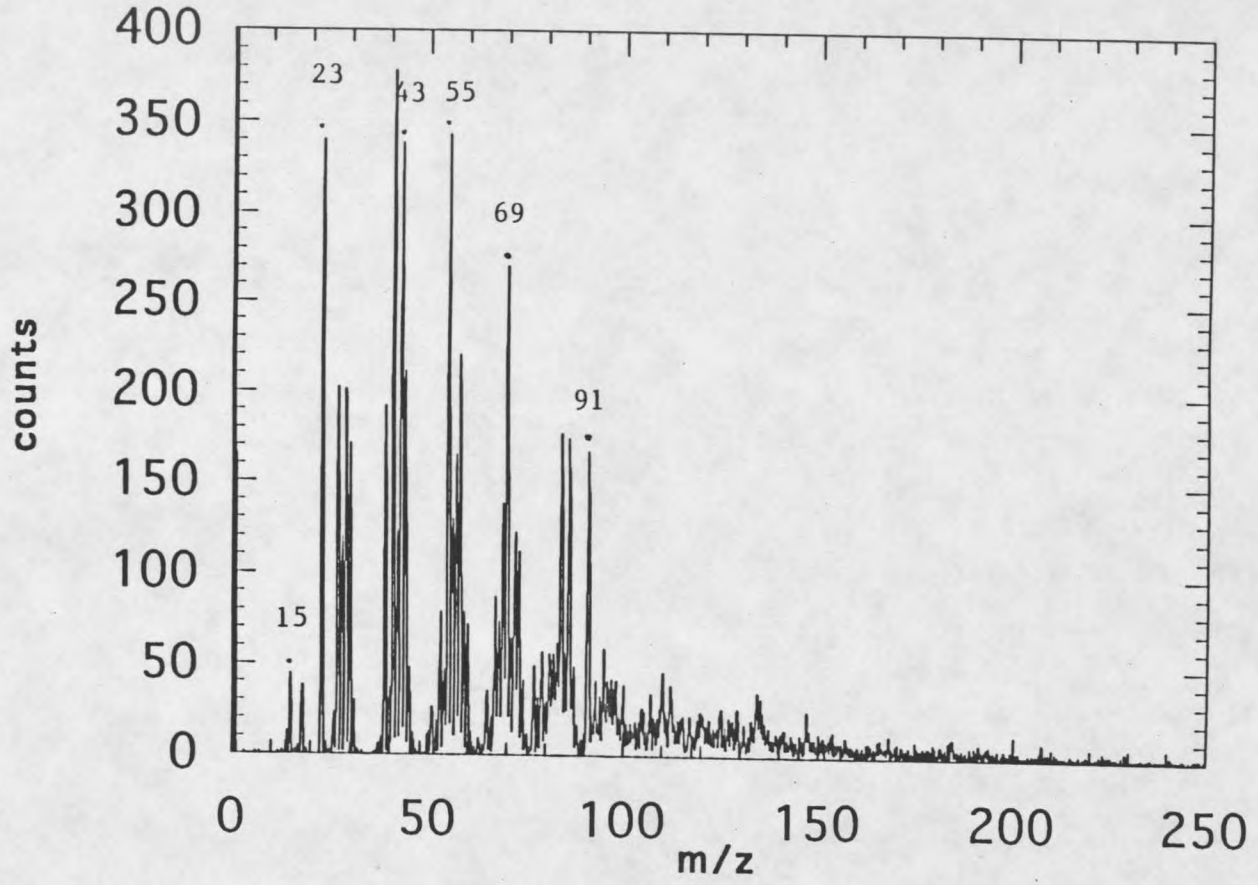

Figure 56. Positive ion static SIMS spectrum of *C. albicans* cell wall crude antigen

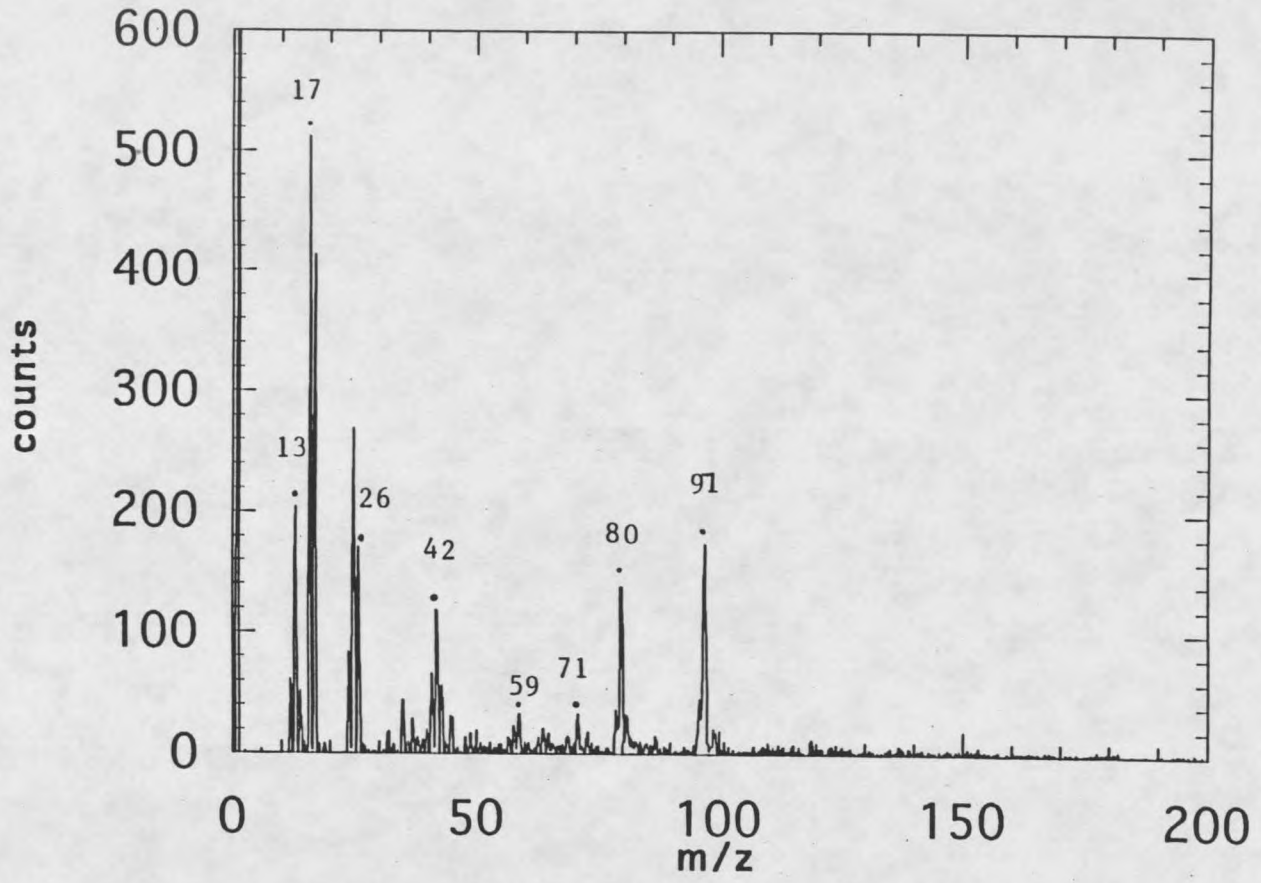

Figure 57. Negative ion static SIMS spectrum of *C. albicans* cell wall AgH9

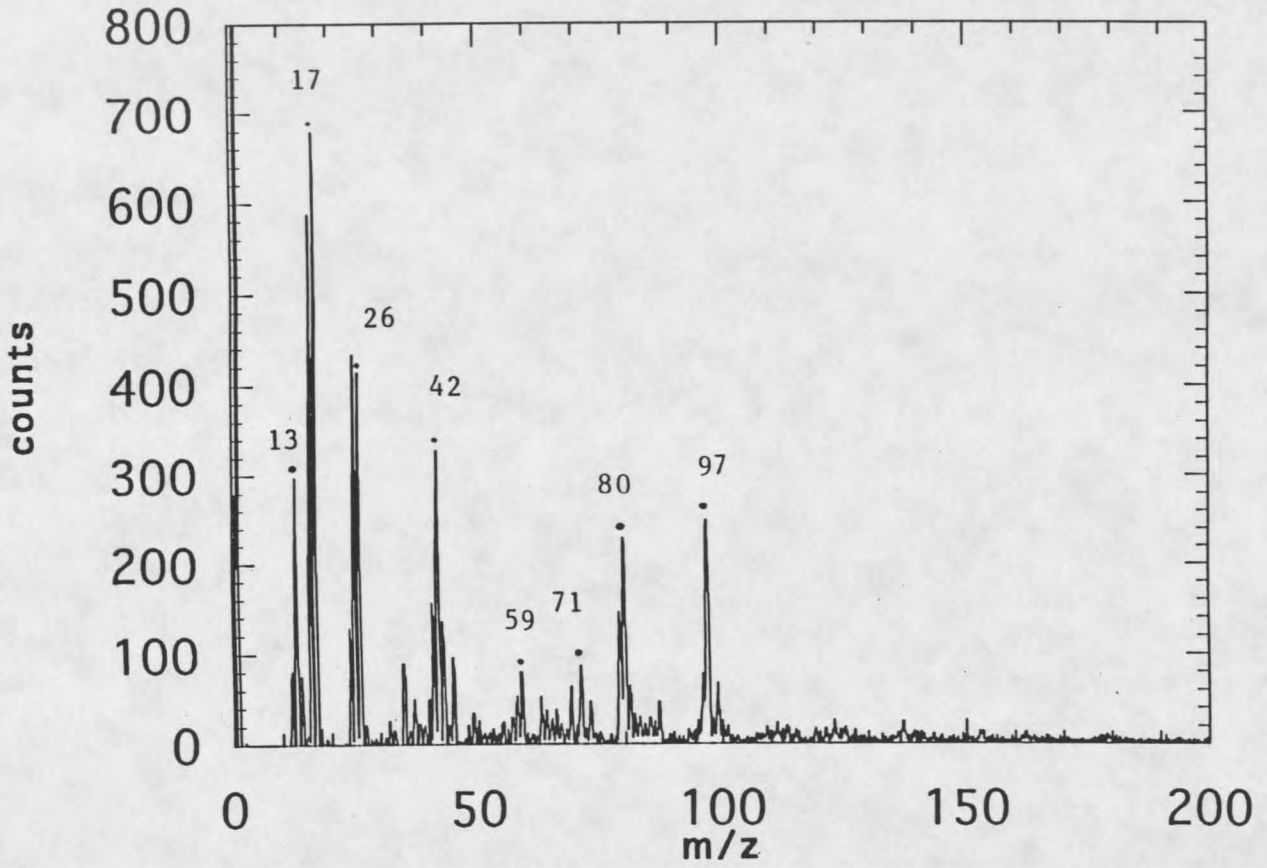

Figure 58. Negative ion static SIMS spectrum of *C. albicans* cell wall AgC6

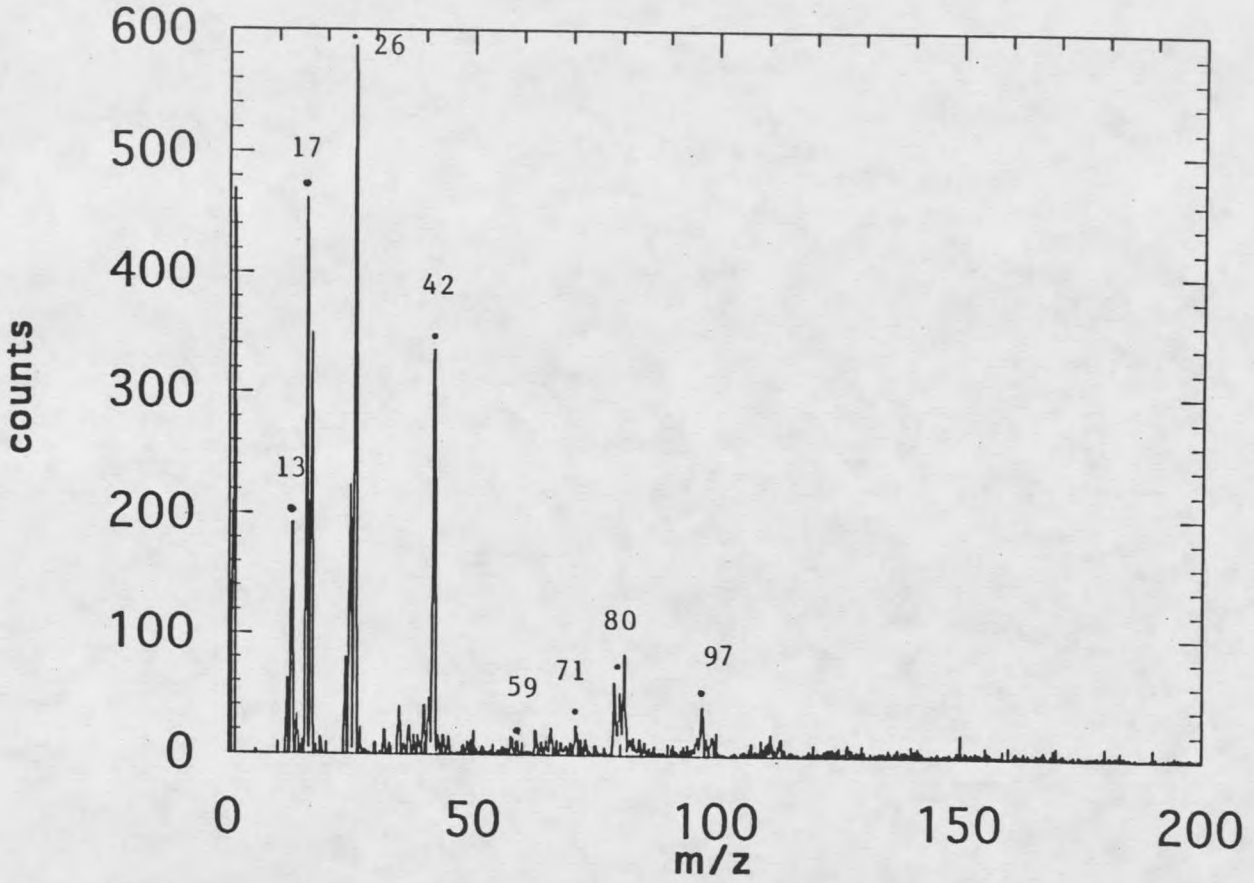

Figure 59. Negative ion static SIMS spectrum of *C. albicans* cell wall crude antigen

CONCLUSION

1. Stereoisomers looked identical in ESCA analysis, while a difference was seen in SIMS analysis. The SIMS spectra of glucose, mannose and galactose slightly differed, but the SIMS spectra of cellobiose were quite different from the SIMS spectra of maltose.

2. The positive ion SIMS spectrum of *C. albicans* cell wall purified antigen was more like the positive ion SIMS spectrum of mannose than any other spectrum. However, the negative ion SIMS spectrum clearly indicated the involvement of amino acids. No difference was seen between cell wall AgH9 and AgC6 from their ESCA and SIMS analyses. ESCA and SIMS analyses showed a higher nitrogen percentage in crude antigen than in purified antigen.

3. The use of ESCA and SIMS for the study of saccharides and *C. albicans* cell wall has never been done. The ESCA and SIMS spectra shown in this experiment were the first report of saccharides and *C. albicans*. The protocol for spectral interpretation described here should be generally useful in ESCA and static SIMS saccharides, polysaccharides, saccharide acid and protein interpretation. This experiment contributed the fundamental work for further adhesion study.

REFERENCES CITED

1. Kennedy, M.J., Rogers, A.L., and Yancey, R.J., "Environmental Alteration and Phenotypic Regulation of Candida albicans Adhesion to Plastic", Infection and Immunity, 57, 3876, (1989).

2. Hawser, S.P., and Douglas, L.J., "Biofilm Formation by Candida Species on the Surface of Catheter Materials In Vitro", Infection and Immunity, 62, 915, (1994).

3. Hazen, B.W., and Hazen, K.C., "Dynamic Expression of Cell Surface Hydrophobicity During Initial Yeast Cell Growth and Before Germ Tube Formation of Candida Albicans", Infection and Immunity, 56, 2521, (1988).

4. Kennedy, M.J., "Adhesion and association mechanisms of Candida albicans", Curr. Top. Med. Mycol., 73, 169, (1988).

5. Locci, R., Peters, G., and Pulverer, G., "Microbial Colonization of Prosthetic Devices. IV. Scanning Electron Microscopy of Intravenous Catheters Invaded by yeasts", Zentralbl. Bakteriol. Abt. Orig., 173, 419, (1981).

6. Rotrosen, D., Gibson, T.R., and Edwards, J.E., "Adherence of Candida Species to Intravenous Catheters", J. Infect. Diseases, 147, 594, (1983).

7. Benninghoven, A., Hagenhoff, B., and Niehuis, E., "Surface MS: Probing Real World Samples", Anal. Chem., 65, 630, (1993).

8. Walls, J.M., and Smith, R., "Surface Science Techniques", Vacuum, 45, 649, (1994).

9. Watson, J.T., Introduction to Mass Spectrometry, Raven Press Books, (1985). QD 96.S43 B46

10. Benninghoven, A., Rudenauer, F.G., and Werner, H.W., Secondary Ion Mass Spectrometry, Basic Concepts, Instrumental Aspects, Applications and Trends, John Wiley & Sons, (1987).

11 Waller, G.R., Biochemical Applications of Mass Spectrometry, John Wiley & Sons, (1979).

12. McEwen, C.N., and Larsen, B.S., Mass Spectrometry of Biological Materials, Marcel Dekker, (1990).

13. Mantus, D.S., Ratner, B.D., Carlson, B.A., and Moulder, J.F., "Static Secondary Ion Mass Spectrometry of Adsorbed Proteins", Anal. Chem., 65, 1431, (1993).

14. Rose, M.E., and Johnstone, R.A.W., Mass Spectrometry for Chemists and Biochemists, the Press Syndicate of the University of Cambridge, (1982).

15. Gilbert, J., Applications of Mass Spectrometry in Food Science, Elserier Applied Science Publishers, (1987).

16. Ratner, B.D., and Castner, D.G., Electron Spectroscopy for Chemical Analysis, John Wiley & Sons, UK, (1992).

17. Odds, F.C., Candida and Candidosis, Bailliere Tindall, London, (1988).

18. Calderone, R.A., and Braun, P.C., "Adherence and Receptor Relationships of Candida Albicans", Microbiological Reviews, 55, 1, (1991).

19. Kwon-Chung, K.J., and Bennett, J.E., Medical Mycology, Lea & Febiger, Philadelphia, (1992).

20. Brawner, D.L., and Cutler, J.E., "Ultrastructural and Biochemical Studies of Two Dynamically Expressed Cell Surface Determinants on *Candida albicans*", Infection and Immunity, 51, 327, (1986).

21. Brawner, D.L., and Cutler, J.E., "Variability in expression of a cell surface determinant on *Candida albicans* as evidenced by an agglutinating monoclonal antibody", Infection and Immunity, 43, 966, (1986).

22. Rakoff, H., and Rose, N.C., Organic Chemistry, the Macmillan Company, NY, (1966).

23. Fieser, L.F., and Fieser, M., Advanced Organic Chemistry, Reinhold Publishing, NY, (1961).

24. Karrer, P., Organic Chemistry, Elsevier Publishing, (1950).

25. Campbell, M.K., Biochemistry, Saunders College Publishing, (1991).

26. Zimmerman, P.A., and Hercules, D.M., "Effect of Stereoregularity on TOP-SIMS Spectra of Polymers", Applied Spectroscopy, 48, 620, (1994).

27. Newman, J.G., Carlson, B.A., Michael, R.S., and Moulder, J.F., Static SIMS Handbook of Polymer Analysis, Perkin-Elmer Corporation, (1991).

28. Briggs, D., Brown, A. and Vickerman, J.C., Hankbook of Static Secondary Ion Mass Spectrometry (SIMS), John Wiley and Son, (1989).